DOCTOR OF PHILOSOPHY

Two-phase Flow Modelling of Mud Flocs Sedimentation in Coastal Waters

Xu, Chunyang

Award date:
2016

Two-phase Flow Modelling of Mud Flocs Sedimentation in Coastal Waters

Chunyang Xu

A thesis submitted for the degree of Doctor of Philosophy

Division of Civil Engineering

The University of Dundee

January

2016

TABLE OF CONTENTS

List of Figures

List of Tables

Notation

A	Coefficient in calculating dissipation coefficients of eddy viscosity and diffusivity
A'	Constant coefficient in Manning equation
$\hat{A}$	Peak value of orbital excursion
B	Coefficient in calculating dissipation coefficients of eddy viscosity and diffusivity
B'	Constant coefficient in Manning equation
B_1	Coefficient calculating yield stress of mud flocs
C	Mass sediment concentration
C'	Constant coefficient in Manning equation
C_d	Drag coefficient
$\overline{C_{\max}}$	Maximum depth-averaged sediment concentration
C_{gel}	Mass concentration of cohesive sediment at gelling point
C_1	Coefficient in permeability formulae
C_2	Coefficient in permeability formulae
C_3	Coefficient in effective stress formulae
C_4	Coefficient in effective stress formulae
C_5	Coefficient in effective stress formulae
C_6	Coefficient in effective stress formulae

D	Floc size
D'	Constant coefficient in Manning equation
D_c	Characteristic size of flocs
D_{eq}	The equilibrium floc size
E	Shear modulus
E_{de}	Deposition sediment flux
E_{up}	Upward erosion sediment flux
F_c	Characteristic fractal dimension
$F_{c,p}$	The cohesive force between primary particles
F_d	Dissipation coefficient of eddy diffusivity
F_{diff}	Dissipation coefficient of eddy diffusivity
F_v	Dissipation coefficient of eddy viscosity
F_y	Mud floc yield stress
G	Shear parameter
H	Wave height
K	Hydraulic permeability
L	Wave length
M	Erosion coefficient
M_s	Eroded sediment
$\overline{P}$	Pressure
R_e	Particle Reynolds number
R_i	Richardson number
T	Wave period

T_{fzz}	Shear stress of fluid phase in the vertical direction
T_{ij}	Stress tensor
T_{rel}	Relaxation time
T_{szz}	Shear stress of solid phase in the vertical direction
T_{xz}	Shear stress term in the horizontal direction
$\overline{U}$	Ensemble mean velocity
$\widehat{U}$	Peak value of orbital velocity
a	Empirical coefficient in settling velocity account for turbulent shear
b	Empirical coefficient in settling velocity account for turbulent shear
d	Primary particle size
d_*	Dimensionless particle parameter
$\widehat{d}$	Non-dimensionalized intra-particle distance
e	Void ratio
e_c	Efficiency parameter
e_d	Parameter describing turbulent diffusion
f_i	Momentum transfer between fluid and solid phase
f_s	Shape factor of particle
f_w	Friction Factor
m	Exponent in settling velocity formulae
m_σ	Coefficient in calculating effective stress
n	The number of flocs per unit fluid volume
nf	Fractal dimension
$nf_{\max}$	Maximum fractal dimension that allow flocs to breakup
n_{RZ}	Empirical coefficient in Richardson-Zaki equation
j	Index in vertical direction

$k_A^{'}$	Coefficient in flocculation model
$k_B^{'}$	Coefficient in flocculation model
k_w	Wave number
k_1	Constant empirical coefficient in settling velocity formulae
p	Coefficient in flocculation model
$\tilde{p}$	Total pressure
q	Coefficient in flocculation model
t	Time
t_t	Turbulent shear strength
u_m	Volume-averaged velocity
w_{hin}	Hindered settling velocity
w_s	Settling velocity
w_s^{gel}	Settling velocity of sediment when the concentration reaches gelling point
$w_{s,r}$	Sediment reference settling velocity
$w_{\sup}$	Settling velocity calculated using Maximum fractal dimension
w_{slow}	Settling velocity calculated using Minimum fractal dimension
w_{s0}	Sediment settling velocity in dilute case
x	Spatial co-ordinate in the horizontal direction
z	Spatial co-ordinate in the vertical direction
Δz_j	Grid size
α	Coefficient in the formulae calculating fractal dimension
α_1	Empirical coefficient in calculating standard deviation
α_s	Volumetric fraction of sediment
$\alpha_s^{\max}$	maximum volumetric fraction of sediment

α_s^{gel}	Volumetric fraction of sediment at gelling point
α_s^*	Loose packed volumetric sediment fraction
$\alpha_1^{'}$	Coefficient in calculating sediment erosion
$\alpha_2^{'}$	Coefficient in calculating sediment erosion
$\alpha_3^{'}$	Coefficient in calculating sediment erosion
β	Coefficient in the formulae calculating fractal dimension
β_e	Empirical erosion flux coefficient
β_1	Amplification factor of viscosity
χ	Coefficient in calculating settling velocity in the permeability regime
δ_{ij}	Kronecker delta
ϕ	Volumetric concentration of mud flocs
$\phi_{\max}$	Maximum floc volumetric concentration
γ_s	Unit weight of sediment
γ_w	Unit weight of fluid
μ	Dynamic viscosity
μ_D	Mean fractal dimension
μ_{eff}	Effective dynamic viscosity
ν	Molecular viscosity
ν_p	Poisson rate
ν_T	Eddy viscosity
ρ_w	Density of fluid
ρ_{mix}	Fluid bulk density
$\Delta\rho$	Effective density of sediment
$\Delta\rho_e$	Effective density of sediment considering the normal distribution of fractal dimension

σ_D	Standard deviation of fractal dimension
σ_e	Effective stress
σ_T	Prandtl Schmidt number
σ_0	Reference effective stress
τ	Shear stress
τ_b	Bed shear stress
τ_c	Critical shear stress for sediment erosion
τ_{cd}	Critical bed shear stress for sediment deposition
τ_{cw}	Combined shear stress
τ_m	Averaged total shear stress
τ_w	Shear stress due to waves
Γ_T	Eddy diffusivity
Δ	Average compressive volume strain

Acknowledgement

Completion of my thesis would have been impossible without hard work and help from others. I would like to take this opportunity to thank some of the people who have given me precious help and support.

I would like to express my deepest appreciation to my PhD supervisor, Prof. Ping Dong in University of Dundee, UK for his guidance and inspiration throughout my studies and living at University of Dundee. His professionalism and broad view on research had a great impact on me. His constructive suggestions and guidance about this thesis are highly appreciated.

Lots of thanks to Dr. Chunyan Zhou, Dr. Yiqiang Chen, Dr. Qinqin Gui, Dr. Teng Liang, Ph.D. Jiaqi Liu, Ph.D. Jian Gou, Ph.D. Ke Wang, Ph.D. Xiaojing Zhong and Ph.D. Yiming Jin from University of Dundee for their help, discussion and good memory together.

I’d like to thank my parents for their support, encouragement and love.

I hereby certify that the work embodied in this dissertation is the result of original research and has not been submitted for a higher degree to any other University or Institution.

_____

Chunyang Xu

Abstract

Cohesive sediments can be found widely such as on continental shelves, at estuaries and in coastal waters. Various engineering problems such as siltation of navigation channels and polluting coastal environment can be caused by the cohesive sediments. To solve these problems, field/lab experiments and numerical models are widely used to study the cohesive sediment transport processes.

The flocculation process is usually neglected in the conventional cohesive sediment transport models, despite the fact that flocculation process can significantly influence the dynamics and fate of cohesive sediment. In the last decades, a large number of studies had attempted to describe flocculation effects by relating the settling velocity of mud flocs with mud flocs properties (size, shape and effective density) empirically based on various flocculation models for dilute suspension. A few investigations have also been reported on the cohesive sediment transport processes with high concentration, but the interactions of fluid and high-concentrated suspended sediment under the action of combined waves and currents remain poorly understood. This thesis investigates the cohesive sediment transport process in coastal waters numerically, especially focusing on the flocculation process. The investigation covers a number of aspects of sedimentation processes of cohesive sediments and the insight gained and models developed represent a major advance in understanding the cohesive sediment transport in coastal estuarine waters.

Firstly, mud flocs are treated as self-similar fractal entities with the fractal dimension being considered as either a constant or a simple function of the mean floc size

in most previous theoretical descriptions. This deterministic description of fractal dimension has recently been found to be inadequate, because for a given size class, fractal dimension of the mud flocs is not a single value but distributed over a certain range. To address this problem, a new flocculation model is proposed in the thesis in which the fractal dimensions for a given floc size class D are taken to be normally distributed rather than a constant. The model is fully validated with available experimental data on the temporal evolution of floc size.

Secondly, a two-phase model for prediction of cohesive sediment suspension is developed and validated using lab experiments. The flocculation process is taken into consideration by incorporating a new drag force closure into the two-phase flow model. This new drag force closure is related to the settling velocity of mud flocs affected by suspended sediment concentration (SSC). The new two-phase model is applied to the simulation of sediment suspension at EMS/Dollard estuary for two measuring period (in June and August 1996). Numerical results are compared with the measured variations of bed shear stresses and sediment concentrations at different elevations above the sea bed where the flocculation process is known to influence the vertical profile of settling velocities and thus the distribution of SSC throughout the water column.

Finally, the two-phase flow model is applied to predict sedimentation processes under both wave and current conditions. The momentum transfer between the two phases is represented by a drag term and the mixing length model is modified to take into account the buoyancy effects due to the gradient of suspended sediment concentration near the seabed. Quantitative comparisons for intra-tide variations of flow properties and mud concentration between the model and the measurements are presented. An

interpretation on how the existence of a fluid mud layer may affect the calculated concentration profile and aspects for further improvement of the model are discussed.

Chapter 1 Introduction

1.1 Research context

Throughout the history of humans, civilization started along the fertile rivers such as Yellow River in China and Nile River in Egypt (Winterwerp and Van Kesteren, 2004)，because these areas are productive due to the existence of cohesive sediment which contains abundant nutrients for aquatic product and crops. Cohesive sediment can be found widely especially in the estuaries, lagoons and coastal areas, such as in the Ems estuary (Van Der Ham *et al.*, 2001; van Leussen, 1999), the Yellow River estuary (Van Maren *et al.*, 2009; Zhou *et al.*, 2015), the Yangtze River estuary (Shi *et al.*, 2012; Zhu *et al.*, 2014), the Ria de Aveiro lagoon (Lopes *et al.*, 2006) and the Yellow Sea (Bian *et al.*, 2013). The presence of cohesive sediment can cause various engineering problems. The sedimentation and accumulation of cohesive sediment may hinder the navigation channels and harbour basins (van der Ham and Winterwerp, 2001), influence the safety of hydraulic structure and cause economic loss. For example, due to the serious sedimentation in the Yanshan port, further construction of harbours has been stopped (Ying *et al.*, 2012). It was reported that about 1.0×10^6 m^3 of sediment has to be dredged to keep the safe navigation in Rotterdam port and the cost to maintain the harbour basin is high (Winterwerp and Van Kesteren, 2004). When designing the ponds or dams, the sediment load that can deposit is one of the most important parameters that should be considered. Because of the poorly estimated amounts of clay, the sidewalls started to leak and eventually failed, which caused the 300 acres of land flooded at the Kinston Fossil Plant in 2008 (Heiliger, 2010). Due to the cohesive characteristics, a lot of pollutants

such as organic materials and heavy metals are absorbed by the flocculated mud flocs which will pollute rivers and coastal waters (Maggi, 2005). The thick layer of fluid mud has been found in the sea bed, continental shelves and mudflat (Zhu *et al.*, 2014) and becomes unstable. Mudflows generated under the natural or human disturbances may result in the damage of cables (van der Ham and Winterwerp, 2001). Therefore, it is necessary to carry out study on the cohesive sediment processes. Due to the complex flocculation process, both the floc size and effective density are varying in time and space, which makes it difficult to predict the settling velocity of cohesive sediment using numerical models (Cuthbertson *et al.*, 2010) or to observes them in filed measurements and laboratory test (Cuthbertson *et al.*, 2010; Manning, 2004a). The understanding of mechanisms influencing the flocculation process and further the cohesive sediment transport processes are limited. A fluid mud layer may exist in a fluid-like state and exhibits a non-Newtonian behavior especially at the bottom of tidal channels (Huang and Aode, 2009). Though a lot of studies (Shi *et al.*, 2012; Winterwerp, 2006) have been carried out on the high concentrated cohesive sediment, the non-Newtonian effects and the interaction between fluid and cohesive sediment under combined currents and waves at the water-bed interface is still poorly understood.

During recent years, a lot of experiments have been carried out to study flocculation process of mud flocs (Manning *et al.*, 2011; Spearman *et al.*, 2011; Vahedi and Gorczyca, 2012), which give the potential capability for further investigation on the flocculation mechanisms. More numerical models especially the two-phase model have been developed to simulate the physical processes of cohesive sediment processes (Chauchat *et al.*, 2013; Cheng *et al.*, 2015; Hsu *et al.*, 2009). The increased knowledge on physical

processes of cohesive sediment and the gradually matured two-phase model provide a good opportunity for the study on cohesive sediment sedimentation processes in coastal waters.

1.2 The composition and characteristics of cohesive sediment

By definition, cohesive sediment is a mixture of organic material, silt, clay, fine sand and water. The composition and thus the mechanical behavior of cohesive sediment vary in time and space (Kranenburg, 1994; Mehta, 1986). The main composition of cohesive sediment, thus its behavior and characteristics are summarized as follows (Winterwerp and Van Kesteren, 2004):

- Organic material is one of the main components of cohesive sediment and can have large effects on the flocculation process and the mud floc size which will complicate the behavior of cohesive sediment. The main organic substances are polysaccharides, lipids and humic acids. These large (compared to clay particle) organic matters can connect with clay particles at several locations and form mud flocs with long loops or tails. It can be seen in Figure 1.1 that the mud flocs are fluffy. The sizes of mud flocs shown in Figure 1.1 (a_1 and a_2) are around 300 μm.
- Mineral materials often perform as a major part of cohesive sediment. Clay minerals, such as kaolinite and montmorillonite, are dominated in the clay fraction (particle size less than 2 μm). The silt fraction (2 μm <particle size< 63 μm), are mainly composed of quartz, feldspar and carbonates. It should be mentioned that due to the micro-size and special shape of clay particles, which

cause a specific electrical charge distribution, cohesion is addressed as one of the most important characteristics of cohesive sediment.

- Due to the cohesive characteristics, pollutants such as heavy metals usually appear within mud flocs. Though these pollutants share a low percentage of the mass, they may have a significant influence on the environment in estuaries and coastal waters.

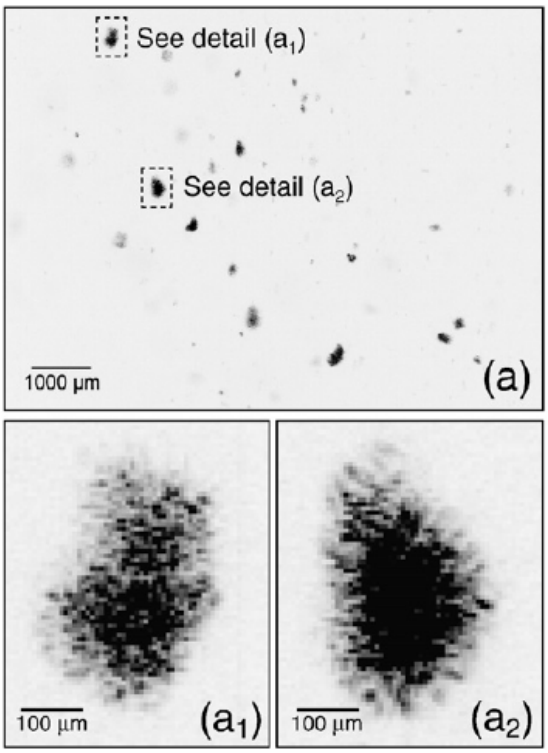

Figure 1.1 Mud flocs (Cuthbertson *et al.*, 2010)

1.3 Cohesive sediment processes

The key process of cohesive sediment processes are briefly described as follows.

1) Flocculation is one of the main characteristics which distinguish between the non-cohesive sediment and cohesive sediment (Van, 2013). Large mud flocs are formed by

small primary particles of cohesive sediment and break up due to Brownian motion, differential settling and turbulence.

2) Settling velocity is the key parameter determining the cohesive sediment flux. Accurate prediction of cohesive sediment transport cannot be obtained without fully understanding the settling process of cohesive sediment (Cheng *et al.*, 2015). For cohesive sediment, the settling velocities are related to floc sizes, floc densities and floc shapes in dilute situations. In highly suspended sediment concentration (SSC), the settling velocities will be influenced by hindrance effects (Dankers and Winterwerp, 2007).

3) Self-weight consolidation is introduced in the present research. Under the self-weight of cohesive sediment, water is expelled out from the inside and between the mud flocs, during which the pore pressure decreases and the effective stress of mud flocs increases.

4) Erosion and entrainment of sediment from the bed is an important process for large scale transport of cohesive sediment. According to our knowledge, the mechanisms determining critical shear stress for erosion in the case of cohesive sediment is still not fully understood yet. Only the physical processes of cohesive sediment listed here and the interaction between fluid and cohesive sediment will be illustrated in the description of numerical model.

1.4 Models for cohesive sediment sedimentation processes

Generally speaking, models for cohesive sediment transport can be summarized into two groups. One is the single-phase numerical model (Hsu and Balachandar, 2009;

Spearman *et al.*, 2011; van der Ham and Winterwerp, 2001), in which the velocity of cohesive sediment is assumed as the same as flow velocity except in the vertical direction. Winterwerp (2006) presented a classic single-phase model and applied it to Ems/ Dollard estuary. The 1DV model is driven by the averaged fluid velocity $\overline{U}$ and the turbulence is simulated by combining a $k-\varepsilon$ model. The concentration is obtained by solving an advection-diffusion term. Traditionally the single-phase models are based on the hypothesis that the SSC has no effects on the flow structure. While in the work of van der Ham and Winterwerp (2001), a dissipation term is introduced into the $k-\varepsilon$ model to account for the buoyancy effects.

As for the settling type, the theory of Kynch (1952) has been widely used to simulate settling experiments for non-cohesive sediment as well as cohesive sediment. It has been proved that the settling types of highly concentrated cohesive sediment depend on the initial concentration when using Kynch's analytical method (Dankers and Winterwerp, 2007).

After the cohesive sediment settles on the bed, a solid structure is formed and the deformation of soil structure is described using consolidation theory by Terzaghi (1923), which is named as small strain consolidation theory only applicable to primary stage (elastic deformation appears on the subsoil) of self-weight consolidation, or by Gibson *et al.* (1967) and Gibson *et al.* (1981), which is addressed as large strain consolidation theory.

Alternatively, recently two-phase models are more popular in the simulation of cohesive sediment sedimentation processes (Boulton *et al.*, 2006; Chauchat and Guillou,

2013; Hsu *et al.*, 2007; Nguyen *et al.*, 2009; Teisson *et al.*, 1992; Torres-Freyermuth and Hsu, 2010). In the two-phase models, the continuity equations and momentum equations for both phases (solid phase and fluid phase) are solved respectively. The momentum transfer between two phases is implemented using the drag force closure (Chauchat *et al.*, 2013; Teisson *et al.*, 1992). A variety of turbulence closures have been used in the simulation of non-cohesive sediment transport. The eddy viscosity can be calculated either using a specified profile (Jiang *et al.*, 2004), or using a Prandtl Mixing theory (Liu and Sato, 2005; Zhang and Dong, 2000), or by solving a complete two equations turbulence closures $k-\varepsilon$ model (Hsu *et al.*, 2003). The $k-\varepsilon$ turbulence closures are used in most of the two-phase models designed for cohesive sediment (Nguyen *et al.*, 2009; Torres-Freyermuth and Hsu, 2010). To account for the bed deformation under self-weight, the concept of effective stress for solid structure is introduced. In the two-phase model, effective stress is given by a particle pressure σ_e closure (Chauchat *et al.*, 2013).

Overall, although useful in predicting general flow features, the single-phase models do not address the fundamental mechanisms between the interaction of suspended sediment and fluid in a completely rational way (Dong and Zhang, 1999). It means that the settling velocity of suspended sediments is not calculated directly and an empirical settling velocity formula has to be adopted instead to account for the hindered settling effect which is particularly important in the sedimentation processes in hyper concentration. A fictive bed is assumed for the single-phase model and the determination of sediment flux between the bed and water column is complex. The two-phase model allows the extension of calculation domain which is from the water surface to the consolidated bed.

1.5 Aim and objectives of the research

In the most researches, the flocculation process has been described by simply relating settling velocities with characteristics of mud flocs such as size, density and shape using empirical equations. The mechanisms of flocculation process of mud flocs are still not fully understood. Few researches have focused on the interaction between fluid and high concentrated mud under the combined action of currents and waves, which remains poorly understood. The overall aim of this research is to investigate the sedimentation processes of mud flocs in coastal waters. To be specific, the mechanisms influencing the flocculation process will be further studied and the effects of flocculation process on the sedimentation processes of cohesive sediment are taken into account using a two-phase model in which the settling velocities of mud flocs will be calculated directly. And also the interactions between fluid and high concentrated mud under combined waves and currents are further studied to improve the understanding of sedimentation processes of cohesive sediment.

The identified objectives presented in this thesis have been summarized and listed as follows:

- Investigate the time evolution of mud flocs under different shear conditions, using a flocculation model of mud flocs based on the normal distribution of fractal dimension and yield stress.
- Validate the presented two-phase model using data of settling tanks experiments and prove the efficiency of the two-phase model in the simulation of cohesive sediment sedimentation-consolidation process.

- Quantify the effects of flocculation process of mud flocs on the transport of cohesive sediment by comparing results from presented two-phase model with the data measured in Ems/ Dollard estuary.
- Investigate sedimentary processes of cohesive sediment on an erosional intertidal mudflat with the two-phase model. An interpretation on how the fluid mud layer affects the calculated concentration profile under combined waves and currents actions is discussed.

1.6 Outline of the thesis

The dissertation is organized as followings:

Chapter 1 (Introduction of dissertation) provides the background information of studies on cohesive sediment sedimentation processes, especially for the progress of numerical models. The models used to simulate the transport of cohesive sediment are briefly discussed. It also outlines the key objectives and aims of the current research as well as the structure of the dissertation.

Chapter 2 A comprehensive review on the cohesive sediment dynamics is presented. It covers flocculation process, settling/hindered settling process, consolidation process, and the interaction between fluid and cohesive sediment is also mentioned. The physical processes of cohesive sediment are illustrated in detail and the model or mathematical formulae used to describe the sediment dynamics are reviewed and discussed. Comprehensive literature review on the models adopted in the cohesive sediment transport is given. The single-phase models are compared with two-phase models and the

strengths and weaknesses of both model groups (single-phase model and two-phase model) are concluded.

Chapter 3 A flocculation model based on the normal distribution of fractal dimension and yield stress is developed. Based on the experiments data, the presented flocculation model is validated and applied to study the time evolution of mud floc size under different shear conditions.

Chapter 4 A two-phase model is developed for validation and application in the next Chapter. All the stress terms and boundary conditions are listed in detail.

Chapter 5 The two-phase model was validated using experiments data derived from settling tanks and then applied to field measurements. Both settling experiments of non-cohesive sediment and cohesive sediment are simulated by the two-phase model with different drag force and effective stress closures. The two-phase model is applied to the simulation of cohesive sediment transport in Ems/Dollard estuary based on the data measured in two different periods to investigate the effects of flocculation on the cohesive sediment dynamics. Also the two-phase model is applied to study the sedimentary processes on an erosional mudflat at Yangtze River Delta, China and produce quantitative comparisons for intra-tide variations of flow properties and mud concentration between the model and the measurements.

Chapter 6 (conclusions) The major findings of this study are summarised and recommendations for future research are proposed.

Chapter 2 Sediment dynamics and numerical studies on the cohesive sediment transport

2.1 Sediment dynamics

The commonly accepted key processes of cohesive sediment (see Figure 2.1) are briefly discussed in Chapter 1. In this chapter, the main processes of the cohesive sediment, as well as the mathematical formulae used to describe the physical processes, are reviewed in detail.

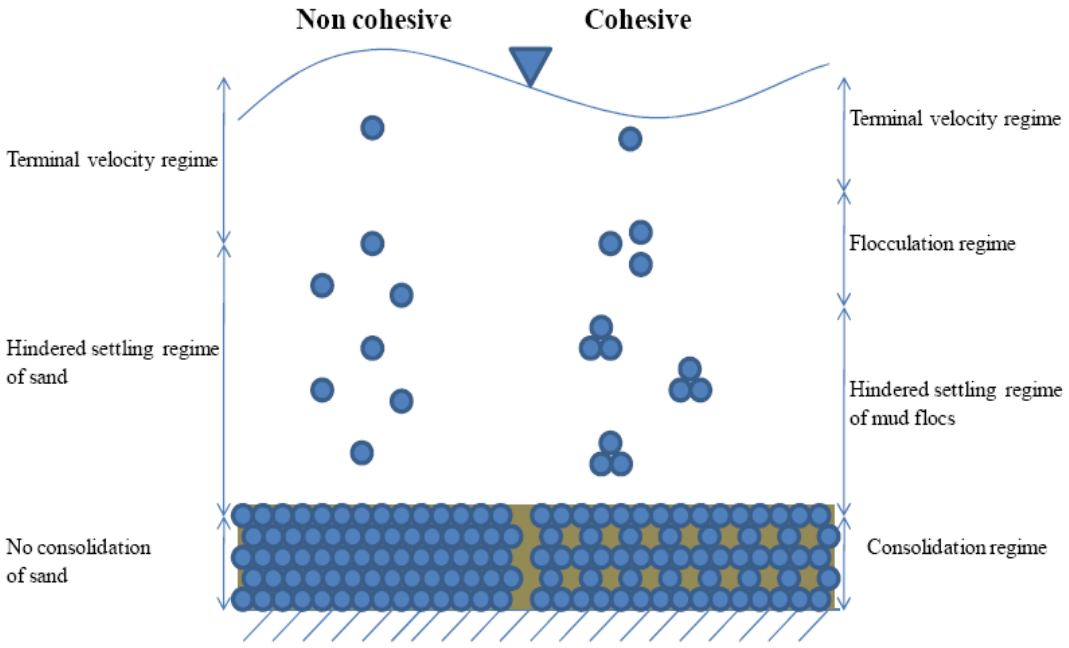

Figure 2.1 Settling processes of non-cohesive sediment (left) and cohesive sediment (right), adopted from Van (2013)

2.1.1 Flocculation processes

2.1.1.1 *The concept of flocculation*

Compared to non-cohesive sediment, flocculation process is a special process that distinguish between the behavior of the cohesive sediment and that of non-cohesive sediment (Klimpel and Hogg, 1986). Single particles and organic matter are caused to collide and get aggregation to form large flocs (Burban *et al.*, 1989; Lick *et al.*, 1992). This process, namely flocculation, which strongly influences the settling velocity of sediment in aquatic environment, is acknowledged widely as a special part of transport processes for cohesive sediment and complicates the process of sediment transport (Winterwerp, 1998). The flocculation mechanism turns slowly sinking matter such as organic matter, single particles and contaminates into large, rapidly sinking flocs. Consequently, the dynamical and physical properties of flocs are different with that of single particles, organic matter and contaminates.

2.1.1.2 *Factors controlling the flocculation process*

It is well known that at least three mechanisms are operative during the flocculation process (Lee *et al.*, 2011; Winterwerp, 1998):

1) Brownian motion: particles move randomly and collide with each other, which may cause aggregation.

2) Differential settling: in a settling column, particles or larger flocs with a larger settling velocity may overtake particles or small flocs with smaller settling velocity. Collisions between these particles or flocs have probability to make particles or flocs get aggregation, the process of which is addressed as flocculation by differential settling.

3) Turbulent motion: in the turbulent flow, particles, organic matter and contaminants will move along with the flow, be carried by turbulent eddies, which may result in large floc aggregation. Obviously, disaggregation may happen and flocs begin to break up when the turbulent shear stress is large enough.

It has been concluded that the disaggregation of mud flocs is dominated by Brown motions, and the effects of differential settling and fluid shear can be negligible for small particles or when sediment concentration is less than 1 g/L (Burban *et al.*, 1989; Lick *et al.*, 1992; McCave, 1984; van Leussen, 1999). However, it has been argued that the differential settling mechanism is important in still water environment such as water treatment installations (Lick *et al.*, 1993). The effect of turbulent motions has been mostly focused by the scholars (McCave, 1984; Son and Hsu, 2008; Son and Hsu, 2009; Spicer and Pratsinis, 1996; Winterwerp, 1998; Winterwerp *et al.*, 2006) and was introduced into many flocculation models as one of the key factors controlling the flocculation process. Another key parameter that controls the flocculation process is the cohesive sediment concentration. It has been found that the sizes of mud flocs increase with the sediment concentration (Dyer, 1989). It can be explained as that the opportunity for primary particles or small mud flocs to collide increases with the increase of sediment concentration, which will result in large mud flocs. Though turbulent intensity and concentration of sediment have the major influence on the flocculation (van Leussen, 1999, 2011), other factors, such as organic matter or dissolved contaminants also have effects on the aggregation of sediment particles through electrochemical or biochemical attraction, which is named as the cohesive characteristics, and further on the settling velocity, that cannot be neglected.

From the discussion mentioned above, it can be concluded that the particle collisions are related to sediment concentration and turbulence intensity. In other words, high concentration and shear intensity increase the opportunity for particles to collide, while other biological or chemical parameters, such as salinity and organic contents, increase the efficiency of sediment particles getting aggregation, which is defined as flocculation ability by van Leussen (1999).

2.1.1.3 *Models describing the flocculation process*

Settling velocities related to flocculation process

For cohesive sediment, primary particles and microflocs aggregate during the flocculation process and form larger mud flocs whose densities, sizes and shapes are changed and thus the settling velocities (van der Ham and Winterwerp, 2001). A large number of literatures try to relate the settling velocities of mud flocs to cohesive sediment concentration (denoted as $w_s - C$ relationship). The $w_s - C$ relationship has been applied to various field or lab experiments to describe the settling velocities of cohesive sediment due to flocculation (van der Ham and Winterwerp, 2001; Van der Lee, 2000; van Leussen, 1999).

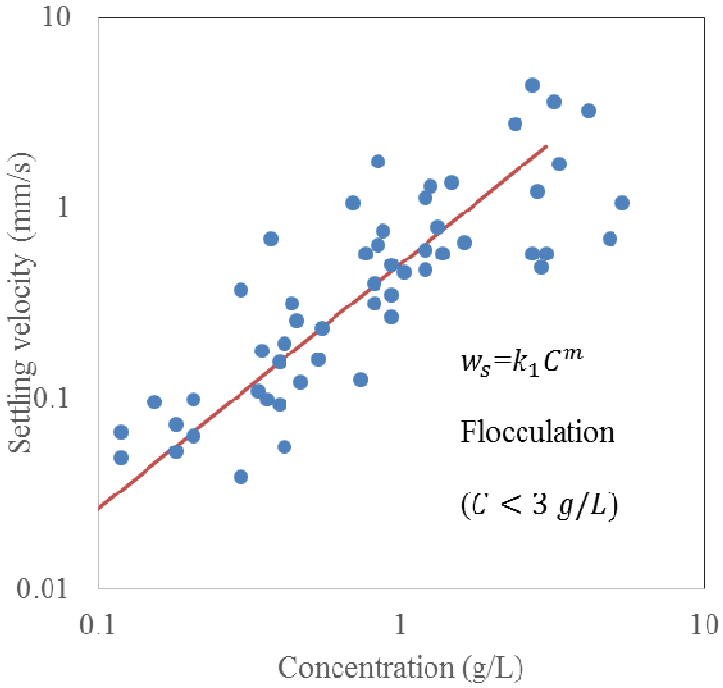

Figure 2.2 The relationship between settling velocities and SSC of cohesive sediment, redrawn from Thorn (1981)

$$w_s = k_1 C^m \tag{2.1}$$

where w_s is the settling velocity, k_1 is an constant empirical coefficient, C (kg/m^3) is the sediment concentration and m is the exponent (Figure 2.2).

The constant k_1 depends on the sediment type and is suggested to be specified as 0.001 and m is equals to 1 (Van, 2013). In the 1DV model of van der Ham and Winterwerp (2001), k_1 and m are specified as 0.0015 and 1.2 respectively. Calibrated based on the field measurements, m varies from 0.61 in the Humber estuary to 2.6 in the Elbe estuary (Van der Lee, 2000). According to van Leussen (1999), there is no unique relationship existing between settling velocities and SSC, even along the river axis in the same estuary. This was confirmed in the work of Van der Lee (2000) which further

concluded that the settling velocities correlate with SSC on a tidal time scale. The Equation (2.1) is very simple and easy to be implemented into numerical models in addition to the sediment concentration. The turbulence intensity also plays an important role in the flocculation process. Most experiments (Manning, 2004a; Manning, 2004b; Mehta, 1986) showed that the measured mud floc sizes decrease with the increase of fluid shear intensity when the turbulence shear stress exceeds a critical value, whereas an opposite phenomenon is observed when the turbulence shear is less than the critical value. To take the effects of fluid shear intensity on flocculation into consideration, Dyer (1989) presented an empirical formulae (Equation (2.2)):

$$w_s = w_{s,r} \frac{1 + aG}{1 + bG^2} \tag{2.2}$$

where G is shear parameter, $w_{s,r}$ is reference settling velocity, a and b are empirical coefficients. This formula implies that the floc sizes firstly increase with shear stress and then followed by a decrease. This equation is further illustrated in Figure 2.3:

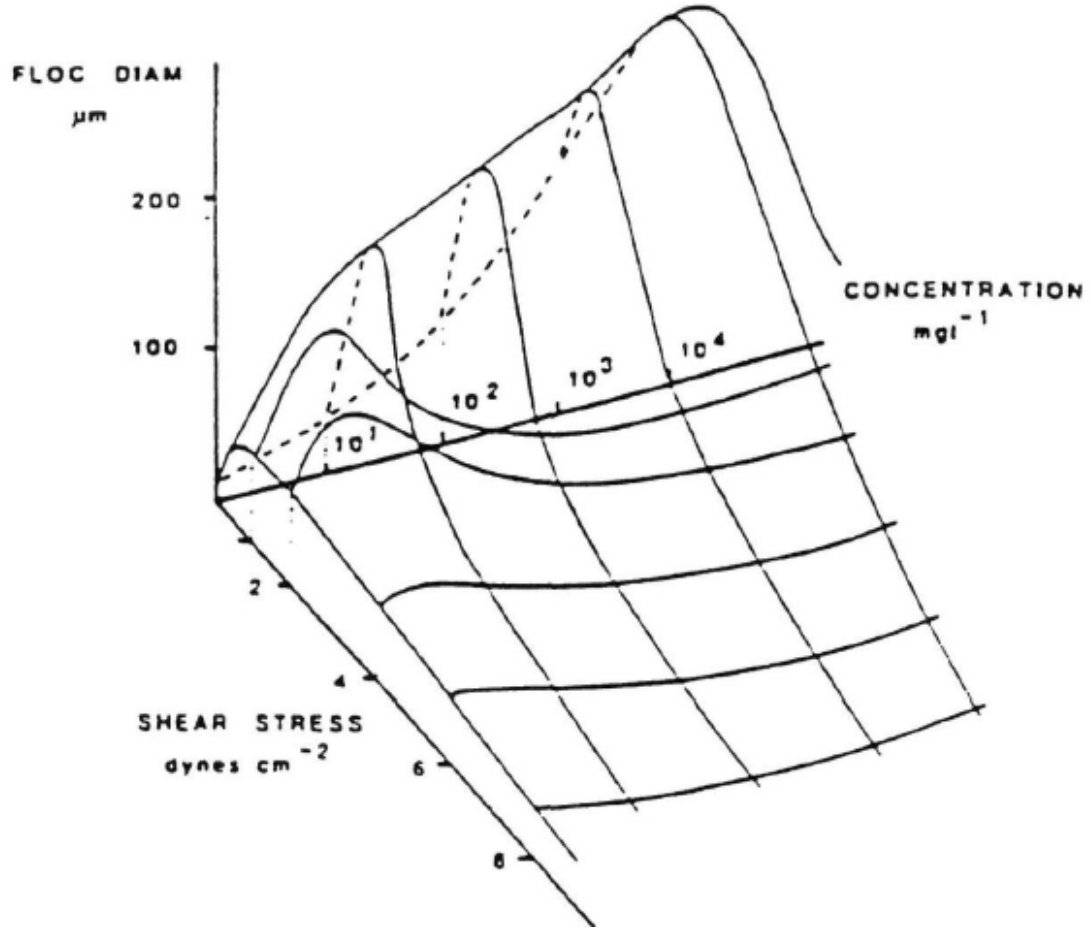

Figure 2.3 Relation of floc sizes against sediment concentration and shear stress (Dyer, 1989)

To combine the effects of turbulence and SSC on the calculation of settling velocities, a series of empirical models have been developed by Manning *et al.* (2011):

$$w_s = A' + B'\tau + C'\tau^2 + D' \times \mathrm{SPM} \tag{2.3}$$

where A', B', C' and D' are constant coefficients which need to be specified according to the proportion of mud content and shear stress, τ is the shear stress at the elevation z above the bed and SPM is the suspended particulate matter (mg/L). As the Equation (2.3)

is restricted to the study area and a lot of coefficients need to be specified, it is not easy to be incorporated into the sediment transport model.

Equations (2.1), (2.2) and (2.3) are trying to describe the effects of factors such as sediment concentration and turbulence intensity on the flocculation process by introducing parameters related to sediment concentration and turbulence intensity directly into the formulae calculating settling velocities of mud flocs. Other researches focus on the prediction of floc sizes.

Floc sizes related to flocculation process

For cohesive sediment, the floc sizes change constantly under the effects of turbulence and SSC due to the biochemical and electrochemical characteristics. As the floc size is one of the key parameters determining the settling velocities of mud flocs in the water column with dilute sediment concentration, accurate prediction of the temporal floc size is essential in understanding the sediment transport process. Based on the assumption of constant fractal dimension, Winterwerp (1998) developed a flocculation model considering the effects of SSC, fluid shear intensity and the flocculation ability:

$$\frac{dD}{dt} = \frac{k_A^{'}}{nf}\frac{C}{\rho_s} G d^{nf-3} D^{4-nf} - \frac{k_B^{'}}{nf}\left(\frac{\mu}{F_y}\right)^q G^{q+1} \times d^{-p} D^{2q+1} (D-d)^p \tag{2.4}$$

where D is floc size, d is the size of primary particle, t is time and nf is fractal dimension. p and q are coefficients and specified as 1 and 0.5 respectively. The yield stress of flocs is denoted as F_y, μ is the dynamic viscosity. ρ_s is the density of sediment. In Equation (2.4), coefficients $k_A^{'}$ and $k_B^{'}$ are defined as:

$$k_A^{'} = (3e_c \pi e_d) / 2f_s \tag{2.5}$$

$$k_B^{'} = a^{'} e_b \tag{2.6}$$

where e_c is an efficiency parameter describing the possibility of the collisions that will result in flocculation. And e_b is an efficiency parameter for floc break. As discussed by Lick *et al.* (1992), e_c is a function of floc size and floc density which is difficult to be determined at present. Therefore e_c is assumed to be constant for simplicity. e_d is a parameter describing the turbulent diffusion. f_s is the shape factor of particle and $a^{'}$ is an coefficient.

The flocculation model presented by Winterwerp (1998) linearly connects the aggregate and break-up processes. It can predict the temporal floc sizes and thus the settling velocities. Inspired by the work of Winterwerp (1998), Son and Hsu (2008) extended the flocculation model considering the variable fractal dimension with floc size:

$$\frac{dD}{dt} = \frac{Gd^{\beta}}{\beta \ln \frac{D}{d} + 1} \left[\frac{Ce_c \pi e_d}{2\rho_s f_s} d^{nf-3} D^{-nf+4-\beta} - \frac{e_b a^{'}}{3} \left(\frac{\mu G}{F_y} \right)^q d^{-p} D^{-\beta+2q+1} (D-d)^p \right] \tag{2.7}$$

where $\beta = \dfrac{\log(F_c / 3)}{\log(D_c / d)}$, D_c is a characteristic size of flocs and set to be 2000 μm and F_c is a characteristic fractal dimension and is set to be 2.

Son and Hsu (2009) further extended the flocculation model by taking the variable yield stresses of flocs into consideration:

$$\frac{dD}{dt}=\frac{Gd^{\beta}}{\beta\ln(D/d)+1}\left[\frac{k_A^{'}}{3}\frac{C}{\rho_s}d^{nf-3}D^{-nf+4-\beta}-\frac{k_B^{'}}{3}(\frac{\mu G}{B_1})^{q}D^{1-\beta+(2q/3)(3-nf)}d^{-p+(2q/3)nf}(D-d)^{p}\right] \tag{2.8}$$

where B_1 is an coefficient and calculated as:

$$B_1=(\frac{\pi}{6})^{-2/3}F_{c,p} \tag{2.9}$$

where $F_{c,p}$ is the cohesive force between primary particles.

2.1.2 Settling process

Gravitational settling is one of the basic sediment processes in a fluid (Burban *et al.*, 1990; Cheng, 1997a; Strom and Keyvani, 2011). The settling velocities are not only determined by the characteristics of sediment particles/sediment flocs such as shape, size and density but also depend on the viscosity and density of the fluid (Fennessy *et al.*, 1994; Reed and Anderson, 1980). For cohesive sediment in high concentration, the settling velocities also depend on SSC and factors can affect the flocculation ability such as PH and salinity of the fluid.

2.1.2.1 *Settling velocities calculation in dilute sediment concentration*

Many attempts have been made to calculate the settling velocity which is usually regarded as a function of floc shape, density and size in a specific water circumstance with a dilute sediment concentration. The Stokes equation or the modified Stokes equations, which are obtained from a balance between gravitational force and drag force, is applied to infinite dilute situation:

$$w_s = \frac{(\rho_s - \rho_w)gD^2}{18\mu} \tag{2.10}$$

where ρ_w is the density of fluid, g is the acceleration due to gravity. For $Re > 1$ various empirical formulae have been developed such as Equation (2.11) by Cheng (1997b):

$$\frac{w_s d}{\nu} = (\sqrt{25 + 1.2d_*^2} - 5)^{1.5} \tag{2.11}$$

where ν is the kinematic viscosity and d_* is a dimensionless particle parameter and defined as:

$$d_* = (\frac{\Delta g}{\nu^2})^{1/3} d \tag{2.12}$$

Though the equations mentioned above are specifically designed for non-cohesive sediment particles, Equation (2.10) has been used to calculate the effective density of mud flocs (Khelifa and Hill, 2006; Manning, 2004a) and Equation (2.11) has been successfully applied to calculate the settling velocities of mud flocs (Cuthbertson *et al.*, 2008). To calculate the settling velocities of cohesive sediment, the key parameter is to determine the effective density of mud flocs (Dyer, 1989; Gibbs, 1985; van Leussen, 1999), because the effective densities of mud flocs have been changed during the flocculation process, which are completely different from that of the primary particles. Winterwerp (1998) treated the mud flocs as fractal entities and developed a settling model for mud flocs based on the assumption of constant fractal dimension:

$$w_s = \frac{f_s}{18} \frac{(\rho_s - \rho_w)\mathrm{g}}{\mu} d^{3-nf} \frac{D^{nf-1}}{1 + 0.15Re^{0.687}} \tag{2.13}$$

in which Re is the particle Reynolds number and defined as:

$$Re = w_s D / \nu \tag{2.14}$$

2.1.2.2 *Settling velocities calculation in high sediment concentration (hindered settling velocity)*

Section 2.1.2.1 discussed about the settling velocities for individual particles or mud flocs in dilute sediment concentration. Under low concentration conditions (C< 0.01 g/L), the effects of particle interaction can be neglected and the settling velocity of flocs is equal to the terminal velocity. As the concentration of the suspension increases, the floc properties (size, density) vary and the settling velocity increases at first. For large concentration, a transition value occurs: settling velocity decreases when suspended concentration is larger than a transition value. As large amount of mud flocs exist in the water column, the interactions between the flocs are drastic and hindered effects appear (Winterwerp, 2002).

Hindered effects

Various studies have been focused on the hindered settling velocities of sand particles (Baldock *et al.*, 2004; Masliyah, 1979; Richardson and Zaki, 1954; Tomkins *et al.*, 2005). As for mud flocs, though few researches are published, the rationales from the sand particles can be applied to mud flocs. Winterwerp and Van Kesteren (2004) proposed that the following seven processes have significant effects on settling velocities of individual particles in a suspension: 1) particle-particle collisions, 2) cloud formation

or settling convection, 3) wake formation and return flow, 4) dynamic and flow effect, 5) viscosity of the flow, 6) interactions between particles, 7) buoyancy or effective density.

Usually three hindered effects are adopted:

- Wake and return flow: a wake and return flow will be generated when the mud flocs settle in a fluid. For other mud flocs settle within the wake and return flow, the ultimate settling velocity will be influenced. In fact the effective settling velocity will be decreased as the direction of the wake and return flow is opposite to the direction of settling velocity.
- Viscosity of the flow: it has been found that the viscosity of the flow will increase with the increase of suspended sediment concentration. Thus the increased viscosity results in a decrease of settling velocities of mud flocs.
- Buoyancy or effective density: the effective density increases with the increase of cohesive sediment concentration, which will result in a larger buoyancy (a smaller effective gravitational force) force acting on the mud flocs. As the terminal settling velocities are calculated from the effective gravitational force and drag force, thus the effective settling velocities of mud flocs will decrease.

Formulae describing the hindered effects

As discussed above, the increase of viscosity with concentration is one of the main factors resulting in hindered effects on settling velocities of mud flocs. The relation between effective viscosity of fluid and suspended matter was first proposed by Einstein (1905):

$$\mu_{eff} = \mu(1+2.5\alpha_s) \tag{2.15}$$

where μ_{eff} is the effective dynamic viscosity of fluid and α_s is the volumetric fraction of sediment.

The Equation (2.15) proposed by Einstein (1905) is for dilute situation. For dense suspension, the calculation of effective dynamic viscosity was proposed by Frankel and Acrivos (1967):

$$\mu_{eff} = 8/9\mu[(\alpha_s^{\max}/\alpha_s)^{1/3} - 1]^{-1} \tag{2.16}$$

in which $\alpha_s^{\max}$ is the sediment volumetric fraction when it reaches maximum packing.

Graham (1981) presented a new model for the calculation of effective dynamic viscosity, the results of which are consistent with Equation (2.15) and Equation (2.16) in dilute and dense concentration respectively:

$$\mu_{eff} = \mu(1+\beta_1\alpha_s) \tag{2.17}$$

in which β_1 is the amplification factor of viscosity and defined as:

$$\beta_1 = \frac{5}{2} + \frac{9}{4}\frac{1}{1+\hat{d}}\left(\frac{1}{2\hat{d}} - \frac{1}{1+2\hat{d}} - \frac{1}{(1+2\hat{d})^2}\right)\frac{1}{\alpha_s} \tag{2.18}$$

where $\hat{d}$ is the non-dimensional intra-particle distance and calculated as:

$$\hat{d} = [1-(\alpha_s/\alpha_s^{\max})^{1/3}]/(\alpha_s/\alpha_s^{max})^{1/3} \tag{2.19}$$

Richardson and Zaki (1954) developed the well-known hindered settling formulae:

$$w_{hin} = w_{s0}(1-C)^{n_{RZ}} \tag{2.20}$$

where w_{s0} is the sediment settling velocity in dilute case, n_{RZ} is an empirical coefficient used to consider the decrease of sediment velocity due to the increase of sediment concentration.

Equation (2.20) can be applied to calculate sand particle settling velocities in suspension. As for cohesive sediment, a modified formula of Equation (2.20) by Mehta (1986) is proposed for mud flocs:

$$w_{hin} = w_{s0}(1-k_1\alpha_s)^{n_m} \tag{2.21}$$

in which n_m is a function of particle Reynolds number.

This model is reanalyzed by Winterwerp and Van Kesteren (2004) and this leads to a new hindered settling Equation (2.22), which has been successfully applied to the modelling of high concentrated cohesive sediment settling process:

$$w_{hin} = w_{s0}\frac{(1-\phi)^{m_1}(1-\alpha_s)}{1+2.5\phi} \tag{2.22}$$

in which ϕ is volumetric concentration of mud flocs and defined as $\phi = C/C_{gel}$ and C_{gel} is the mass concentration of sediment at gelling point, m_1 is a coefficient to account for the non-linearity.

In Equation (2.22), the $1-\alpha_s$ term is used to account for the buoyancy or reduced gravity, the term $1+2.5\phi$ is for the increase of viscosity and the term $(1-\phi)^{m_1}$ is for the

wake or return flow. It should be noted that the volumetric concentration of mud flocs ϕ is used in Equation (2.22) because the cohesive sediment settles as flocs, which is a mixture of sediment and water (Winterwerp and Van Kesteren, 2004). As the value of C_{gel} is crucial and has a large variability for different sediment types, Camenen and Pham van Bang (2011) argued that the definition of $\phi = C / C_{gel}$ maybe not appropriate and the maximum floc volumetric concentration $\phi_{\max}$ is introduced:

$$w_{hin} = w_{s0}(1-\alpha_s)^{nf/2}(1-\phi)^{nf/2-1}(1-\frac{\phi}{\phi_{\max}})^{\phi_{\max}} \tag{2.23}$$

To apply the Equation (2.23), the fractal dimension of mud flocs nf , which varies with floc size (Khelifa and Hill, 2006), and the maximum floc concentration should be specified. Due to the uncertainties and the inherent variability of cohesive sediments, the two variables should be further investigated.

2.1.3 Consolidation process

Consolidation is an important phenomenon of sediment dynamics (see Figure 2.4) which needs to be taken into consideration in cohesive sediment transport models (Hawlader *et al.*, 2008; Winterwerp and Van Kesteren, 2004). Usually two types of consolidation are considered, namely the primary and secondary stages of consolidation. During the primary stage of consolidation, elastic deformation appears on the subsoil. The primary stage of consolidation occurs when the self-weight of sediment exceeds the seepage force, the pore water begins to be expelled out from inside and between the mud flocs, during which sediment flocs get closer. Secondary stage of consolidation begins when the effective stress between sediment particles is larger than zero, which means the

structure residence occurs. Secondary stage of consolidation causes large deformations of the bed. In this section the general theories for self-weight consolidation of cohesive sediment and closures for effective stress and permeability of mud flocs will be reviewed and discussed.

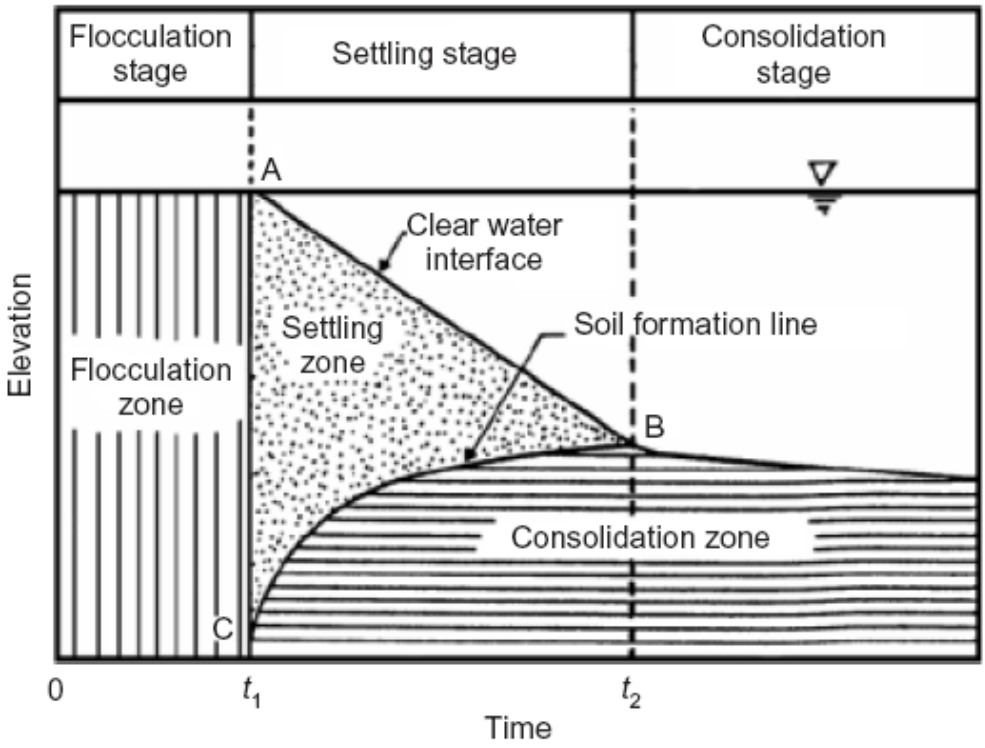

Figure 2.4 General characteristics of sediment dynamics (Imai, 1981)

2.1.3.1 *Self-weight consolidation*

Based on the assumption that the compressibility and permeability is constant during the process of consolidation, Terzaghi established the so-called small strain consolidation theory which is approximately satisfied when applied to the primary stage of one dimensional consolidation of saturated clays. Due to the strict assumption of small strain theory , it was extended to large strain theory by Gibson *et al.* (1967):

$$\frac{\partial e}{\partial t}+(1+e)^2\left(\frac{\rho_s-\rho_w}{\rho_w}\right)\frac{\partial}{\partial z}\left(\frac{k}{(1+e)^2}\right)+\frac{(1+e)^2}{g\rho_w}\frac{\partial}{\partial z}\left(\frac{k}{1+e}\frac{\partial \sigma_e}{\partial z}\right)=0 \tag{2.24}$$

in which e is the void ratio, k is the hydraulic permeability (m/s) and σ_e is the effective stress.

The theory of Gibson *et al.* (1967) has taken both the variations of soil compressibility and permeability into consideration and has been applied to various numerical models (Been and Sills, 1981; Toorman, 1999; Toorman, 1996; Van Bang *et al.*, 2008). Toorman (1996) concluded that though sedimentation and consolidation processes are of interest of different scientific fields, they can be expressed within one united theory:

$$\frac{\partial \alpha_s}{\partial t}=\frac{\partial}{\partial z}\left(w_0\alpha_s+\frac{w_0}{\gamma_s-\gamma_w}\frac{\partial \sigma_e}{\partial z}+D_B\frac{\partial \alpha_s}{\partial z}\right) \tag{2.25}$$

in which γ_w and γ_s are the unit weights of fluid and sediment, D_B is the suspension diffusivity coefficient and w_0 is defined as:

$$\frac{w_0}{\gamma_s/\gamma_w-1}=\frac{k}{1+e} \tag{2.26}$$

The united theory is consistent with chemical and geotechnical models and especially with the equation of Gibson *et al.* (1967).

2.1.3.2 *Closures for effective stress and permeability*

Although various consolidation theories have been established, these equations can only be solved when the closures for effective stress σ_e and permeability k are specified. And the accuracy in predicting the consolidation process of cohesive sediment mostly depends on the appropriate chosen of material functions.

As concluded by Van (2013), the following forms are the typical closure functions for permeability:

$$\begin{cases} k = C_1 e^{C_2} \\ k = C_1 \phi_p^{-C_2} \\ k = \exp(-C_1 + C_2 e) \end{cases} \tag{2.27}$$

where C_1 and C_2 are coefficients, ϕ_p is volumetric concentration of sediment particles.

Closures for effective stress:

$$\begin{cases} e = -C_3 \sigma_e^{C_4} + C_5 \\ \sigma_e = C_3 \phi_p^{C_4} \\ e = C_3 (\sigma_e + C_4)^{-C_5} \\ \sigma_e = \exp(C_5 + C_6 e) \end{cases} \tag{2.28}$$

in which $C_3 - C_6$ are coefficients.

As pointed out by Winterwerp and Van Kesteren (2004), a physical concept is incorporated into the power law type functions which have a larger validity range. Based on the physical concept, these kind of formulae are more popular. For example, Merckelbach and Kranenburg (2004) treated the cohesive sediment bed as accumulated

by mud flocs and established the relationships of effective stress and permeability, which were expressed as the functions of sediment fraction and fractal dimension:

$$k = C_1 \alpha_s^{-2/(3-nf)} \tag{2.29}$$

$$\sigma_e = C_3 \alpha_s^{2/(3-nf)} \tag{2.30}$$

However, the proposed model have two severe limitations (Chauchat *et al.*, 2013):

- When the sediment concentration approaches zero, an infinite permeability k is obtained through Equation (2.29). In fact, a finite and constant value should be obtained for permeability k.
- The effective stress appears only when the sediment concentration exceeds a critical value that can allow the formation of networks for sediment flocs. When the sediment concentration is lower than the critical value, the networks do not exist and the effective stress vanishes.

To overcome the limitations mentioned above, Chauchat *et al.* (2013) presented new formulae for effective stress and permeability:

$$k = w_s / [\alpha_s (\rho_s / \rho_f - 1)] \tag{2.31}$$

$$w_s = \begin{cases} w_0 (1-\alpha_s)^{nf/2} (1-\phi)^{nf/2-1} (1-\dfrac{\phi}{\phi_{\max}}), \alpha_s \le \dfrac{\alpha_s^{gel}}{\chi} \\ w_s^{gel} (\dfrac{\chi \alpha_s}{\alpha_s^{gel}})^{-2/(3-nf)+1}, \alpha_s > \dfrac{\alpha_s^{gel}}{\chi} \end{cases} \tag{2.32}$$

in which w_s is empirical settling velocity near the bed including the hindered settling effects. The value of $\phi_{\max}$ corresponds to the gelling fraction α_s^{gel}, and χ is a coefficient. w_s^{gel} equals w_s when $\alpha_s = \alpha^{gel}$. ρ_f is the density of mud flocs.

$$\sigma_e = \begin{cases} 0, \alpha_s < \alpha_s^{gel} \\ \sigma_0[(1-\frac{\alpha_s - \alpha_s^{gel}}{\alpha_s^{\max}})^{-2/(3-nf)} - 1], \alpha_s \geq \alpha_s^{gel} \end{cases} \tag{2.33}$$

where $\alpha_s^{\max}$ and σ_0 are coefficients need to be calibrated.

The main processes of sediment dynamics (flocculation, settling/hindered settling, and consolidation) are introduced. In the current research, all the processes mentioned above will be implemented into the presented two-phase model (Chapter 4). The interaction between sediment and fluid is also very important and incorporated into the two-phase model as well.

It should be mentioned that another important process of sediment dynamics is sediment erosion. On the bottom bed which consists of cohesive sediment, a lot of pollutants such as organic materials, heavy metals accumulate. Thus the knowledge on the erosional process is essential for the management of water quality (De Sutter *et al.*, 1999). Furthermore, the erosion process controls the amount of sediment mass suspended in the water column in some coastal waters, the cohesive sediment transport cannot be accurately predicted without fully understanding the erosion process of cohesive sediment (Hir *et al.*, 2008; Jacobs *et al.*, 2011; Thomsen and Gust, 2000; Whitehouse *et al.*, 2000). Partheniades-Krone formulation was adopted by van der Ham and Winterwerp (2001) to simulate the erosion process of EMS/Dollard estuary. In the current study

Partheniades-Krone formulation is incorporated into the two-phase model to study the erosion process of EMS/Dollard estuary. Then it is also modified and applied to Yangtze River.

2.2 Numerical studies on the cohesive sediment transport

The cohesive sediment dynamics are comprehensively reviewed in Section 2.1 and the numerical studies on the cohesive sediment transport are reviewed in this Section in order to establish the current knowledge about cohesive sediment transport.

2.2.1 Single-phase models

The single-phase models have been widely applied to the study of cohesive sediment transport in estuaries, lagoons and coastal waters (Lopes *et al.*, 2006; Lumborg and Pejrup, 2005; Maggi *et al.*, 2007; Spearman *et al.*, 2011; van der Ham and Winterwerp, 2001). In the single-phase models, the horizontal momentum equation can be written as (van der Ham and Winterwerp, 2001):

$$\frac{\partial \overline{U}}{\partial t}+\frac{1}{\rho_{mix}}\frac{\partial \overline{P}}{\partial x}=\frac{\partial}{\partial z}((\nu+\nu_T)\frac{\partial \overline{U}}{\partial z}) \tag{2.34}$$

where $\overline{U}$ is ensemble mean velocity in the horizontal direction, ρ_{mix} is fluid bulk density. ν_T is eddy viscosity respectively. $\frac{\partial \overline{P}}{\partial x}$ is horizontal pressure gradient in the x direction.

As the 1DV single-phase model is driven by measured depth averaged and time varying velocityU_m, to solve Equation (2.34), the calculated depth averaged velocity U_d is adjusted to equal as U_m:

$$\frac{1}{\rho_{mix}}\frac{\partial \overline{P}}{\partial x} = -\frac{\tau_b}{\rho_{mix} h} + \frac{U_d - U_m}{T_{rel}} \tag{2.35}$$

where h is the water depth and T_{rel} is a relaxation time, τ_b is the bed shear stress.

The balance equation of sediment concentration can be written as (Spearman *et al.*, 2011):

$$\frac{\partial \overline{C}}{\partial t} = \frac{\partial}{\partial z}(\Gamma_T \frac{\partial \overline{C}}{\partial z} + w_s \overline{C}) \tag{2.36}$$

where Γ_T is eddy diffusivity.

The single-phase models have been extensively applied to model the cohesive sediment transport processes. A 1DV sediment transport model was developed by *Teisson et al.* (1992) to study the vertical distribution of suspended sediment concentration by considering the interactions between fluid and sediment, while the hindered settling effects were not incorporated into the model. A Reynolds stress turbulence model was introduced to study the buoyancy effects through a sediment induced buoyancy term included in the vertical stress equations. The model results showed that the flow structure was altered and the bed shear stress was reduced due to the existence of cohesive sediment even at very low concentration of 1 kg/ m^3 .

Kranenburg (1998) carried out a simulation of sediment transport in the saturation concentration which means the settling of particles are counteracted by turbulence and the vertical sediment flux equals to zero. The model was developed based on the Prandtl-mixing theory and used a modified turbulence damping functions by extending the Monk-Anderson damping equations. With the derived damping functions introduced, Kranenburg (1998) concluded that a stronger damping effects for increasing gradient

Richardson number and a better agreement with the field measurements were obtained compared to other functions . It has been stressed that it is not recommended to replace the standard $k-\varepsilon$ model with the new derived damping model, because it may not so generally applicable.

A more comprehensive study on the interaction of turbulence and suspended sediment was carried out by Toorman *et al.* (2002). The full hydrodynamic equation and sediment balance equation are solved and implemented with Prandtl mixing length and standard $k-\varepsilon$ turbulence model. In terms of the high order turbulence model such as Reynolds stress model, Toorman (2002) argued that no better results are predicted but at a higher calculation cost.

The model results showed that the introduced buoyancy effects explained the decrease of Von Karman constant. And the dissipation is very strong around the lutocline and near the bottom, according to which a more comprehensive two layer approach was recommended by Toorman *et al.* (2002).

van der Ham and Winterwerp (2001) reported their simulations of cohesive sediment transport in the Ems-Dollard estuary with a $k-\varepsilon$ turbulence model. In their work, the flocculation process was simulated using Equation (2.1) and (2.2), the sediment availability was introduced by limiting the depth-averaged sediment concentration $\overline{C}$ less than the maximum depth-averaged sediment concentration of $\overline{C}_{\max}$. A buoyancy destruction of turbulent kinetic energy term was included in the transport equation of turbulent kinetic energy k .

The results indicated that the buoyancy effects can results in the rapid decrease of sediment concentration close to the slack water. Due to the availability of sediment, the

increase of sediment concentration stops before the maximum current velocity is reached. The results also showed that the consideration of flocculation process is of little use, which is not consistent with observations in the Ems/Dollard estuary that the flocculation process is important in the formation of floc sizes/settling velocities and thus the cohesive sediment transport process (Van der Lee, 2000; van Leussen, 1999, 2011).

Later, Winterwerp (2002) presented a three dimensional model to study the variation of settling velocity and floc size at estuaries. In this study, both the flocculation and hindered settling models (Equation (2.22) are implemented into the model. It was concluded that the observed features cannot be properly simulated using a constant settling velocity because of the flocculation process. Due to the temporal variation of floc size and settling velocity, the gelling concentration varies over a large range and thus the concentration of fluid mud layers.

To specify the flocculation process on the transport of cohesive sediment transport, Son and Hsu (2011) applied a 1DV model to simulate the SSC at Ems/ Dollard Estuary. The extended flocculation model based on the semi-empirical lagrangian flocculation model developed by Winterwerp (1998), which can quantitatively predict the floc sizes (Figure 2.5) and settling velocities, are incorporated into 1DV model. The effects of flocculation efficiency, turbulence shear rate, SSC and yield stress of flocs are taken into consideration in the flocculation model.

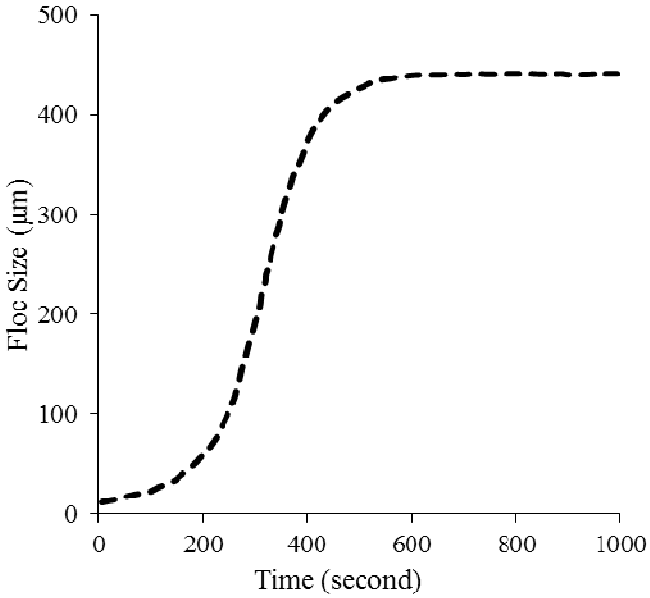

Figure 2.5 Temporal evolution of floc size predicted using flocculation model of Son and Hsu (2009).

The models results capture the essential features of cohesive sediment transport observed at Ems/Dollard Estuary. However, the model results agrees less favorably with field measurements than the results from van der Ham and Winterwerp (2001). The calculated SSC at 0.7 m and 0.3 m above the bed are both less than the field measurements. Also, it has been observed that a time lag exists between the flow velocity and sediment concentration (Dyer et al., 2000; van Leussen, 1999, 2011), which is explained as the erosion/deposition features in Ems. However, the time lag disappears in the model results of Son and Hsu (2011), as the calculated SSC peaks always appear earlier than measurements. This may because the complex flocculation model, though takes variable other effects into consideration, may not address the main factors such as SSC controlling the flocculation process. As it has been found by Van der Lee (2000) that the floc sizes and settling velocities correlate with suspended sediment concentration on a tidal time scale at the Ems/Dollard estuary.

Son and Hsu (2011) also investigated the effects of erodibility on the cohesive sediment transport and suggested that it is essential to adopt the variable critical shear stress, which is related to eroded sediment mass M_s (Equation (2.37)), when calculating upward sediment flux E_s.

$$E_s = \mathrm{Max}[\beta_e(\frac{\tau_b}{\tau_c(M_s)} - 1), 0] \tag{2.37}$$

$$\tau_c = \alpha_1^{'}(M_s - \alpha_2^{'})^{\alpha_3^{'}} \tag{2.38}$$

where β_e is an empirical erosion flux coefficient and M_s is eroded sediment. $\tau_c(M)$ is critical shear stress calculated by Equation (2.38). $\alpha_1^{'}$, $\alpha_2^{'}$ and $\alpha_3^{'}$ are coefficients.

These single-phase models are based on the assumption of sediments being passive scalar and following the movement of fluid flow with negligible inertia effects (Nguyen *et al.*, 2009). Although acceptable predictions using this type of single-phase models have been reported for specific problems, their representation of the actual physical processes is rather crude. For example, the impact of suspended sediment on flows and particle-particle interactions is often ignored (Nguyen *et al.*, 2009). To describe the sediment settling velocity, which is the key variable in understanding the cohesive sediment transport process and cannot be calculated directly, site-specific model parameters have to be adopted in the models (Camenen and Pham van Bang, 2011). The settling velocity of the flocs generally depends not only on the floc size and floc density but also on the concentration. To account for different settling regimes such as flocculation and hindered settling regimes, different empirical formulae are used and thus a large amount of calibration work needs to be done in order to determine the empirical coefficients.

Furthermore, the cohesive sediment depostion and erosion occurs at the surface of the bed where usually a layer of fluid mud is formed (McAnally *et al.*, 2007). Sediment processes such as sedimentation and consolidation occur within this layer. Since the consolidation process can not be included in the single-phase models, an assumption of a fictive bed should be made to define the calculation domain. To simulate the cohesive seidment transport proceses from the surface of water columm to the 'real bed', where the bed is under the fluid mud, well consolidated and difficult to be eroded, these single-phase models should be coupled with models for settling and consolidation bed which is available from Winterwerp and Van Kesteren (2004).

2.2.2 Two-phase models

Models for sediment transport are basically classified into two groups, namely, single-phase model and two-phase model. Recently the two-phase models are becoming more and more popular in the research of sediment transport. In such models, the continuity equations and momentum equations for both phases (fluid and solid phase) are solved separately. In this section, two-phase models used in the simulation of cohesive sediment transport are comprehensively reviewed to prepare for the development of two-phase model in the current dissertation.

For 1DV two-phase models, the continuity and momentum equations for solid phase and fluid phase are derived separately by averaging the local instantaneous conservation equations. The continuity equation for both phases can be written as (Dong and Zhang, 1999):

$$\frac{\partial \rho_k \alpha_k}{\partial t} + \frac{\partial \rho_k u_{kj}}{\partial x_j} = \frac{\partial \rho_k \overline{\alpha_k' u_{kj}'}}{\partial x_j} \tag{2.39}$$

where k is the solid or the fluid phase, x_j (j=1,2,3) is the Cartesian coordinate system, α_k, ρ_k, u_{kj} and p_k are the volumetric concentration, density, velocity vector and pressure of phase k ,respectively.

The momentum equation for both phases is:

$$\frac{\partial \rho_k \alpha_k u_{ki}}{\partial t} + \frac{\partial \rho_k \alpha_k u_{ki} u_{kj}}{\partial x_j} = -\rho_k \alpha_k g \delta_{i2} - \alpha_k \frac{\partial p_k}{\partial x_i} + \frac{\partial T_{ij}}{\partial x_j} - f_i \tag{2.40}$$

where f_i is the momentum transferred between fluid and solid phase. T_{ij} is stress tensor, and δ_{ij} is the Kronecker delta.

Two-phase models have been widely applied to the study of non-cohesive sediment transport (Amoudry et al., 2005; Amoudry, 2008; Hsu et al., 2004; Hsu et al., 2003; Liu and Sato, 2005; Villaret and Davies, 1995) and recently more and more two-phase models are applied to the simulation of cohesive sediment transport processes (Chauchat and Guillou, 2013; Safak *et al.*, 2010). Teisson *et al.* (1992) is probably the first to apply a two-phase model in cohesive sediment study and focused on the two way coupling between suspended sediment and fluid, namely, how the cohesive sediment alters the flow features and vice versa how the flow influences the settling process of sediment. It was concluded that with the two-phase fluid approach, the calculation domain of the model can be applied from the water surface to the bed without considering the interface between water and sediment bed in particular.

Hsu (2003) developed a two-phase model to calculate the dilute sediment

concentration and velocity profiles. The results were compared to the lab experiments carried out in a steady and uniform open channel. The turbulent energy was modeled using a standard $k-\varepsilon$ model, in which the dissipation of turbulence, due to the presence of suspended sediment was accounted. With the two-phase approach, the fluid turbulence damping was identified which is caused by the drag between sediment and fluid. Furthermore, the decrease of Von Karman parameter or the Prandtl mixing length can be explained.

Recently, a 2-D vertical two-phase model has been applied to simulate the turbidity maximum in Seine estuary (Chauchat *et al.*, 2009). From the model results, a layer of high concentrated fluid mud was identified and the advantage of using a two-phase model for sediment transport was illustrated. The two-phase model allows the modelling domain can be applied from bottom of the bed to the water surface and most of the settling processes of cohesive sediment are included (see Figure 2.6).

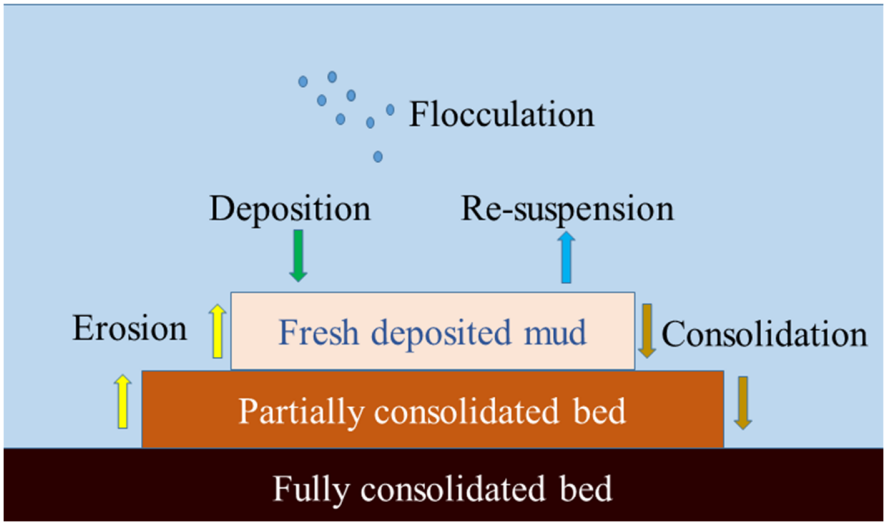

Figure 2.6 The settling processes of cohesive sediment (Leupi, 2005)

Son and Hsu (2011) applied a simplified 'two-phase' model (in fact it is a single-phase model) to study the resuspension of cohesive sediment in which the flocculation

process is modelled through linearly combining the aggregation and break up processes. Their results showed that the mud flocs settling processes were much better predicted when flocculation process was incorporated into the sediment transport model. More realistic properties of mud flocs are accounted using variable fractal dimensions and yield strenghts to describe the flocculation process.. However, a notable drawback in the model is that the settling velocity of mud flocs is calculated using empirical equations rather than directly calculated based on an adopted mechanism (Zhang and Dong, 2000).

Chauchat *et al.* (2013) presented a 1DV two-phase model to simulate the sedimentation-consolidation processes for both non-cohesive sediment and cohesive sediment. However, horizontal velocity and sediment processes such as hindered settling and consolidation processes were not taken into consideration. Though the model results showed a good agreement with lab measurements, the proposed source term for effective stress is only the function of concentration and loses sight of the history effects of aggregate structure evolution. Also a constant fractal dimension was adopted to describe the structure of mud flocs, which is not appropriate.

Overall, the two-phase approach allows the modelling domain covers from the suspension surface to the bottom bed and has a major advantage when compared to the model of Kynch (1952) or Gibson *et al.* (1967). Furthermore, this work provided a framework for the study of sedimentation of mud flocs in coastal waters.

Most two-phase models focused on the settling processes of mud flocs and interactions between fluid and suspended sediment. Safak *et al.* (2010) adopted the two-phase model, which was presented by Hsu *et al.* (2009), for the study of coupling of mud flocs and near bed wave-current generated turbulent flows. The model results indicated

that the turbulence dissipation caused by density effects is important when calculating the kinetic energy equation. The gradient Richardson number decreased significantly within the wave boundary layer.

2.2.3 On the necessity of two-phase model development

For single-phase models, one of the most important advantages is that they can provide acceptable results in some circumstances less computer calculation (Nguyen *et al.*, 2009). Sediment-fluid interaction, inter-particles interaction and fluid-bed interaction are important but are difficult to be implemented into the single-phase models. When doing cohesive sediment transport simulation with low sediment concentration, the inter-particle stresses and sediment-fluid interaction can be neglected (Lopes *et al.*, 2006; Lumborg, 2005). When sediment availability is limited, a fictive bed, which cannot be eroded, can be assumed to avoid the fluid-bed interaction (Spearman *et al.*, 2011). The results predicted by single-phase models may perform adequately compared to two-phase models. When dealing with the problems of high-concentrated cohesive sediment transport in estuaries such as Yangtze River Estuary, where a layer of fluid mud should be considered, a two-phase model should be used.

As discussed above, a number of two-phase models have been developed, some of which are specially designed for modelling mud sedimentation dynamics (Boulton *et al.*, 2006; Chauchat *et al.*, 2013; Hsu *et al.*, 2007; Nguyen *et al.*, 2009). The theoretical soundness and predictive capability of these models have been shown for various flow conditions. However, due to the lack of detailed data, two-phase mud flow models have largely been applied to or validated against laboratory measurements in simple settling tank or open channel experiments (Chauchat and Guillou, 2013; Chauchat *et al.*, 2013;

Torres-Freyermuth and Hsu, 2010) or limited field measurements of concentration change over a relatively long time scale (Son and Hsu, 2011).

In the current dissertation, the sediment suspension in Ems/Dollard Estuary and sedimentary processes on an erosional mudflat at Yangtze River Delta will be studied. The Ems/Dollard Estuary is ebb current dominate (Dyer *et al.*, 2000; Talke and de Swart, 2006). Flocculation process is observed and is important in determining floc sizes, settling velocities and the cohesive sediment transport in Ems/ Dollard estuary (Van der Lee, 2000; van Leussen, 1999, 2011). However, the model results calculated from van der Ham and Winterwerp (2001) show that the flocculation process hardly influences the suspended sediment distribution in the water column. This may be because the improper coefficients were selected for the empirical-formulae to calculate settling velocities in single-phase model.

In terms of the mudflat at Yangtze River Delta, though located in the transition zone between Yangtze Estuary and Hangzhou Bay, the coastal evolution is governed by Yangtze River. The surface suspended sediment concentration at Luchaogang ranges from < 0.1 kg/m^3 to > 2 kg/m^3 (Zhu *et al.*, 2014), which means sediment processes such as flocculation, hindered settling and inter-particle stresses should be included in the numerical model. Seasonal bed level change is up to 40 cm , which indicates that a strong fluid-bed interaction occurs on this mudflat. Furthermore, the mudflat evolution is under the combined action of strong tidal currents and waves, which will further complicate the sediment processes.

To study the sedimentary processes in areas mentioned above, a two-phase model is developed in Chapter 4. In the two-phase model, most of the important sediment

processes including hindered settling, fluid-mud interactions and especially the flocculation process, which has not been considered in other two-phase models, are incorporated. Essential forces such as inter-particle stresses and shear stresses under combined waves and currents are included. The source term of fluid stress in horizontal direction is modified to account for the turbulence dissipation caused by cohesive sediment, especially the fluid mud. The two-phase model will be validated and applied to field measurements in Chapter 5.

Chapter 3 A dynamic model for coastal mud flocs with distributed fractal dimension

In this chapter, a flocculation model is developed based on the normal distribution of fractal dimension of mud flocs. As the flocculation process has been comprehensively reviewed in Chapter 2, here only references related to the development of flocculation model are introduced to specify the knowledge gaps and explain the necessity of developing the new flocculation model.

3.1 Introduction

Cohesive sediment transport in estuaries and coastal areas is one of the most important processes controlling their morphological evolution. An accurate determination is required for the settling velocity of the material in suspension in order to predict the transport of cohesive sediments. Different from the sands and gravels, whose physical properties such as shape, density and particle size are relatively constant and the settling velocities can be estimated fairly accurately using various empirical formulae, muddy sediments appear as flocs in suspension due to flocculation process (Son and Hsu, 2011; Spicer and Pratsinis, 1996; Winterwerp, 2002). The transport process of cohesive sediment is significantly affected by flocculation during which the slowly sinking primary particles aggregate and form large, rapidly sinking flocs (Winterwerp, 1998). The dynamical and physical properties of mud flocs are completely changed and further the sedimentation, consolidation and resuspension processes of cohesive sediment will be significantly affected.

In recent years, considerable efforts have been made to study the flocculation processes and quantify floc properties through either laboratory experiments or theoretical models (Biggs and Lant, 2000; Keyvani and Strom, 2014; Lee *et al.*, 1994; McAnally and Mehta, 2000; Son and Hsu, 2009; Winterwerp, 1998). To better understand the coupled effect of suspended particle mass concentration and turbulence on flocculation, field measurements were also carried out on muddy estuaries and shelves (Safak *et al.*, 2013). Mud flocculation under different shear intensities was investigated and significant sediment supply associated with high level turbulence shear was suggested as a main cause for the breakup of macroflocs. To investigate the effect of multiple shear cycles on the equilibrium flocs size, Keyvani and Strom (2014) conducted laboratory experiments using a mixture of sediment containing 80% kaolinite and 20% montmorillonite. Their results showed that the equilibrium flocs size only depends on shear intensity.

Treating flocs as self-similar fractal entities (see Figure 3.1) requires the determination of the fractal dimension as it will affect the calculation of the effective density of flocs and settling velocity. Based on the constant fractal dimension assumption, Winterwerp (1998) developed a flocculation model by linearly combining aggregation and break-up processes. Although describing all flocs with a single fractal dimension is convenient for calculation, it is inadequate to represent the complex geometry of mud flocs formed under varying shear and concentration conditions. Martinis and Risovic (1998) suggested that the value of fractal dimension decreases from 3 to 1.2 when diameters of cohesive sediments increase from small particles to large aggregates. The experimental results by Dyer and Manning (1999) showed that the flocs geometry can

only be well described using fractal dimensions ranging from 3 to 1 instead of an optimal fixed value 2. Many other researchers also concurred that fractal dimensions are not constant under different flow conditions, for different floc sizes and aggregation mechanisms (Khelifa and Hill, 2006, Maggi *et al.*, 2007, Vahedi and Gorczyca, 2011).

To predict the settling velocity and effective density of flocs, Khelifa and Hill (2006) processed a large number of data sets involving flocs ranging from 1.4 to 25500 μm and found that a power law distribution of fractal dimension can fit data and predict the mean value of the settling velocity with large data scatter. This is because in reality, a range of settling velocities can usually be found for any given floc size as shown in many field measurements (Dyer and Manning, 1999; Gibbs, 1985; Sternberg, Berhane and Ogston, 1999). Because the structure of muddy flocs was different and so was the effective density. To account for the large range of settling velocities for the same sized flocs, Vahedi and Gorczyca (2012) suggested that multiple exponents should be used to predict the settling velocity. In their study, a normal distribution of fractal dimensions is assumed and the results agree well with experimental measurements data. One floc size with multiple fractal dimensions may have multiple yield strengths which will strongly influence the break-up process of flocculation. Son and Hsu (2009) improved the existing flocculation model by taking into the consideration of variable fractal dimension suggested by Khelifa and Hill (2006) and provided the expression for variable yield strengths of flocs.

The aim of this Chapter is to improve the description of floc properties and develop a time-dependent flocculation model by taking into consideration the distributions of fractal dimensions and yield strengths. The model developed will be limited to the effect

of turbulent shear as among the three mechanisms, those are known to affect the flocculation process, i.e. Brownian motion, turbulent shear and differential settling, the turbulence shear effect is usually dominant in coastal environment (Lee *et al.*, 2011; Winterwerp, 1998). The model has been validated against available experimental data.

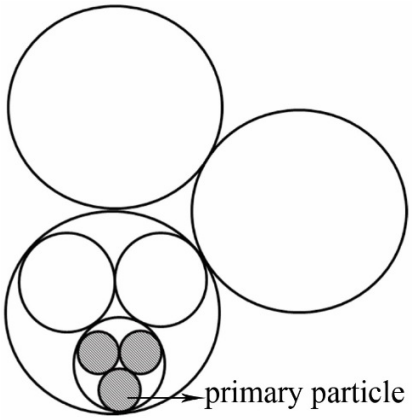

Figure 3.1 Virtual structure of mud flocs which are treated as the self-similar fractal entities. The two-dimensional fractal dimension of the presented flocs is $nf = 1.43$

3.2 Research methods

The formation and deposition of mud flocs in estuaries and coastal waters is an unsteady process as floc size, density and settling velocity can all vary with time and are critically dependent on the distribution of fractal dimensions of the flocs. Therefore, in formulating the present floc model, fractal dimensions of flocs, settling velocity, and floc development addressing flocculation and break up processes are treated separately as described below.

3.2.1 Fractal dimensions of flocs

To reflect the fact that the fractal dimension of mud flocs are generally not constant but distribute over a certain range, we assume fractal dimension for a given floc size class

D to be normally distributed as suggested by Vahedi and Gorczyca (2012):

$$P(nf)_D = \frac{1}{\sqrt{2\pi}\sigma_D}\exp(-\frac{(nf-\mu_D)^2}{2\sigma_D^2}) \tag{3.1}$$

where μ_D and σ_D are the mean and standard deviation of nf, respectively.

For flocs in size class D, the mean value of fractal dimension μ_D should be determined first. Vahedi and Gorczyca (2011) divided flocs into large groups (>50 μm) and small groups (<50 μm) and within each group a linear relationship is used to represent the variation of mean fractal dimension with floc size. Khelifa and Hill (2006) suggested that the fractal dimension of floc will decrease as the floc size increases and the mean fractal dimension value is calculated using a power law of the ratio between floc size D and primary particle size d. This relationship is adopted in the present study which is:

$$\mu_D = \alpha(\frac{D}{d})^{\beta} \tag{3.2}$$

where α and β are empirical coefficients and equal to 3 and $\log(F_c/3)/\log(D_c/d)$ respectively in which D_c is a characteristic size of flocs and set to be 2000 μm and F_c is a characteristic fractal dimension and is set to be 2 (Khelifa and Hill, 2006).

As to the standard deviation σ_D, it needs to reflect the variation range of fractal dimensions in the available data. Due to the differences in aggregation mechanisms, the fractal dimension values around 1.8-1.9 are reported for cluster-cluster aggregation; 2.5-2.51 for Brownian flocculation; 1.6-2.2 for diffusion-limited colloidal aggregation and 1.8-2.1 for reaction-limited colloidal aggregation (Maggi *et al.*, 2007; Meakin, 1983; Risović and Martinis, 1996). For inorganic flocs, the values determined by Li and

Ganczarczyk (1989) are in the range of 1.59-2.85. For very fragile flocs, the values are found to be around 1.4 or lie between 1.52-1.72 (Dyer and Manning, 1999; Li and Logan, 1995). Based on these results, the fractal dimension can be taken as falling within [1.6 2.4] for large fragile flocs, whereas it is very close or equal to 3 for small particles. Therefore, the standard deviation of fractal dimension should range from zero ($\sigma_D = 0, D = d$) for primary particles (smallest) to a value appropriate for larger fragile flocs. In the literature, both a logarithmic and a linear increase of the variance of fractal dimension are discussed by Vahedi and Gorczyca (2012). As the logarithmic increase of the variance of fractal dimension is physically more realistic than the linear one, it is adopted here:

$$\sigma_D = \alpha_1 \ln(D / d) \tag{3.3}$$

in which α_1 is an empirical coefficient. σ_D is zero when the floc size approaches d, the size of the primary particle. When the floc size becomes D_c the fractal dimension is specified to be within the range of [1.6, 2.4]. For a normal distribution the probability within plus and minus 4 times σ_D, $P(\mu - 4\sigma < x < \mu + 4\sigma)$, is more than 99.9%. We can thus estimate the standard deviation ($\sigma_{D=D_c}$) according to the suitably prescribed characteristic floc size D_c as $\sigma_{D=D_c}$ = (2.4-1.6)/8=0.1. α_1 can be easily determined as $\alpha_1 = \sigma_{D=D_c} / \ln(D_c / d)$.

3.2.2 Settling velocity

According to previous investigations (Kranenburg, 1994; Winterwerp, 1998), the relationship between effective density and fractal dimension of a single floc is given by:

$$\rho_f - \rho_w = (\rho_s - \rho_w)(\frac{D}{d})^{nf-3} \tag{3.4}$$

Based on Stokes Law, Winterwerp (1998) obtained the settling velocity expression Equation (2.13) on the basis of balancing drag and gravitational forces and incorporating Equation (3.4), for simplicity the equation is rewritten here as:

$$w_s = \frac{f_s}{18} g \frac{\rho_s - \rho_w}{\mu} \frac{D^2}{1 + 0.15\,\mathrm{Re}^{0.687}} (\frac{D}{d})^{nf-3} \tag{3.5}$$

As the fractal dimension is now considered to decrease with the increase of floc size, according to Equation (3.2), the relationship between the floc density and mean value of fractal dimension can be determined as:

$$\begin{cases} \Delta\rho = \rho_f - \rho_w = (\rho_s - \rho_w)(\frac{D}{d})^{nf-3} \\ nf = \mu_D = \alpha(\frac{D}{d})^{\beta} \end{cases} \tag{3.6}$$

where $\Delta\rho$ is the effective density. Combining Equations (3.5) and (3.6) leads to the new settling velocity equation:

$$\begin{cases} w_s = \frac{f_s}{18} g \frac{\rho_s - \rho_w}{\mu} \frac{D^2}{1 + 0.15\,\mathrm{Re}^{0.687}} (\frac{D}{d})^{nf-3} \\ nf = \mu_D = \alpha(\frac{D}{d})^{\beta} \end{cases} \tag{3.7}$$

Vahedi and Gorczyca (2012) calculated the settling velocities with a power law variation for mean and a logarithmic variation for the standard deviation of the normal distribution. The results of calculated settling velocities fitted well with the data collected for the settling velocities of lime softening flocs.

Inspired by this work, the distribution of fractal dimension is incorporated in calculating the excess density of mud flocs in this study. Different from the Vahedi and Gorczyca (2012) model in which scatters of settling velocities for floc size class D were randomly generated, Equation (3.8) is used in the current study to take account the effects of distribution of fractal dimension. The advantage of this approach is that it is easier to be incorporated into sediment transport models and it is also more representative in calculating the effective density with Equation (3.8) instead of Equation (3.4). The effective (or mean) density of mud flocs $\Delta\rho_e$ for a given floc size class D is calculated by:

$$\Delta\rho_e = \rho_f - \rho_w = (\rho_s - \rho_w)\int_{\mu_D-4\sigma_D}^{\mu_D+4\sigma_D} (\frac{D}{d})^{nf-3} \frac{1}{\sqrt{2\pi}\sigma_D} \exp(-\frac{(nf-\mu_D)^2}{2\sigma_D^2}) dnf \tag{3.8}$$

Replacing $\Delta\rho$ in Equation (3.6) with $\Delta\rho_e$ given by Equation (3.8) leads to the mean settling velocity for floc size class *D*:

$$w_s = \frac{f_s}{18\mu} g \frac{D^2 \Delta\rho_e}{1+0.15\,\mathrm{Re}^{0.687}} \tag{3.9}$$

Equation (3.5) clearly shows that w_s increases with nf but now nf can have values within the interval $[\mu_D - 4\sigma_D, \mu_D + 4\sigma_D]$. To illustrate the settling velocity distribution more clearly, two boundary lines corresponding to the upper and lower limits of nf are calculated instead of generating random scatter points, as:

$$w_{s_{up}} \quad when \quad nf = \mu_D + 4\sigma_D = \alpha(\frac{D}{d})^{\beta} + 4\sigma_D \tag{3.10 a}$$

$$w_{s_{low}} \quad when \quad nf = \mu_D - 4\sigma_D = \alpha(\frac{D}{d})^{\beta} - 4\sigma_D \tag{3.10 b}$$

Figure 3.2 shows the calculated results as compared with field and laboratory data

collected by Khelifa and Hill (2006) from various sources. The middle line is calculated with Equation (3.9) while the upper and lower lines are calculated with Equations (3.10a) and (3.10b) respectively. As the large flocs are very fragile and few data points can hardly represent the true distribution of settling velocities we have limited our study on the floc size less than 2100 μm for the largest floc size classes. It is of interest to note that the data points within the boundary lines are not evenly distributed with most being gathered around the middle line and the data points become sparser when approaching to the boundary lines.

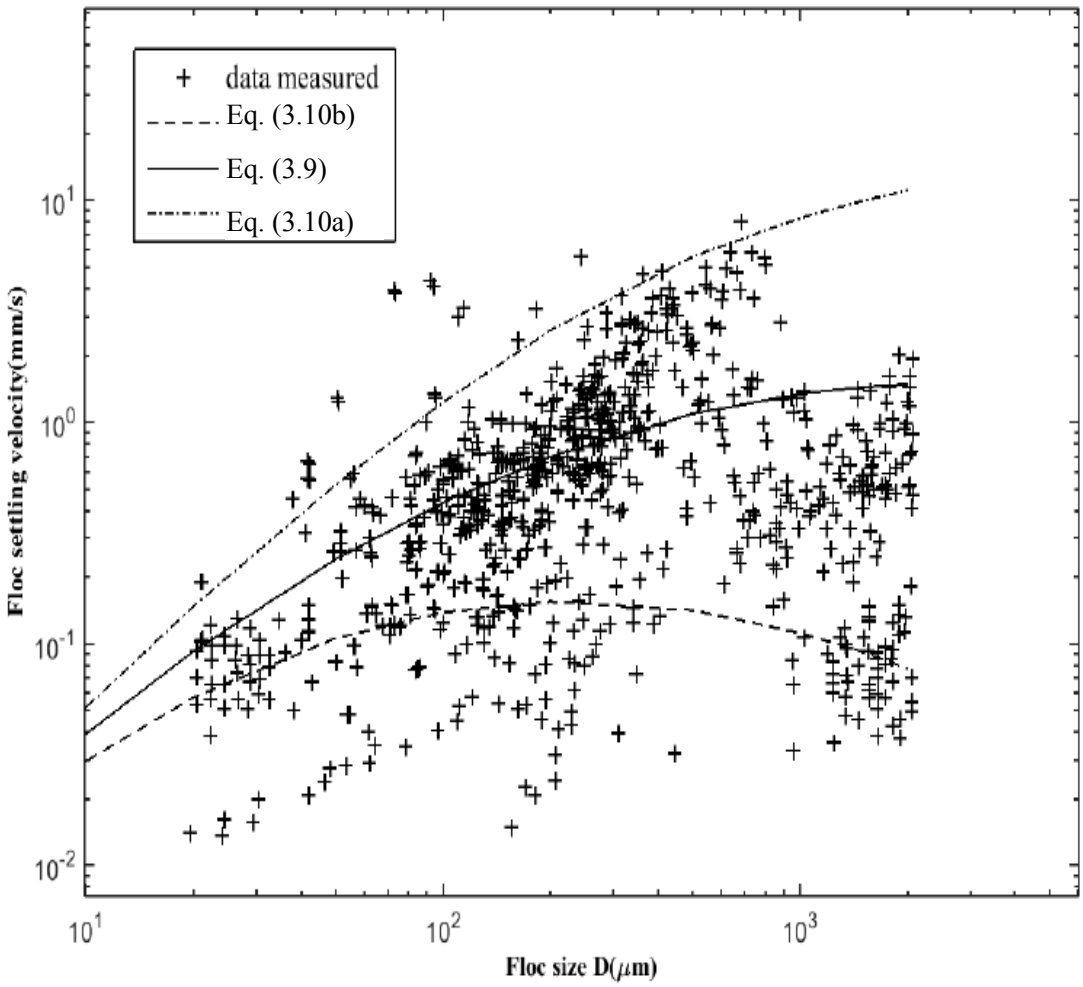

Figure 3.2 The middle line is calculated with Equation (3.9) which is based on a normal distribution of fractal dimension for each floc size class D. The upper and lower lines are calculated with Equations (3.10a) and (3.10b) respectively. The data are collected by Khelifa and Hill (2006) from various sources and in the predicted floc size is limited to less than 2100 μm

3.2.3 Floc development model

Following Winterwerp (1998), the relationship between the volumetric concentration, mass concentration C and the number of flocs per unit fluid volume n is taken as:

$$\phi = \left(\frac{\rho_s - \rho_w}{\rho_f - \rho_w} \right) \frac{C}{\rho_s} = f_s n D^3 \tag{3.11}$$

Levich (1963) deduced the particles flocculation rate due to flow turbulence by integrating the diffusion equation over a finite volume:

$$\frac{dn}{dt} = -\frac{3}{2} e_c \pi e_d G D^3 n^2 \tag{3.12}$$

As discussed by Lick *et al.* (1992) e_c is a function of floc size and floc density and is difficult to be determined. Therefore e_c is assumed to be constant for simplicity. As $\alpha = 3$, dn/dD can be derived as the following from Equations (3.2), (3.4) and (3.11):

$$\frac{dn}{dD} = -\frac{3C}{\rho_s f_s} d^{nf-3-\beta} D^{-nf-1+\beta} (\beta \ln \frac{D}{d} + 1) \tag{3.13}$$

Combining Equations (3.12) and (3.13) gives:

$$\frac{dD}{dt} = \frac{C e_c \pi e_d}{2 \rho_s f_s} G d^{nf-3+\beta} D^{-nf+4-\beta} \frac{1}{\beta \ln(D/d) + 1} \tag{3.14}$$

In describing the floc breakup process, the flocs size is assumed small enough so that the effects of inter-particle collisions on flocs break-up can be ignored and only the effects due to turbulent shear are taken into account. Based on dimensionless analysis, Winterwerp (1998) suggests that the floc break-up process has a relationship with floc size, D, the floc yield strength τ_y and dissipation parameter G:

$$\frac{dn}{dt} = n e_b G a (\frac{D-d}{d})^p (\frac{\tau_t}{F_y})^q \tag{3.15}$$

where τ_t is the shear strength due to turbulence. F_y is floc yield strength. In the analysis

of Winterwerp (1998), F_y is regarded as a constant. The values of p=1 and q=0.5 suggested by Son and Hsu (2009) and Winterwerp (1998) are used in this study.

By assuming that the floc yield strength is a function of the number of primary particles and the cohesive force of each particle in the rupture plane, the following equation is proposed (see more details in Son and Hsu (2009)).

$$F_y = B_1(\frac{D}{d})^{2nf/3} D^{-2} \tag{3.16}$$

where $B_1 = (\pi/6)^{-2/3} F_{c,p}$.

In Equation (3.15), the floc break up rate dn/dt is proportional to the ratio between turbulent shear stress (τ_t) and floc yield strength (F_y), here we assume that only flocs with yield strength smaller than turbulent shear τ_t contribute to the flocs break up rate. As F_y is a function of floc size D and fractal dimension nf, Equation (3.15) in terms of mean turbulence shear is rewritten as:

$$\frac{dn}{dt} = ne_b Ga(\frac{D-d}{d})^p \int_{\mu_D-4\sigma_D}^{nf_{\max}(D)} (\frac{\tau_t}{F_y(D,nf)})^q \frac{1}{\sqrt{2\pi}\sigma_D} \exp(-\frac{(nf-\mu_D)^2}{2\sigma_D^2}) dnf \tag{3.17}$$

where $nf_{\max}(D)$ is the maximum fractal dimension that allows F_y smaller than τ_t for a given floc with size D.

Equation (3.16) shows that τ_y increases as nf increases for a given floc size D. The maximum $nf_{\max}(D)$ can be calculated as:

$$B_1(\frac{D}{d})^{2nf_{\max}(D)/3} D^{-2} = \tau_t \tag{3.18}$$

where $\tau_t = \mu G$ (see Winterwerp (1998) for more details), then

$$nf_{\max}(D) = \frac{3}{2}\log(\mu G D^2 / B_1) / \log(D/d) \tag{3.19}$$

Using the chain rule, from Equations (3.13) and (3.17), the floc break-up process is obtained:

$$\begin{aligned}\frac{dD}{dt} = &-\frac{e_b G a}{3}(\frac{\mu G}{B_1})^q D^{1-\beta+2q} d^{\beta-p}(D-d)^p \frac{1}{\beta\ln(D/d)+1} \\ &\times\int_{\mu_D-4\sigma_D}^{nf_{\max}(D)}(\frac{D}{d})^{-\frac{2q}{3}nf}\frac{1}{\sqrt{2\pi}\sigma_D}\exp(-\frac{(nf-\mu_D)^2}{2\sigma_D^2})dnf\end{aligned} \tag{3.20}$$

By combing linearly the preceding formulae derived for aggregation and break-up processes the complete time-dependent flocculation model can be obtained as:

$$\begin{aligned}\frac{dD}{dt} = \frac{Gd^\beta}{\beta\ln(D/d)+1}\Bigg[&\frac{k_A^{'}}{3}\frac{c}{\rho_s}d^{nf-3}D^{-nf+4-\beta} \\ &-\frac{k_B^{'}}{3}(\frac{\mu G}{B_1})^q D^{1-\beta+2q}d^{-p}(D-d)^p\int_{\mu_D-4\sigma_D}^{nf_{\max}(D)}(\frac{D}{d})^{-\frac{2q}{3}nf}\frac{1}{\sqrt{2\pi}\sigma_D}\exp(-\frac{(nf-\mu_D)^2}{2\sigma_D^2})dnf\Bigg]\end{aligned} \tag{3.21}$$

where $k_A^{'} = (3e_c\pi e_d)/2f_s$ and $k_B^{'} = ae_b$

In the results section, the new model is denoted as model A, which accounts for the normal distribution of fractal dimension and yield stress of mud flocs, and the model proposed by Son and Hsu (2009) as Model B, which adopted a single value of fractal dimension for a given floc size class.

3.3 Results

To use the flocculation model, the coefficient B_1 needs to be determined first. Here we assume that all the yield strengths of flocs are smaller than turbulent shear when the mean floc size reaches the equilibrium floc size.

$$B_1(\frac{D_{eq}}{d})^{\frac{2}{3}nf(D_{eq})}D_{eq}^{-2} = \mu G \tag{3.22}$$

where D_{eq} is the equilibrium floc size, $nf(D_{eq}) = \mu_{D_{eq}} + 4\sigma_{D_{eq}}$ then:

$$B_1 = \mu G D_{eq}^2(\frac{D_{eq}}{d})^{-\frac{2}{3}nf(D_{eq})} \tag{3.23}$$

For both models we assume the floc size growth rate $\frac{dD}{dt}$ equals zero when the floc size equals D_{eq} and then $\frac{k_A^{'}(B_1)^q}{k_B^{'}}$ (for Model A) and $\frac{k_A^{'}}{k_B^{'}}$ (for Model B) are both constant values. The parameters $k_A^{'}$ and $k_B^{'}$ are selected based on the best fit between the predicted curves and experiment data.

Model A, Equation (3.21) has been applied to four experimental datasets from various sources. To better present the effect of fractal dimension distribution on the temporal evolution of flocculation, Model A is compared with the model presented by Son and Hsu (2009) (to be referred to as Model B) which is based on a single fractal dimension for each floc size class.

The first dataset is from the experiment carried out by Spicer *et al.* (1998) (denoted as case 1) and is used to validate both flocculation models. The experiment was carried out in a stirred tank to investigate effect of shear rate $G = \sqrt{\varepsilon / \upsilon}$ on the floc properties (floc size, floc structure and floc density) during flocculation process. The shear rate *G* was specified as 50 s^{-1} during the floc size growth process. Flocs are formed by spherical, polystyrene primary particles with a diameter of 0.87 μm and a density of 1050 kg/m^3 (Spicer and Pratsinis, 1996). The primary particles are mixed in a 2.8 L tank and the

initial particle number concentration was set as 4×10^{7} cm^{-3} from which the volume concentration ϕ was calculated to be 1.4×10^{-5}. As the mass concentration will be used in the flocculation model, the value is calculated as C= 0.0147 kg/m^3. Three techniques are used for withdrawal of a sample using: a hand pipette, a syringe pump and a peristaltic pump. To keep consistent with Son and Hsu (2009), the experimental data obtained using the third technique is chosen to validate the models, because the data show largest numbers and stable curve as explained by Hsu and Balachandar (2009).

It was assumed that when $t=0$ the floc size is equal to 10 μm for both models. It needs to be mentioned here that the primary particle diameter has to be set as 1 μm in order to avoid numerical instability (see, Son and Hsu (2009)). The maximum floc size is assumed as the equilibrium floc size. From the assumptions above all, the parameters are determined and summarized in Table 3.1.

The temporal evolutions of floc size calculated using both models are presented in Figure 3.3 together with the experiment data of Spicer *et al.* (1998). As it can be seen both models predict a 'S' shaped curve as observed or predicted previously (Winterwerp, 1998). The curves increase quickly initially and gradually reach the equilibrium size near the end of flocculation process. In other words, the floc size increase rate is decreasing during the flocculation process, because the compactness of flocs decreases with the increase of floc size and the flocs become more fragile when the floc size increases. This provides the evidence that the incorporation of variable fractal dimension by both models contribute to the 'decrease' of floc size increase rate of the curves. When compared with each other, Model A which is based on a normal distribution of fractal dimension seems to perform better than Model B which based on a single fractal dimension value for each

fixed floc size class. The increase rate of the curve by Model A is higher than Model B at the initial time, and the situation reverses near end of the flocculation process.

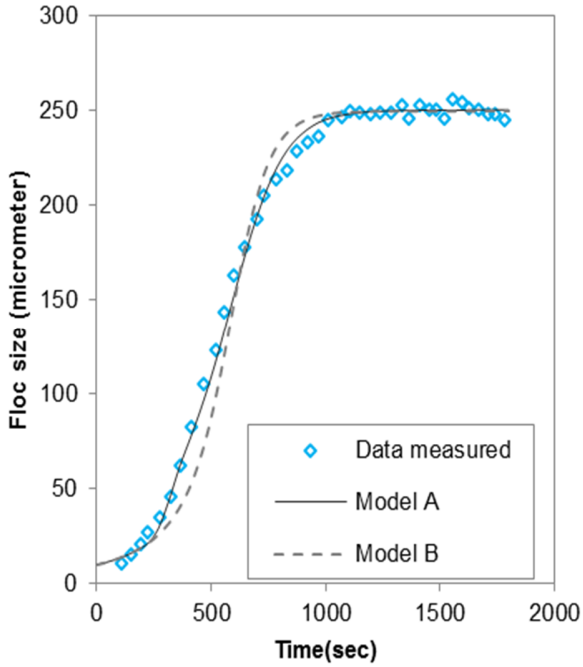

Figure 3.3 Experimental data of Spicer *et al.* (1998) and model predictions

Table 3.1 Parameters used in the flocculation models for experiment (Spicer *et al.*, 1998)

Model	$k_A^{'}$	$k_B^{'}$	B_1
A	3.59	6.617×10^{-6}	2.197×10^{-13}
B	6.74	4.59×10^{-6}	2.63×10^{-14}

Colomer *et al.* (2005) carried out an experiment (denoted as case 2) to investigate the particle flocculation process under low-shear conditions. In the experiments, a spherical flask was placed within an orbital shaking table and the shear rate G was set from 0.45 to 2.40 s^{-1}. Primary particles chosen are sulfate polystyrene latex particles with a diameter of 2.1 μm and the density is 1.055 g/cm^3. The volume concentration ranges

from 0.2 to 10×10^{-5}, from which the mass concentration can be calculated to be from 2.1 to 105 g/m^3. To reduce the effects of differential settling on the flocculation process, a density-matched aqueous environment was created by adding 99.5% NACL into water. The Brownian motion effect is present at the initial stage of flocculation process and can be ignored when the shear condition dominates the flocculation process. The shear rate G= 0.45 s^{-1} is selected and volume concentration of 2×10^{-5} are used to validate the numerical models.

The experimental data by Colomer *et al.* (2005) and model predictions are presented in Figure 3.4. The size of primary particle is set as 2.1 μm for both models. Other coefficients used are summarized in Table 3.2. The results of Model A and Model B perform well and the two curves predicted are almost identical. The reason is likely to be that the experiment was carried out under low-shear conditions, which can guarantee the collisions needed for aggregation and is also small enough for the aggregation to dominate in the aggregation-breakup balance (Colomer *et al.*, 2005). The generated flocs are relatively small and have narrow fractal dimension variance ranging from 2.67 to 2.84 for equilibrium floc size. This implies that break-up formulation in flocculation Model A, which is based on a normal distribution of fractal dimension, is less effective when applied to flocculation process with small equilibrium floc size, unlike in the case of experiments by Spicer *et al.* (1998) in which the shear-condition (G= 50 s^{-1}) and the equilibrium floc size (D= 250 μm) are much larger and Model A performs clearly better than Model B.

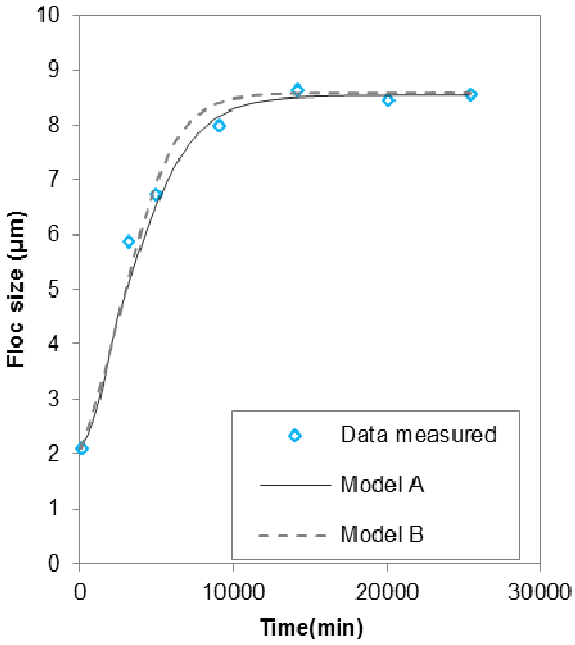

Figure 3.4 Experimental data of Colomer *et al.* (2005) and model predictions

Table 3.2 Parameters used in the flocculation models for experiment (Colomer *et al.*, 2005)

Model	$k_A^{'}$	$k_B^{'}$	B_1
A	1.567	1.313×10^{-5}	2.10×10^{-15}
B	1.994	2.35×10^{-5}	4.2×10^{-15}

The third experimental dataset used to validate the numerical models is from Biggs and Lant (2000). The shear rate is set as G= 19.4 s^{-1}. Due to the lack of information about the density of sludge and primary particle diameter, which are needed for determining the model parameters, we follow the assumptions made by Son and Hsu (2009). The density of sludge and primary particle are assumed as 1.3 g/cm^3 and 2.65 g/cm^3 respectively. Then the mass concentration is calculated as 24.19 kg/m^3 and the diameter of primary particle used is 4 μm. Other parameters are listed in Table 3.3. The fourth case considered

in the study is the experiment carried out by Keyvani and Strom (2014). A mixture of kaolinite and montmorillonite clay, the concentration of which is 50 mg/L, was used to investigate the growth path and equilibrium floc size. Under the shear rate of G= 35 s^{-1} the clay was mixed in the chamber to obtain the flocculation process. Other parameters relevant are listed in Table 3.4.

Table 3.3 Parameters used in the flocculation models for experiment (Biggs and Lant, 2000)

Model	$k_A^{'}$	$k_B^{'}$	B_1
A	1.125×10^{-2}	2.07×10^{-5}	7.362×10^{-13}
B	0.02	2.82×10^{-5}	4.2×10^{-13}

Table 3.4 Parameters used in the flocculation models for experiment (Keyvani and Strom, 2014)

Model	$k_A^{'}$	$k_B^{'}$	B_1
A	0.135	3.5×10^{-7}	1.174×10^{-13}
B	0.1995	1.0×10^{-6}	4.2×10^{-13}

Model results and data from Biggs and Lant (2000) (denoted as case3) and Keyvani and Strom (2014) (denoted as case4) are plotted in Figure 3.5 and Figure 3.6 respectively. All the curves predicted by Model A and Model B seem to follow the data trend with a high increasing rate initially and gradually reaching the equilibrium floc size near the end of flocculation process.

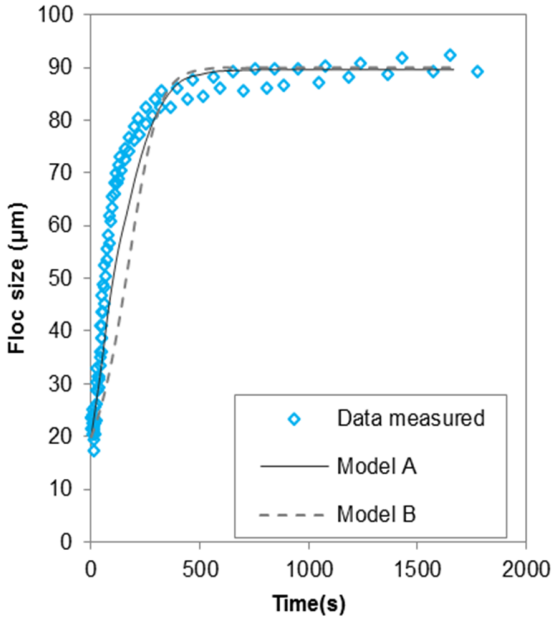

Figure 3.5 Experimental data of Biggs and Lant (2000) and model predictions

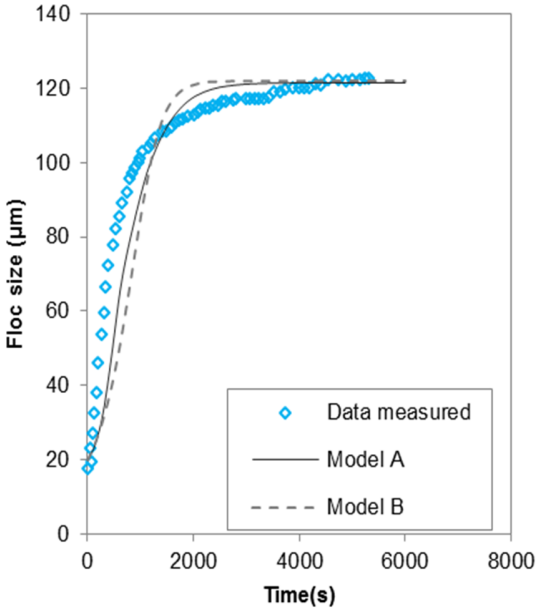

Figure 3.6 Experimental data of Keyvani and Strom (2014) and model predictions

3.4 Discussion

The results (case1, case3 and case4) presented above show that Model A predicts the

experimental data generally better than Model B, especially during the initial part of flocculation process. The reason for this superior performance can be explained as follows:

Both Model A and Model B can simplified as (Keyvani and Strom, 2014):

$$\frac{dD}{dt} = f(A) - g(B) \tag{3.24}$$

where $f(A)$ and $g(B)$ represent the aggregation and breakup processes respectively. Initially the effects of aggregation $f(A)$ are dominant and the flocs grow in size. When the effects of breakup $f(B)$ balance the effects of aggregation $f(A)$, the equilibrium floc size is obtained. According to Equation (3.21), the term accounting for the breakup rate is $(\frac{\tau_t}{F_y})^q$. As Model B is based on a single value of fractal dimension for a given floc size, the term $(\frac{\tau_t}{F_y})^q$ in Model B is rewritten as $[\frac{\tau_t}{F_y(D)}]^q$. On the other hand, as Model A is based on a normal distribution of fractal dimension for one fixed floc size, the term $(\frac{\tau_t}{F_y})^q$ cannot be calculated directly. Instead, the expectation of the term $(\frac{\tau_t}{F_y})^q$, which is denoted as E, is used in Model A.

$$E = \int_{\mu_D - 4\sigma_D}^{nf_{\max}(D)} (\frac{\tau_t}{F_y(D, nf)})^q \frac{1}{\sqrt{2\pi}\sigma_D} \exp(-\frac{(nf - \mu_D)^2}{2\sigma_D^2}) dnf \tag{3.25}$$

As only flocs with yield stress (F_y) less than the turbulent shear will break up which means in Model A, flocs group, whose size is D with fractal dimension only within$[\mu_D - 4\sigma_D, nf_{\max}(D)]$ interval, contributes to the breakup process. While in model B, a single value of fractal dimension is used to represent the whole flocs group whose

size is *D* and thus the whole flocs group contributes to the breakup process. As a result, the curve calculated using Model A show a higher increase rate than Model B. To better illustrate the influence of breakup mechanism on the growth of floc size in both Model A and Model B, the ratios between $\left|\frac{dD}{dt}\right|_B$ ($g(B)$), which is defined as the growth rate of floc size due to breakup, and $\left|\frac{dD}{dt}\right|_A + \left|\frac{dD}{dt}\right|_B$, in which the term $\left|\frac{dD}{dt}\right|_A$ ($f(A)$) is defined as the growth rate of floc size due to aggregation, for different cases (case1-4) are shown in Figure 3.7, Figure 3.8, Figure 3.9 and Figure 3.10 respectively. As mentioned in Section 3.3, the parameters $k_A^{'}$ and $k_B^{'}$ are selected based on the best fit between predicted results and experiment data. As a result, the parameters ($k_A^{'}$ and $k_B^{'}$) used in Model A and Model B are different for the same case. It is meaningless to compare the absolute value of floc size growth rate due to breakup process in Model A and Model B. Consequently, the ratios between $\left|\frac{dD}{dt}\right|_B$ and $\left|\frac{dD}{dt}\right|_A + \left|\frac{dD}{dt}\right|_B$ are used.

It can be seen from Figure 3.7 to Figure 3.10, it can be seen that the ratios between breakup process ($\left|\frac{dD}{dt}\right|_B$) and the sum of floc size growth rate due to breakup process and aggregation process ($\left|\frac{dD}{dt}\right|_A + \left|\frac{dD}{dt}\right|_B$) for both models (Model A and Model B) increase until the breakup and aggregation process are balanced (the ratio is 50%). Initially the ratio of Model A is much less than that of Model B, which can be explained that the initial floc size is close to primary particles and difficult to breakup. However, Model B in which a single value of fractal dimension for floc size D is adopted, overestimates the

breakup process especially at the beginning of floc size evolution (case 1, case 3 and case 4).

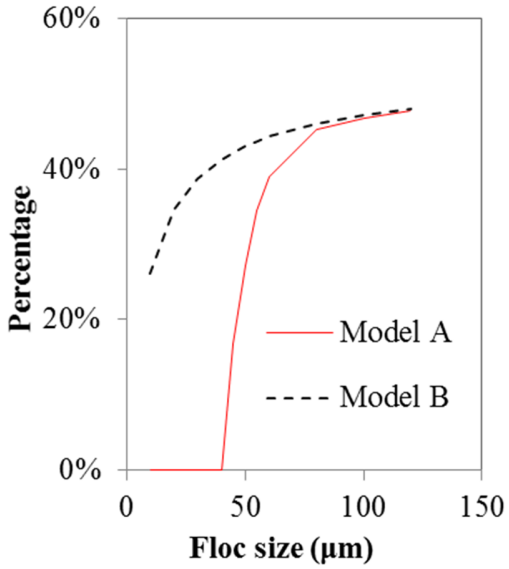

Figure 3.7 The ratios between floc size growth rate due to breakup process ($\left|\frac{dD}{dt}\right|_B$) and the sum of floc size growth rate due to breakup process and aggregation process ($\left|\frac{dD}{dt}\right|_A + \left|\frac{dD}{dt}\right|_B$) for case 1 (Spicer *et al.*, 1998)

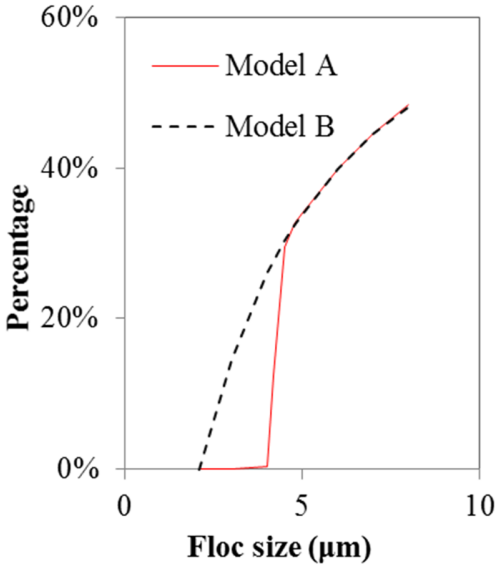

Figure 3.8 The ratios between floc size growth rate due to breakup process ($\left|\frac{dD}{dt}\right|_B$) and the sum of floc size growth rate due to breakup process and aggregation process ($\left|\frac{dD}{dt}\right|_A + \left|\frac{dD}{dt}\right|_B$) for case 2 (Colomer *et al.*, 2005)

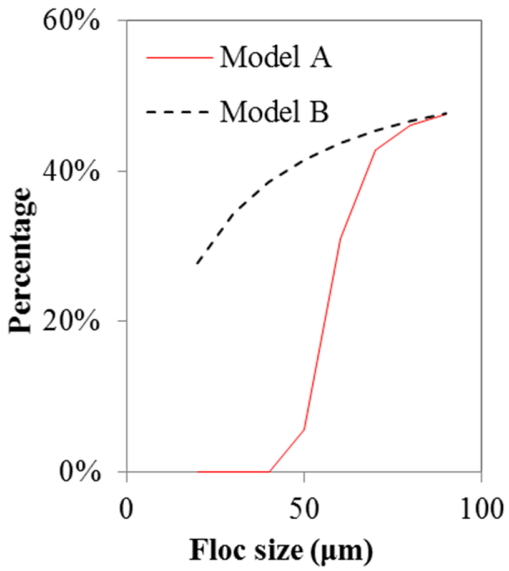

Figure 3.9 The ratios between floc size growth rate due to breakup process ($\left|\frac{dD}{dt}\right|_B$) and the sum of floc size growth rate due to breakup process and aggregation process ($\left|\frac{dD}{dt}\right|_A + \left|\frac{dD}{dt}\right|_B$) for case 3 (Biggs and Lant, 2000)

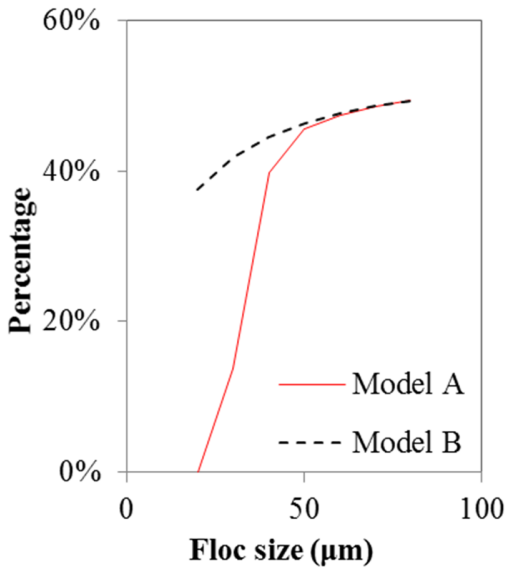

Figure 3.10 The ratios between floc size growth rate due to breakup process ($\left|\frac{dD}{dt}\right|_B$) and the sum of floc size growth rate due to breakup process and aggregation process ($\left|\frac{dD}{dt}\right|_A + \left|\frac{dD}{dt}\right|_B$) for case 4 (Keyvani and Strom, 2014)

3.5 Summary

A new mud flocculation model is presented which is based on the assumption that fractal dimension for each floc size class is normally distributed with both its mean and standard deviation being dependent on the floc size. The model has been validated against four sets of experimental data with satisfactory results. More specifically, under low shear conditions, both the present model and the model by Son and Hsu (2009) give fairly similar predictions for relatively small equilibrium floc sized flocculation process while under high shear-conditions and with a larger equilibrium floc size the new model shows a much better performance. The results demonstrate that the distribution of fractal dimension has a significant effect on the breakup process and the flocculation model using a single value of fractal dimension for a given size class group will overestimate

the effect of breakup process. This deficiency can be effectively removed by incorporating a normal distribution of fractal dimension. Overall, the presented flocculation model considers the distribution of fractal dimension and yield strength to describe the evolution of mud floc size, density and structure, and further settling velocity, which is an essential parameter in the cohesive sediment transport model. However, due to the lack of field measurements of floc evolution process in the research areas of current dissertation, the parameters such as e_c and e_d cannot be calibrated. Thus, this new flocculation model is not incorporated into the two-phase model in Chapter 4, instead the simple concentration-settling velocity relationship Equation (2.1) is adopted to account for the flocculation process. The new flocculation model, as a frame work, has the potential to be combined with two-phase model once the relevant data in study areas are available.

Chapter 4 Two-phase model development

4.1 Governing equations

The two-phase flow model developed in this dissertation is based on the standard theoretical framework detailed in a number of previous works (Chauchat *et al.*, 2013; Dong and Zhang, 1999). The continuity and momentum equations for phase *k* and can be written as:

$$\frac{\partial \rho_k \alpha_k}{\partial t} + \frac{\partial \rho_k u_{kj}}{\partial x_j} = \frac{\partial \rho_k \overline{\alpha_k' u_{kj}'}}{\partial x_j} \tag{4.1}$$

$$\frac{\partial \rho_k \alpha_k u_{ki}}{\partial t} + \frac{\partial \rho_k \alpha_k u_{ki} u_{kj}}{\partial x_j} = -\rho_k \alpha_k g \delta_{i2} - \alpha_k \frac{\partial p_k}{\partial x_i} + \frac{\partial T_{ij}}{\partial x_j} - f_i \tag{4.2}$$

As the two-phase model is designed for transport processes of cohesive sediment particles which are much lighter than sands and thus the inertia effect is usually negligible, the flow and particle may be assumed to have the same mean horizontal velocity. The horizontal momentum equations for both phases are solved together, which is the same as Equation (2.34) (van der Ham and Winterwerp, 2001). The continuity equations and momentum equations in the vertical direction are the same as the model presented by Chauchat *et al.* (2013). It should be mentioned that as there is no horizontal velocity in the work of Chauchat *et al.* (2013), the correlation between velocity fluctuation and concentration is neglected. In this dissertation, the horizontal velocity cannot be ignored in the simulation area.

4.2 .Stress terms

To solve the two-phase equations, the closures, which are interphase momentum

transfer, pressure gradient, intergranular stresses and turbulent stresses should be implemented into the model.

4.2.1 Pressure gradient

The horizontal momentum Equation (2.34) is driven using a depth-averaged velocity U_d and the pressure gradient can be calculated as Equation (2.35). As in the vertical direction, the pressure in the solid phase is different from the fluid pressure, which has the same physical meaning in the single-phase momentum equation, the total pressure $\tilde{p}$ (mixture pressure) has to be considered.

$$\tilde{p} = \alpha_f p_f + \alpha_s p_s \tag{4.3}$$

where p_f is fluid pressure and p_s is the solid pressure. The fluid pressure represents the resistance of fluid to compression, and consists of two parts for the solid pressure: one is from the resistance of fluid filling the pores and the other is due to the contact of solid particles. When the sediment particles settles on the bed and contact with each other, a solid network will be formed and the resistance due to the existence of solid network is named as effective stress σ_e. For the cohesive sediment, the effective stress is found to appear when the concentration exceeds a critical value which is named as gelling concentration (Dankers and Winterwerp, 2007). According to the theory of Terzaghi (1923), the total stress is calculated as:

$$\tilde{p} = p_f + \sigma_e \tag{4.4}$$

Due to $\alpha_s + \alpha_f = 1$, from Equation (4.3) and Equation (4.4), the solid pressure can be calculated as:

$$p_s = p_f + \frac{\sigma_e}{\alpha_s} \tag{4.5}$$

The specific expression of σ_e will be illustrated in detail for non-cohesive sediment and cohesive sediment respectively.

According to Zhang and Campbell (1992), if the concentration of non-cohesive sediment is between loose packed concentration α_s^* and the maximum packed concentration, the behavior of sediment will be in a transition state between the solid-like or fluid like behavior. The normal stress for non-cohesive sediment consists of two parts: one is due to the collisional contribution and the other is due to the enduring contact. Hsu *et al.* (2003) concluded that as the concentration increase larger than α_s^*, normal stress due to the enduring contact is more important.

Hertz contact relation is adopted here:

$$\sigma_e = \frac{m_\sigma}{\pi d^2} K(\alpha_s)\alpha_s (\frac{\Delta}{d})^{3/2} \tag{4.6}$$

where m_σ is a coefficient and given according to the shear modulus E and Poisson ration ν_p of the material (sand particles). $K(\alpha_s)$ is the average number of contacts of per particle and Δ is the average compressive volume strain:

$$m_\sigma = \frac{2}{9\sqrt{3}} \frac{Ed^2}{1-\nu_p} \tag{4.7}$$

Following Hsu *et al.* (2003) the average compressive volume strain can be related to

the difference between loose packing concentration α_s^* and α_s:

$$\frac{\Delta}{d} = (\alpha_s - \alpha_s^*)^{2\chi/3} \tag{4.8}$$

where χ is a coefficient that must be calibrated, then

$$\sigma_e = \begin{cases} 0 & \alpha_s < \alpha_s^* \\ \frac{m_\sigma}{\pi d^2} K(\alpha_s)\alpha_s(\alpha_s - \alpha_s^*)^\chi & \alpha_s^* \le \alpha_s \le \alpha_s^{\max} \end{cases} \tag{4.9}$$

$K(\alpha_s)$ is given as:

$$K(\alpha_s) = 3 + 3\sin[\frac{\pi}{2}(2\frac{\alpha_s - \alpha_s^*}{\alpha_s^{\max} - \alpha_s^*} - 1)], \alpha_s^* \le \alpha_s \le \alpha_s^{\max} \tag{4.10}$$

As for the cohesive sediment, a comprehensive closures for effective stress has been reviewed in Chapter 2. Here we adopt the Equation (2.33) which is modified by Chauchat *et al.* (2013) and is asymptotically consistent with the formulae proposed by Merckelbach and Kranenburg (2004):

$$\sigma_e = \begin{cases} 0, \alpha_s < \alpha_s^{gel} \\ \sigma_0[(1 - \frac{\alpha_s - \alpha_s^{gel}}{\alpha_s^{\max}})^{-2/(3-nf)} - 1], \alpha_s \ge \alpha_s^{gel} \end{cases} \tag{4.11}$$

In this equation, the coefficients σ_0 , α_s^{gel} and $\alpha_s^{\max}$ need to be determined

4.2.2 Interphase momentum transfer

As in the current study, the momentum equations for solid and fluid phase are combined together, only interphase momentum transfer in the vertical direction is considered. For non-cohesive sediment, the drag force, added mass and lift force are the major forces contributing to the interaction force. As in the calculation of Chauchat *et al.*

(2013), the particle Reynolds number (Equation ((4.12)) is around $10^{-3}-10^{-4}$, thus the interphase momentum transfer reduces to simple Stokes drag force:

$$R_e = \rho_f \alpha_f d \left\| w_s - w_f \right\| \frac{1}{\mu_f} \tag{4.12}$$

$$f_i = \frac{3\alpha_s \rho_f}{4d} C_d \left\| w_s - w_f \right\| (w_f - w_s) \alpha_f^{2-n_{RZ}} \tag{4.13}$$

where C_d is drag coefficient and equals to $24/R_e$ at the small Reynolds number, n_{RZ} is an empirical coefficient in the function presented by Richardson and Zaki (1954) to account for the hindered effects.

Due to the biochemical and electrochemical effects of cohesive particles, Equation (4.13) is useless when calculating the interphase momentum transfer for cohesive sediment. Following Chauchat *et al.* (2013), an semi-empirical equation is used:

$$f_i = \frac{\rho_f g}{K} (w_f - w_s) \tag{4.14}$$

where $K\,(ms^{-1})$ is the permeability and can be given in the term of settling velocity w_s (Toorman, 1996):

$$K = \frac{w_s}{\alpha_s (\rho_s / \rho_f - 1)} \tag{4.15}$$

Therefore, the issue to find the closure of permeability K becomes to find the proper settling velocity w_s. Camenen (2008) modified the Richard and Zaki equation to study the effects of concentration on the settling velocity.

$$\frac{w_s}{w_{s0}} = (1-\alpha_s)^{n_{RZ}-2}(1-\phi)(1-\frac{\phi}{\phi_{\max}})^{\phi_{\max}} \tag{4.16}$$

And the coefficient n_{RZ} is assumed to have the same value range proposed by Richardson and Zaki (1954). Camenen and Pham van Bang (2011) assumed the size and density of mud flocs are constant, the hindrance coefficient n_{RZ} is larger than 2 and further modified the equation (Chauchat *et al.*, 2013):

$$\frac{w_s}{w_{s0}} = (1-\alpha_s)^{nf/2}(1-\phi)^{nf/2-1}(1-\frac{\phi}{\phi_{\max}})^{\phi_{\max}} \tag{4.17}$$

Camenen and Pham van Bang (2011) explained that due to the buoyancy effects, a term $(1-\alpha_s)^x$ with $x \geq 1$ should be included in the formulae to calculate the settling velocity at high concentration, while $n-2$ could be less than 1. In the current study, Equation (4.17) is adopted in the two-phase model for the hindrance regime.

When the concentration increases above the gelling concentration α_s^{gel}, which corresponds to the permeability regime, Equation (4.17) is not appropriate. To make the settling velocity in the transition zone (from hindrance regime to permeability regime), the following equations are used:

$$w_s = \begin{cases} w_0(1-\alpha_s)^{nf/2}(1-\phi)^{nf/2-1}(1-\frac{\phi}{\phi_{\max}}), \alpha_s \leq \frac{\alpha_s^{gel}}{\chi} \\ w^{gel}(\frac{\chi\alpha_s}{\alpha_s^{gel}})^{-2/(3-nf)+1}, \alpha_s > \frac{\alpha_s^{gel}}{\chi} \end{cases} \tag{4.18}$$

where w^{gel} equals to w_s when $\alpha_s = \alpha^{gel}$.

It should be noted that the Equations (4.14) and (4.18) only take into account the hindered settling effects, whereas the flocculation process for cohesive sediment is

ignored. The diagram in Thorn (1981) showed that the relationship between particle mass concentration and settling velocities of mud flocs in the flocculation stage can be described using a power law, see Equation (2.1).

To take into consideration the flocculation process, a new closure for the drag force is obtained by combining the Equations (2.1) and (4.18). The effects of flocculation and hindered settling are both included in one single closure relationship, which enable the transition from flocculation regime to hindered settling regime to be determined continuously during the model calculations. The complete form of the new closure is presented as Equations (4.14) and (4.19):

$$w_s = \begin{cases} k_1 C^m (1-\alpha_s)^{n/2} (1-\phi)^{n/2-1} (1-\dfrac{\phi}{\phi_{\max}}), \alpha_s \le \dfrac{\alpha_s^{gel}}{\chi} \\ \mathrm{w}_s^{gel} (\dfrac{\chi \alpha_s}{\alpha_s^{gel}})^{-2/(3-n)+1}, \alpha_s > \dfrac{\alpha_s^{gel}}{\chi} \end{cases} \tag{4.19}$$

4.2.3 Shear stresses

In the horizontal direction, the shear stress T_{xz} is calculated as:

$$T_{xz} = \rho_{mix} (\nu + \nu_T) \frac{\partial \overline{U}}{\partial z} \tag{4.20}$$

The eddy viscosity is calculated using a classic method (Spearman *et al.*, 2011)

$$\nu_T = \kappa^2 z^2 (1-\frac{z}{h}) \frac{\partial u}{\partial z} F_v \tag{4.21}$$

where F_v is the dissipation coefficient of eddy viscosity and κ is the Von Karman constant.

In the vertical direction, the shear stresses of solid phase $T_{s,zz}$ and fluid phase $T_{f,zz}$

are assumed as the same (Chauchat *et al.*, 2013) and equal to the mixture viscous shear stress τ_v which is calculated as:

$$T_{f,zz} = T_{s,zz} = \tau_v \tag{4.22}$$

$$\tau_v = \mu_{eff}[\nabla u_m + (\nabla u_m)^T] \tag{4.23}$$

where u_m is the volume-averaged velocity expressed as:

$$u_m = (1-\alpha_s)u_f + \alpha_s u_s \tag{4.24}$$

4.3 Diffusion coefficient

The remaining term is the correlation between velocity fluctuation and concentration $\overline{\alpha_k' u_{kj}'}$. We follow Dong and Zhang (1999) and $\overline{\alpha_k' u_{kj}'}$ is expressed as a product between the mean concentration gradient and a diffusion coefficient:

$$\overline{\alpha_k' u_{kj}'} = -\Gamma_T \frac{\partial \alpha_k \rho_k}{\partial z} \tag{4.25}$$

where Γ_T is the diffusion coefficient and calculated as:

$$\Gamma_T = \frac{\nu_T F_d}{\sigma_T F_v} \tag{4.26}$$

where the empirical coefficients σ_T is the turbulent Prandtl-Schmidt number and usually specified as 0.7 or 1.0. F_d is the dissipation coefficient of eddy diffusivity due to the buoyancy effects caused by the sediment suspension (Kranenburg, 1998; Toorman, 2002) which may significantly alter turbulent flow structure, as the interaction between turbulent flow and suspended particles dissipates turbulent energy, which keep the

sediment particles in suspension, and the sediment concentration decreases (Toorman, 2002; van der Ham and Winterwerp, 2001; Winterwerp, 2006).

To take account of this effect, a $k-\varepsilon$ model is developed by van der Ham and Winterwerp (2001) and the buoyancy destruction term is introduced into the turbulent kinetic energy transport equation. Simple empirical coefficients are introduced by Toorman (2002) to modify the eddy viscosity F_v and eddy diffusivity F_d, respectively. These coefficients are specified as:

$$F_v = (1+ARi)^{-a} \tag{4.27}$$

$$F_d = F_v(1+BRi)^{-b} \tag{4.28}$$

where A, B, a, b are coefficients and specified as 100,21,1/3 and 0.8 respectively, Ri is the gradient Richardson number and in a 1DV shear flow is defined as:

$$Ri = \frac{-g\frac{\partial \rho_{mix}}{\partial z}}{\rho(\frac{\partial U}{\partial z})^2} \tag{4.29}$$

These eddy viscosity and eddy diffusivity coefficients are re-derived by Kranenburg (1998). Which are based on three conditions: 1) in the equilibrium condition the concentration should fall within a finite interval for all gradients Richardson numbers, 2) keep model stable, 3) the value of flux Richardson number and gradient Richardson number should be reasonable according to the experiment results. The equation calculating eddy viscosity is the same as Equation (4.27), while the equation calculating eddy diffusivity is different:

$$F_d = (1 + BRi)^{-b} \tag{4.30}$$

Suggested by Kranenburg (1998) the coefficients (A , B , a and b) used in Equations (4.27) and (4.30) are specified as 2.4, 2.4, -2 and -4 respectively.

4.4 Boundary conditions

The boundary condition for the horizontal momentum equation is calculated as (van der Ham and Winterwerp, 2001):

$$\tau_c = (\rho_{mix}(\nu + \nu_T)\frac{\partial \overline{U}}{\partial z})\Big|_{z=z_b} \tag{4.31}$$

where τ_c is the shear stress due to currents and z_b is a small distance from the bed usually taken as half of the first computational grid.

As the combined wave and current shear stress is introduced into the boundary condition in the sediment continuity equation for the application to mudflat at Yangtze River Estuary, the shear stress due to waves τ_w needs to be calculated first:

According to Zhu *et al.* (2014), near the wave boundary layer, the peak value of orbital excursion $\widehat{A}$ and velocity $\widehat{U}$ can be calculated as:

$$\widehat{A} = \frac{H}{2\sinh(k_w h)} \tag{4.32}$$

$$\widehat{U} = \frac{\pi H}{T\sinh(k_w h)} \tag{4.33}$$

where H is the wave height, T is the wave period and k_w ($= 2\pi / L$) is the wave number. L is the wave length and is calculated as:

$$L = (gT^2 / 2\pi)\tanh(k_w h) \tag{4.34}$$

The wave shear stress is presented as:

$$\tau_w = \frac{1}{4}\rho_w f_w \hat{U}^2 \tag{4.35}$$

where f_w is the bed friction factor, here we also follow Zhu *et al.* (2014):

$$f_w = \begin{cases} 2(\dfrac{\hat{U}\hat{A}}{\nu})^{-0.5} & \dfrac{\hat{U}\hat{A}}{\nu} < 10^4 \\ 0.09(\dfrac{\hat{U}\hat{A}}{\nu})^{-0.2} & 10^4 < \dfrac{\hat{U}\hat{A}}{\nu} < 10^6, \dfrac{\hat{A}}{k_s} > 10^3 \end{cases} \tag{4.36}$$

where k_s is the effective bed roughness.

The combined wave and current shear stress τ_{cw} can be calculated as Soulsby and Clarke (2005):

$$\tau_{cw} = ((\tau_m + \tau_w|\cos\varphi_{cw}|)^2 + (\tau_w|\sin\varphi_{cw}|)^2)^{1/2} \tag{4.37}$$

where τ_w is the shear stress due to waves, φ_{cw} is the angel between waves and currents, τ_m is the averaged total shear stress:

$$\tau_m = \tau_c[1 + 1.2(\frac{\tau_w}{\tau_c + \tau_w})^{3.2}] \tag{4.38}$$

The bed erodibility is assumed as a constant. For consolidated bed, the assumption is not appropriate while in the current study all the erosion occurs on a layer of fresh-deposited mud which has no consolidation history. The upward erosion sediment flux E_{up} is calculated as:

$$E_{up} = M\rho_s(\left|\frac{\tau_b}{\tau_{cr}}\right| - 1), |\tau_b| > \tau_{cr} \tag{4.39}$$

where τ_b is bed shear stress and equals to τ_c when the currents dominates and equals τ_{cw} when both currents and waves are dominant. M is erosion coefficient, τ_{cr} is critical bed shear stress for sediment erosion. When the bed shear stress is less than the critical bed shear stress sediment will deposit on the bed and the deposition sediment flux E_{de} is given by:

$$E_{de} = w_s\rho_s\alpha_s(\mathrm{z}_b)(1 - \left|\frac{\tau_b}{\tau_{cd}}\right|), |\tau_b| \le \tau_{cd} \tag{4.40}$$

where τ_{cd} is the critical bed shear stress for sediment deposition. Combining Equation (4.39) and Equation (4.40), the boundary condition for the sediment continuity equation can be given as:

$$\Gamma_T \frac{\partial \alpha_s \rho_s}{\partial z} - \alpha_s \rho_s w_s = \begin{cases} M\rho_s(\left|\frac{\tau_b}{\tau_{cr}}\right| - 1), |\tau_b| > \tau_{cr} \\ w_s\rho_s\alpha_s(\mathrm{z}_b)(1 - \left|\frac{\tau_b}{\tau_{cd}}\right|), |\tau_b| \le \tau_{cd} \end{cases} \tag{4.41}$$

Overall, according to the discussion of section 4.2-4.4, we substitute Equations (4.5) and (4.22) in the momentum Equation (4.2) and substitute Equation (4.25) in the continuity Equation (4.1), the governing equations of the two-phase model can be summarised as:

$$\frac{\partial \bar{U}}{\partial t} + \frac{1}{\rho_{mix}}\frac{\partial \bar{P}}{\partial x} = \frac{\partial}{\partial z}((\nu + \nu_T)\frac{\partial \bar{U}}{\partial z}) \tag{4.42}$$

$$\alpha_f + \alpha_s = 1 \tag{4.43}$$

$$\frac{\partial \alpha_f \rho_f}{\partial t} + \frac{\partial \alpha_f \rho_f w_f}{\partial z} - \frac{\partial}{\partial z}[\Gamma_T \frac{\partial \alpha_f \rho_f}{\partial z}] = 0 \tag{4.44}$$

$$\frac{\partial \alpha_s \rho_s}{\partial t} + \frac{\partial \alpha_s \rho_s w_s}{\partial z} - \frac{\partial}{\partial z}[\Gamma_T \frac{\partial \alpha_s \rho_s}{\partial z}] = 0 \tag{4.45}$$

$$\begin{aligned} \frac{\partial \alpha_f \rho_f w_f}{\partial t} + \frac{\partial \alpha_f \rho_f w_f w_f}{\partial z} &= -\alpha_f \frac{\partial p_f}{\partial z} \\ &+\alpha_f \frac{\partial \tau_v^{zz}}{\partial z} - \alpha_f \rho_f g + f_i \end{aligned} \tag{4.46}$$

$$\begin{aligned} \frac{\partial \alpha_s \rho_s w_s}{\partial t} + \frac{\partial \alpha_s \rho_s w_s w_s}{\partial z} &= -\alpha_s \frac{\partial p_f}{\partial z} - \frac{\partial \sigma_e}{\partial z} \\ &+\alpha_s \frac{\partial \tau_v^{zz}}{\partial z} - \alpha_s \rho_s g - f_i \end{aligned} \tag{4.47}$$

4.5 Numerical methods

To solve the 1DV two-phase model, the details concerning the numerical methods are given in this chapter.

4.5.1 Mesh definition

In the current study, a staggered-grid first-order finite-difference method is adopted (Figure 4.1). Finite-difference is one of the simplest method for discretization and has been well developed. Staggered grid combines two types of nodal points located in different locations. Black point represents scalar variables and arrow represents vector variables. For scalar variables (pressure p, sediment volume fraction α_s, fluid volume fraction α_f) are located at the center of the cell. The horizontal velocity u, vertical velocities for both phases (w_f and w_s) are located at the node of computing grid. Δz_j^w represents the distance between the node $j-1$ and node j while Δz_j represents the

distance between the node $j-\frac{1}{2}$ and node $j+\frac{1}{2}$ and equals $0.5(\Delta z_j^w + \Delta z_{j+1}^w)$ see (Figure 4.1).

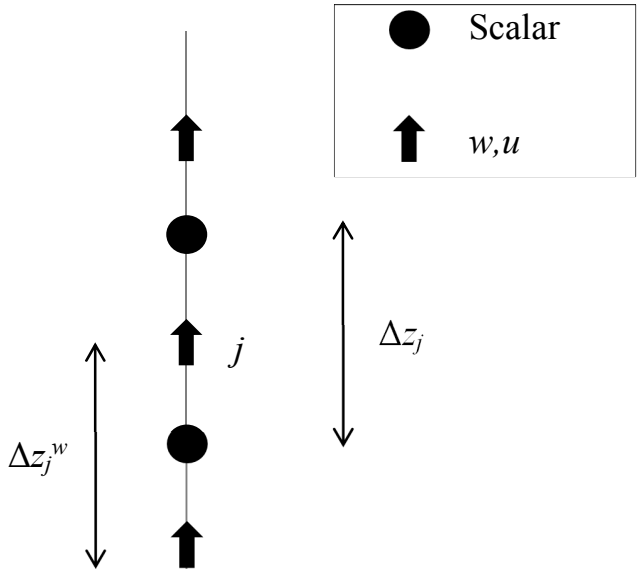

Figure 4.1 Mesh definition

4.5.2 Equation discretization

1) Momentum equation for the horizontal velocity $\overline{U}_j^{n+1}$

$$\frac{\overline{U}_j^{n+1}-\overline{U}_j^{n}}{\Delta t}+\frac{1}{\rho_{mix}}\frac{\partial \overline{P}}{\partial x}=\frac{\nu_{T,j}(\overline{U}_{j+1}^{n+1}-\overline{U}_j^{n+1})}{(z_{j+2}^w-z_{j+1}^w)(z_{j+2}^w-z_j^w)/2} - \frac{\nu_{T,j-1}(\overline{U}_j^{n+1}-\overline{U}_{j-1}^{n+1})}{(z_{j+2}^w-z_j^w)(z_{j+1}^w-z_j^w)/2} \tag{4.48}$$

2) Continuity equation for the solid phase for $\alpha_{s,j}^{n+1}$

$$\frac{\alpha_{s,j}^{n+1}-\alpha_{s,j}^{n}}{\Delta t}+\frac{w_{s,j+1}^{n}(\alpha_{s,j+1}^{n+1}-\alpha_{s,j}^{n+1})}{z_{j+1}-z_{j}}+\alpha_{s,j}^{n+1}\frac{w_{s,j+1}^{n}-w_{s,j}^{n}}{z_{j+1}^{w}-z_{j}^{w}}=$$
$$+\frac{\Gamma_{T,j}(\alpha_{s,j+1}^{n}-\alpha_{s,j}^{n})}{(z_{j+1}^{w}-z_{j}^{w})(z_{j+1}-z_{j})}$$
$$-\frac{\Gamma_{T,j}(\alpha_{s,j}^{n}-\alpha_{s,j-1}^{n})}{(z_{j+1}^{w}-z_{j}^{w})(z_{j}-z_{j-1})} \tag{4.49}$$
$$+\frac{(\Gamma_{T,j+1}-\Gamma_{T,j})(\alpha_{s,j+1}^{n}-\alpha_{s,j}^{n})}{(z_{j+1}-z_{j})(z_{j+1}-z_{j})}$$

3) Volume conservation for α_{f}^{n+1}

$$\alpha_{f}^{n+1}=1-\alpha_{s}^{n+1} \tag{4.50}$$

4) Fluid phase momentum equation for $w_{f,j}^{*}$

$$\frac{w_{f,j}^{*}-w_{f,j}^{n}}{\Delta t}=-w_{f,j}^{n}\frac{w_{f,j}^{*}-w_{f,j-1}^{*}}{z_{j}^{w}-z_{j-1}^{w}}-\frac{1}{\rho_{f}}\frac{p_{f,j}^{*}-p_{f,j-1}^{*}}{z_{j}-z_{j-1}}-g+CFD(w_{s,j}^{n}-w_{f,j}^{*})$$
$$+\mu(1+\beta_{j}\alpha_{s,j}^{n+1})\frac{(\alpha_{f,j+1/2}^{n+1}w_{f,j+1}^{*}-\alpha_{f,j-1/2}^{n+1}w_{f,j}^{*})}{(z_{j+1}^{w}-z_{j}^{w})(z_{j}-z_{j-1})}\frac{1}{\rho_{f}}$$
$$-\mu(1+\beta_{j-1}\alpha_{s,j-1}^{n+1})\frac{(\alpha_{f,j-1/2}^{n+1}w_{f,j}^{*}-\alpha_{f,j-3/2}^{n+1}w_{f,j-1}^{*})}{(z_{j}^{w}-z_{j-1}^{w})(z_{j}-z_{j-1})}\frac{1}{\rho_{f}} \tag{4.51}$$
$$+\mu(1+\beta_{j}\alpha_{s,j}^{n+1})\frac{(\alpha_{s,j+1/2}^{n+1}w_{s,j+1}^{n}-\alpha_{s,j-1/2}^{n+1}w_{s,j}^{n})}{(z_{j+1}^{w}-z_{j}^{w})(z_{j}-z_{j-1})}\frac{1}{\rho_{f}}$$
$$-\mu(1+\beta_{j}\alpha_{s,j-1}^{n+1})\frac{(\alpha_{s,j-1/2}^{n+1}w_{s,j}^{n}-\alpha_{s,j-3/2}^{n+1}w_{s,j-1}^{n})}{(z_{j}^{w}-z_{j-1}^{w})(z_{j}-z_{j-1})}\frac{1}{\rho_{f}}$$

5) Poisson equation for $p_{f,j+1}^{n+1}$

$$\frac{p_{f,j+1}^{n+1}-p_{f,j+1}^{*}-p_{f,j}^{n+1}+p_{f,j}^{*}}{(z_{j+1}-z_j)(z_{j+1}^{w}-z_j^{w})}-\frac{p_{f,j}^{n+1}-p_{f,j}^{*}-p_{f,j-1}^{n+1}+p_{f,j-1}^{*}}{(z_j-z_{j-1})(z_{j+1}^{w}-z_j^{w})}=$$
$$\frac{\rho_f}{\alpha_{f,j}^{n+1}\Delta t}[\frac{\alpha_{f,\mathrm{j}}^{n+1}-\alpha_{f,j}^{n}}{\Delta t}+\alpha_{f,j}^{n+1}\frac{w_{f,j+1}^{*}-w_{f,j}^{*}}{z_{j+1}^{w}-z_j^{w}}+w_{f,j}^{*}\frac{w_{f,j}^{n+1}-w_{f,j-1}^{n+1}}{z_j-z_{j-1}}$$
$$-\Gamma_{T,j}\frac{\alpha_{f,\mathrm{j+1}}^{n}-\alpha_{f,j}^{n}}{(z_{j+1}^{w}-z_j^{w})(z_{j+1}-z_j)}+\Gamma_{T,j}\frac{\alpha_{f,j}^{n}-\alpha_{f,j-1}^{n}}{(z_{j+1}^{w}-z_j^{w})(z_j-z_{j-1})} \tag{4.52}$$
$$-(\Gamma_{T,j+1}-\Gamma_{T,j})\frac{\alpha_{f,\mathrm{j+1}}^{n}-\alpha_{f,j}^{n}}{(z_{j+1}^{w}-z_j^{w})(z_{j+1}-z_j)}]$$

6) Velocity correction $w_{f,j}^{n+1}$

$$\frac{w_{f,j}^{n+1}-w_{f,j}^{*}}{\Delta t}=-\frac{1}{\rho_f}[\frac{p_{f,j}^{n+1}-p_{f,j}^{*}-p_{f,j-1}^{n+1}+p_{f,j-1}^{*}}{z_j-z_{j-1}}] \tag{4.53}$$

7) Solid phase momentum equation for

$$\frac{w_{\mathrm{s},j}^{n+1}-w_{\mathrm{s},j}^{n}}{\Delta t}=-w_{\mathrm{s},j}^{n}\frac{w_{\mathrm{s},j+1}^{n+1}-w_{\mathrm{s},j}^{n+1}}{z_{j+1}^{w}-z_j^{w}}-\frac{1}{\rho_s}\frac{p_{f,j}^{n+1}-p_{f,j-1}^{n+1}}{z_j-z_{j-1}}-g-CFD(w_{s,j}^{n}-w_{f,j}^{*})$$
$$-\frac{1}{\rho_s}\alpha_{s,j-1/2}^{n+1}\frac{\sigma_{e,j}-\sigma_{e,j-1}}{z_j-z_{j-1}}$$
$$+\mu(1+\beta_j\alpha_{s,j}^{n+1})\frac{(\alpha_{f,j+1/2}^{n+1}w_{f,j+1}^{n+1}-\alpha_{f,j-1/2}^{n+1}w_{f,j}^{n+1})}{(z_{j+1}^{w}-z_j^{w})(z_j-z_{j-1})}\frac{1}{\rho_s}$$
$$-\mu(1+\beta_{j-1}\alpha_{s,j-1}^{n+1})\frac{(\alpha_{f,j-1/2}^{n+1}w_{f,j}^{n+1}-\alpha_{f,j-3/2}^{n+1}w_{f,j-1}^{n+1})}{(z_j^{w}-z_{j-1}^{w})(z_j-z_{j-1})}\frac{1}{\rho_s} \tag{4.54}$$
$$+\mu(1+\beta_j\alpha_{s,j}^{n+1})\frac{(\alpha_{\mathrm{s},j+1/2}^{n+1}w_{\mathrm{s},j+1}^{n+1}-\alpha_{\mathrm{s},j-1/2}^{n+1}w_{\mathrm{s},j}^{n+1})}{(z_{j+1}^{w}-z_j^{w})(z_j-z_{j-1})}\frac{1}{\rho_s}$$
$$-\mu(1+\beta_{j-1}\alpha_{s,j-1}^{n+1})\frac{(\alpha_{\mathrm{s},j-1/2}^{n+1}w_{\mathrm{s},j}^{n+1}-\alpha_{\mathrm{s},j-3/2}^{n+1}w_{\mathrm{s},j-1}^{n})}{(z_j^{w}-z_{j-1}^{w})(z_j-z_{j-1})}\frac{1}{\rho_s}$$

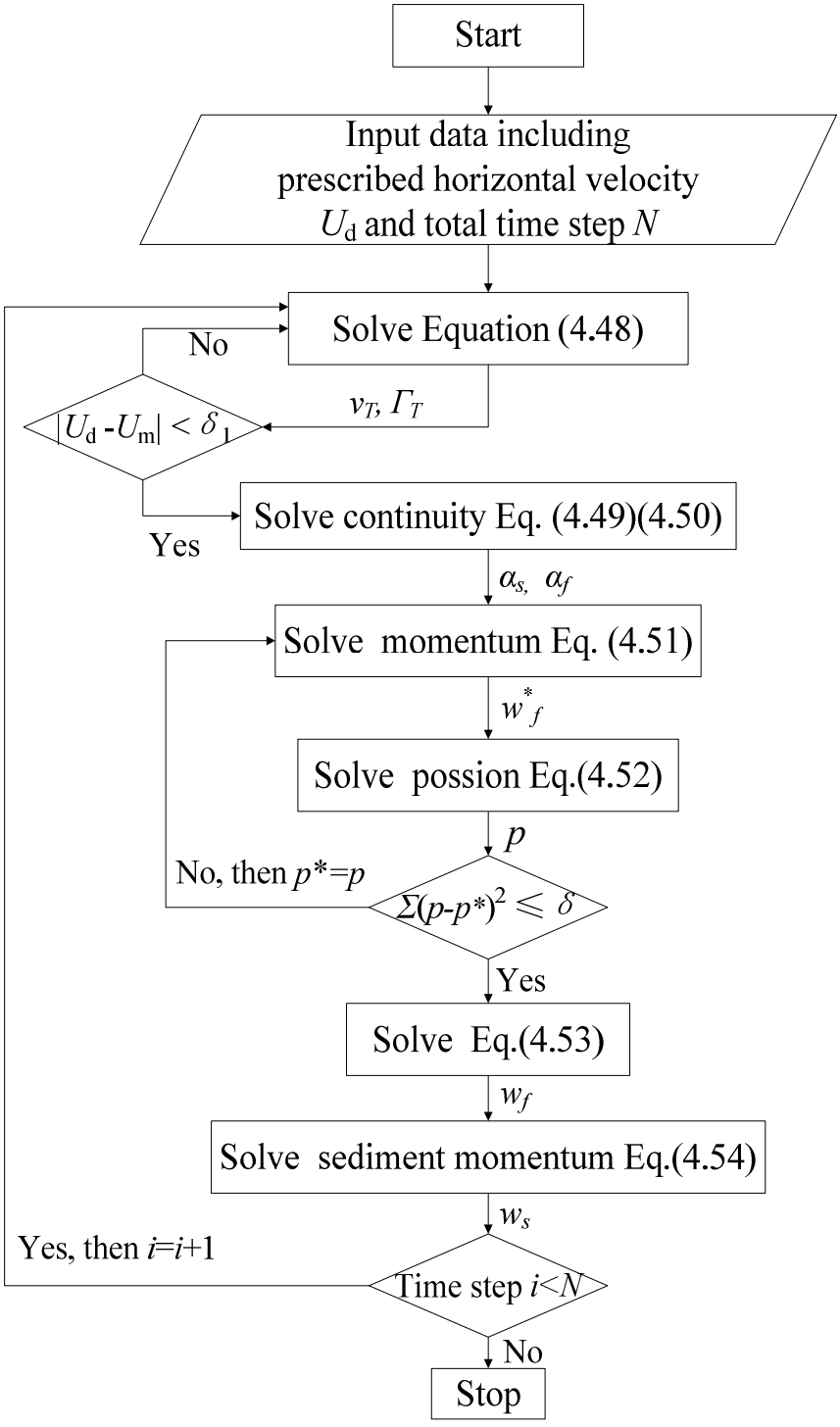

Figure 4.2 Flow Chart

4.5.3 Calculation procedure

As mentioned above, the two-phase model is discretized using finite differences and the discretized equations are solved using explicit-implicit methods. Six unknowns including two vertical velocities w_s and w_f, one horizontal velocity u, two volumetric concentrations α_s and α_f and the pressure p are solved with six equations (Equations (4.42)-(4.47)). The calculations procedures are summarized as below and also see the flow chart in Figure 4.2.

1) Input data including all kinds of initial values of parameters, variations of horizontal depth-averaged velocity U_d, variations of water depth h and total time step N
2) Solve Equation (4.48) for eddy viscosity ν_T and eddy diffusivity Γ_T, while the criteria $|U_d - U_m| < \delta_1$ should be satisfied. If yes, then go to the next step, if not resolve Equation (4.48)
3) Solve discretized Equations (4.49)-(4.50) for the volumetric fractions of fluid and solid phase (α_s, α_f) respectively
4) The pressure is initially set as $p^* = p^n$ and then solve discretized momentum Equation (4.51) for the intermediate fluid velocity w_f^*.
5) Solve discretized Possion Equation for pressure p, if $\sum (p - p^*)^2 \le \delta$ then go to next step, otherwise set $p^* = p$ and resolve the Equation (4.52)
6) Correct the settling velocity w_f of fluid phase and solve the discretized sediment momentum Equation (4.54) for the settling velocity w_s of solid

phase.

7) If time step $i < N$ then $i = i + 1$ and go to step 2. If no, then stop.

Chapter 5 Model validation and application

5.1 Model validation

In this section, the presented two-phase model is validated using experimental data for both cohesive and non-cohesive sediment carried out in vertical settling tanks. As in this study, the research is focused on the sedimentation of cohesive sediment, the stability and sensitivity analysis will be illustrated using cohesive sediment case. As in the vertical tank settling experiments, there is no horizontal velocity, $\overline{U}$ is assumed to be zero and so are the other variables in the model which are related with the horizontal velocity.

5.1.1 Non-cohesive sediment cases

Van Bang *et al.* (2008) carried out an experiments using spherical polystyrene beads settling in Rhodorsil silicone oil which was prepared in a cylindrical container with a base diameter of 50 mm and a height of 100 mm. The diameter and density of polystyrene are 0.29 mm and 1.05 kg/m^3 respectively. As for the Rhodorsil silicone oil the viscosity and density are 2×10^{-2} Pa·s and 0.95 kg/m^3. The polystyrene beads with an an initial solid volume fraction $\alpha_s = 0.48$ are well mixed in the container. During the experiments, the concentration profiles are measured at every 60 s and this data will be compared with numerical results. Equations (4.13) and (4.9) are used as the drag force and effective stress closures.

To set up the two-phase model, the coefficients included in the closures such as E, ν_p, erosion coefficient M, loose packing concentration for non-cohesive sediment α_s^* and maximum packing volume $\alpha_s^{\max}$ should be determined.

For polystyrene beads, the shear modulus E and Poisson ration ν_p are set as 3×10^9 Pa and 0. ξ is set as 4.5 which is determined through a trial and error method (Chauchat *et al.*, 2013). The loose packing concentration $\alpha_s^* = 0.57$ and the max packing sediment volume concentration $\alpha_s^{\max} = 0.6$.

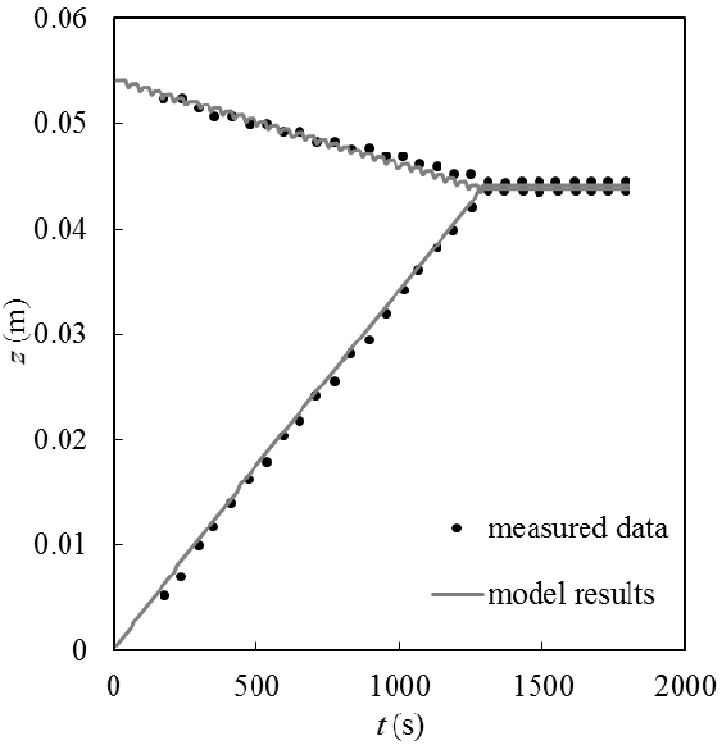

Figure 5.1 Experiments data of Van Bang *et al.* (2008) (black points) and numerical predictions of the interfaces of lower and upper positions (curves)

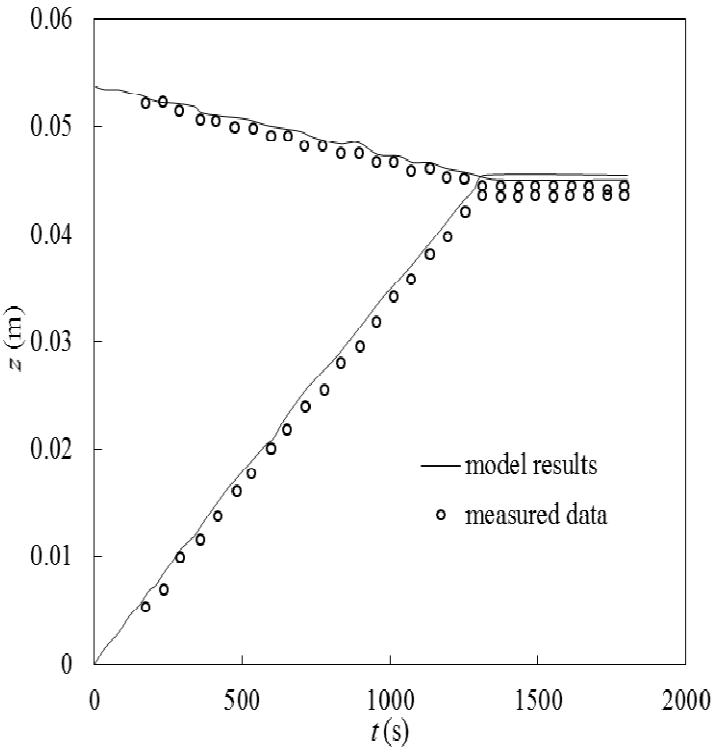

Figure 5.2 Experiments data of Van Bang et al. (2008) (black points) and numerical predictions of the interfaces of lower and upper positions (curves) from Chauchat et al. (2013)

Figure 5.1 shows the numerical results of interfaces (defined as $z_i^{up} = \max\left\{z \middle| \alpha_s \geq \alpha_s^0\right\}$ and $z_i^{low} = \max\left\{z \middle| \alpha_s \geq 0.5(\alpha_s^{\max} + \alpha_s^0)\right\}$) and the experimental data given in Van Bang *et al.* (2008). Figure 5.2 is the results from Chauchat et al. (2013). The predicted upper interface (Figure 5.1), which corresponds to the interface between the fluid phase and the solid phase, decreases linearly and shows a good agreement with the measured data. The lower interface, which is defined as the interface between granular bed and the suspension, increases linearly and meets with the upper interface at roughly 1200s. After that the interface remains constant.

To illustrate the sensitivity of the model results when small changes occur to the concentration that defined as the upper interface and lower interface, the model results

are shown in Figure 5.3 (upper interface) and Figure 5.4 (lower interface). As the upper interface shown in Figure 5.1 is defined as $z_i^{up} = \max\left\{z \middle| \alpha_s \geq \alpha_s^0\right\}$, in which $\alpha_s^0 = 0.48$, the upper interfaces shown in Figure 5.3 are defined as $z_i^{up} = \max\left\{z \middle| \alpha_s \geq \eta\right\}$ (triangles $\eta = 0.46$, diamonds $\eta = 0.47$ and squares $\eta = 0.49$). As the lower interface shown in Figure 5.1 is defined as $z_i^{low} = \max\left\{z \middle| \alpha_s \geq 0.5(\alpha_s^{\max} + \alpha_s^0)\right\}$, in which $0.5(\alpha_s^{\max} + \alpha_s^0) = 0.54$, the interfaces shown in Figure 5.4 are defined as $z_i^{low} = \max\left\{z \middle| \alpha_s \geq \lambda\right\}$ (triangles $\lambda = 0.53$, diamonds $\lambda = 0.545$ and squares $\lambda = 0.55$). From Figure 5.3 and Figure 5.4 it can be seen that the predicted upper/lower interfaces are almost the same when small changes occurs to η / λ, which demonstrates that the model results of predicted interfaces are not sensitive when there are small changes to the definition of upper and lower interfaces.

The numerical results of the transient profiles of sediment concentration and the measured data are presented in Figure 5.5. Also the model results from Chauchat et al. (2013) are presented in Figure 5.2 and Figure 5.6 for comparison. It can be seen that the results of predicted interfaces presented in Figure 5.1 (our model) are better than those in Figure 5.2, while the results of predicted concentration profiles presented in Figure 5.6 are better than those in Figure 5.5 (our model). This maybe because the different values of Richardson-Zaki coefficient are adopted. In the current study, the value is 4.65, which is suggested by.Richardson and Zaki (1954), while in the work of Chauchat et al. (2013), 5.15 is adopted. As the initial condition of sediment concentration gradient is large, oscillations occur in the upper interfaces due to numerical instability. It can be seen that both numerical model results match well with the measured data. And in the lower part of

the sediment concentration profile, the volumetric fraction of sediment particles almost reaches the maximum packing value (around 0.6), which shows a clear demonstration of the capability of the presented model.

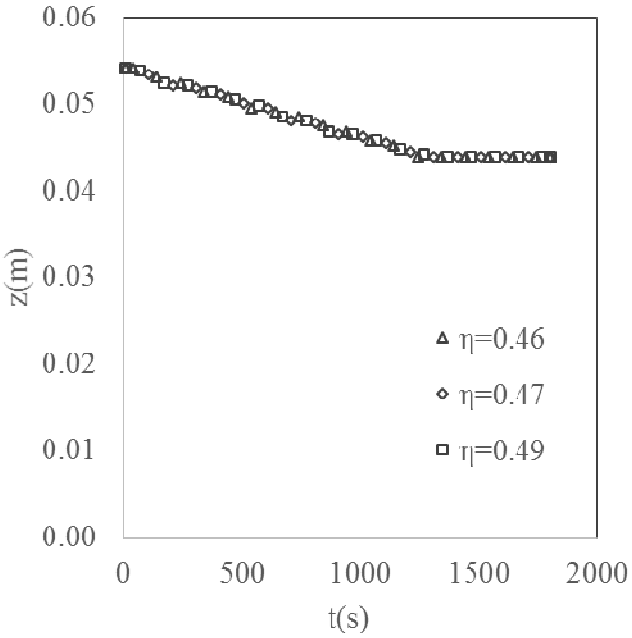

Figure 5.3 Numerical predictions of the interfaces of upper positions. $z_i^{up} = \max\{z|\alpha_s \geq \eta\}$ (triangles $\eta = 0.46$, diamonds $\eta = 0.47$ and squares $\eta = 0.49$).

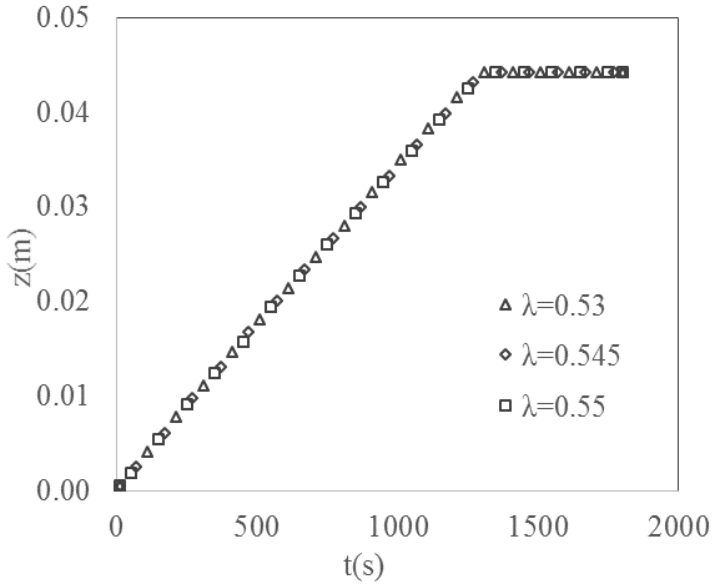

Figure 5.4 Numerical predictions of the interfaces of lower positions. $z_i^{low} = \max\{z|\alpha_s \geq \lambda\}$ (triangles $\lambda = 0.53$, diamonds $\lambda = 0.545$ and squares $\lambda = 0.55$).

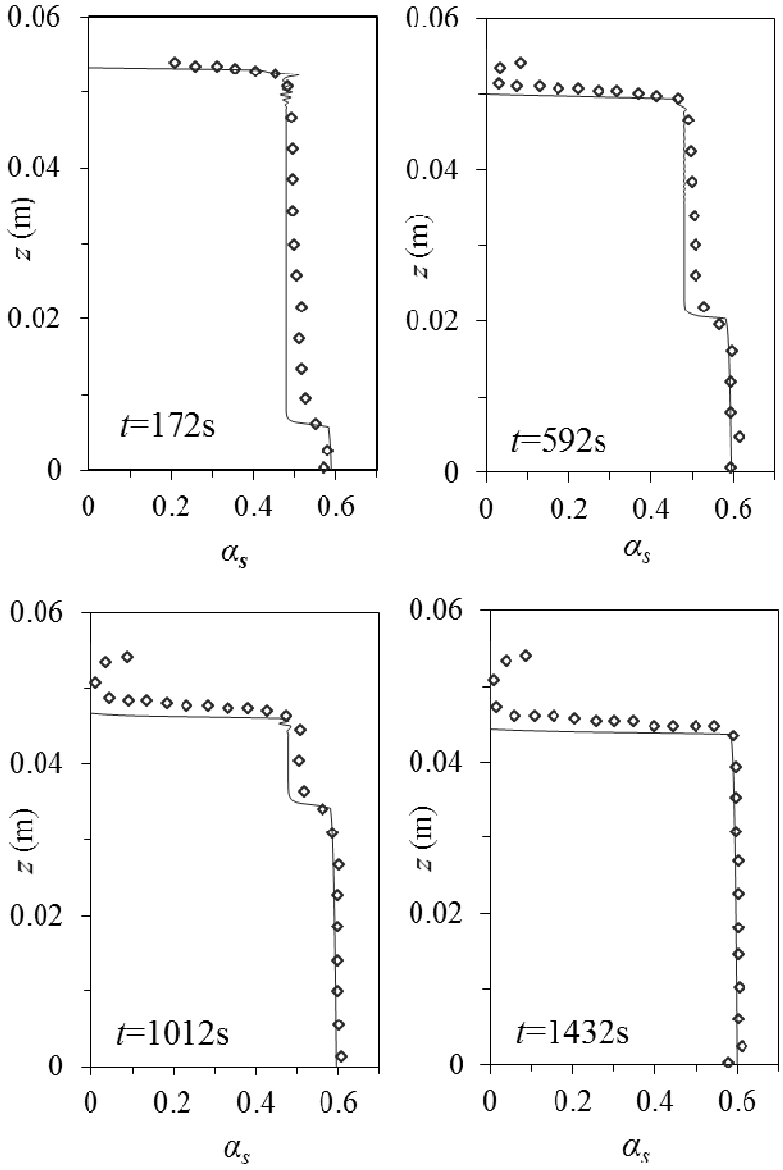

Figure 5.5 Experiment data of Van Bang *et al.* (2008) (diamonds) and calculated sediment concentration profiles (solid curves)

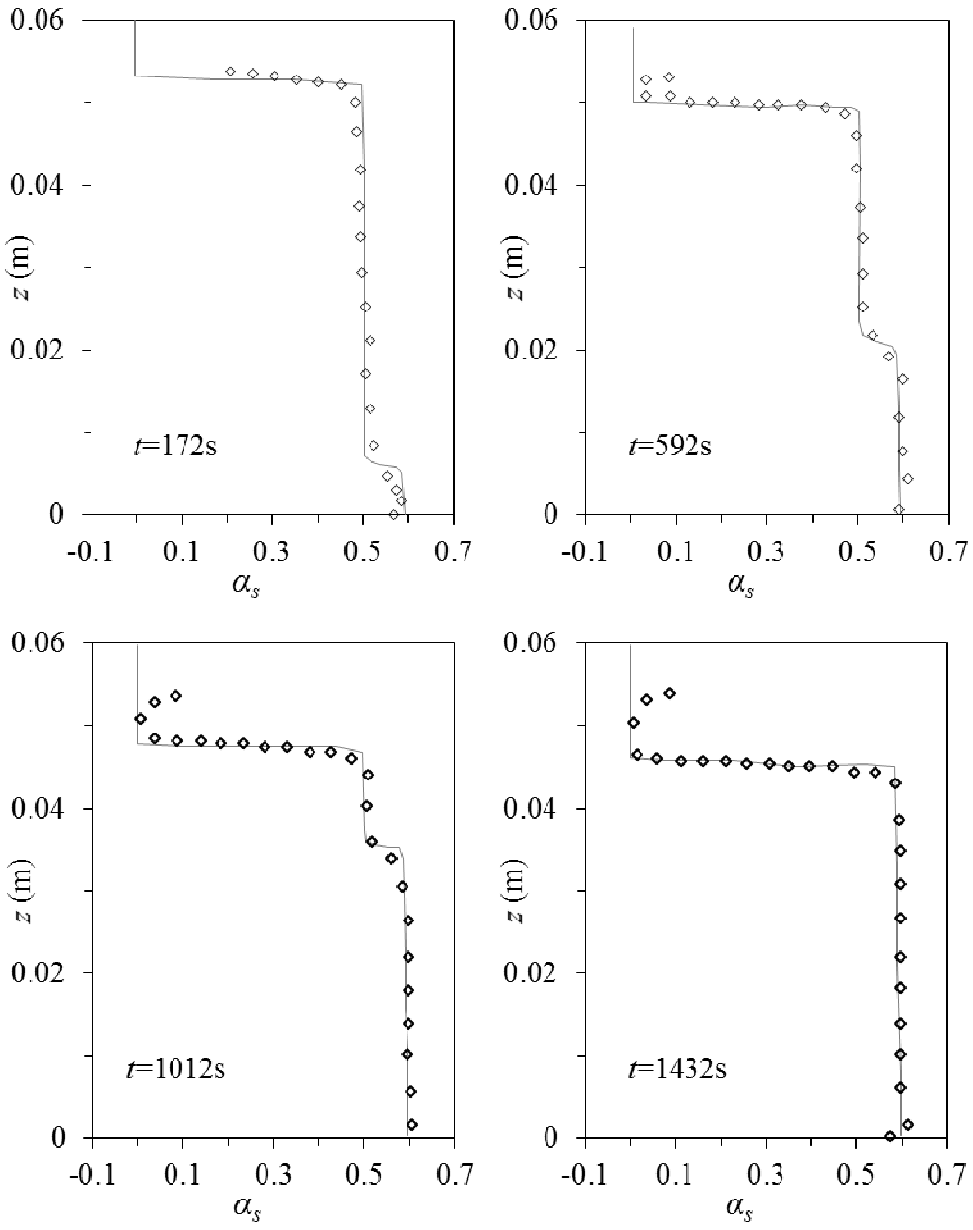

Figure 5.6 Experiment data of Van Bang et al. (2008) (diamonds) and calculated sediment concentration profiles (solid curves) from Chauchat et al. (2013)

5.1.2 Cohesive sediment case

The experimental data from Le Havre (Chauchat *et al.*, 2013) are chosen to validate the two-phase model, especially the drag force and effective stress presented in Equation (4.18) and (4.14). The median diameter and density of the mud are 7.5×10^{-6} m and 2590

kg/m^3, respectively. In the original experiments, the initial volume fractions of 1.2, 2.2 and 5.2% of the mud are homogeneously distributed in the settling column. As these experiments only serve to validate the accuracy of developed two-phase model, the parameters in the various closure models such as W_0 , n , α_s^{gel} , χ , σ_0 and $\alpha_s^{\max}$ are specified using the values obtained by Chauchat *et al.* (2013) based on the same experimental data listed in Table 5.1.

Table 5.1 The fitting parameters used in simulation of sedimentary-consolidation process of cohesive sediment

Parameters	W_0 (m/s)	n	α_s^{gel}	χ	σ_0 (Pa)	$\alpha_s^{\max}$
Value	2×10^{-4}	2.55	0.025	1.283	0.14	0.14

Figure 5.7 shows the calculated and measured interfaces between the clear fluid and suspension zones. The settling curves match well with experimental data for all three initial volume fractions. It is noticed that for the initial volumetric fraction at 1.2%, a slope break occurs as it is in the transition zone from hindered settling to the early stage of consolidation in which permeability is dominant. For the initial volume fraction at 5.2%, the settling velocity of interface is a little bit faster than the measured data, it can be explained that the initial concentration is larger than the gelling concentration and the settling velocity calculated using Equation (4.18), which is calibrated using the lower initial concentration case (1.2%), is not applicable. With the permeability and effective stress calibrated using the initial volumetric solid fraction of 1.2% and 5.2% respectively, the parameters obtained are applied to all of the three settling experiments.

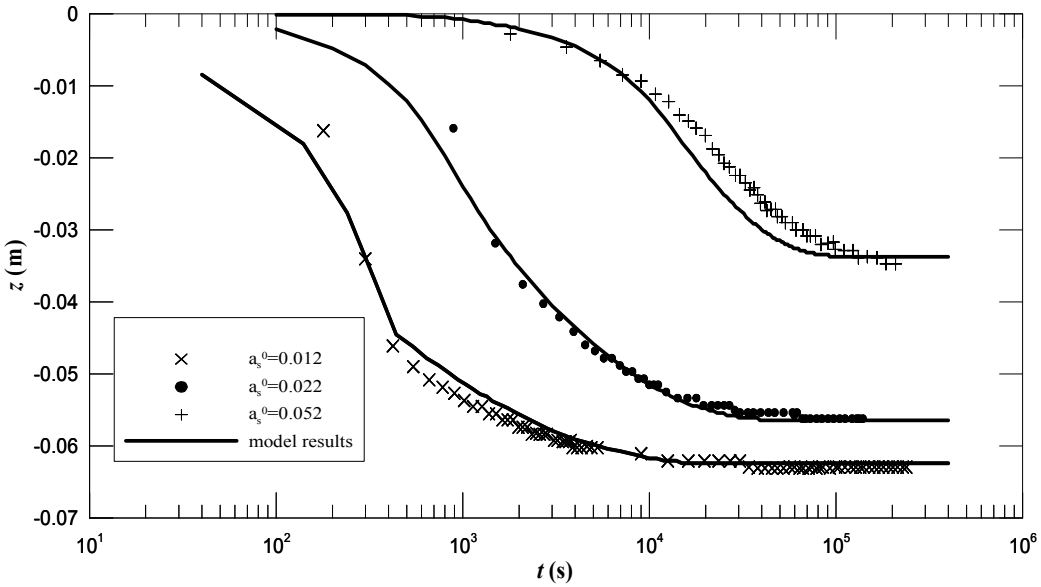

Figure 5.7 The experiments data (symbols) and calculated interface (lines) between clear water and mud suspension with initial sediment volumetric concentration of 1.2, 2.2 and 5.2%.

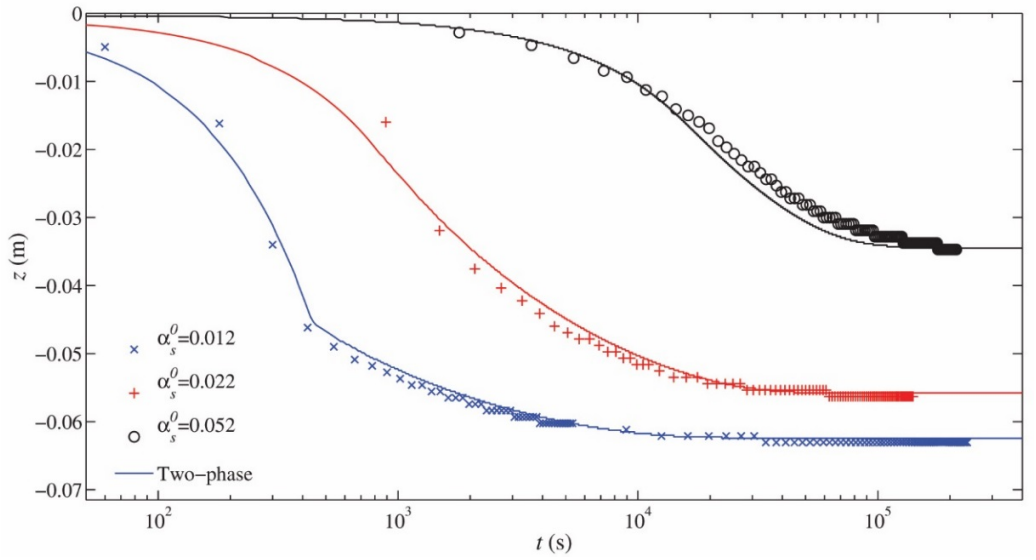

Figure 5.8 The experiments data (symbols) and calculated interface (lines, by Chauchat *et al.* (2013)) between clear water and mud suspension with initial sediment volumetric concentration of 1.2, 2.2 and 5.2%.

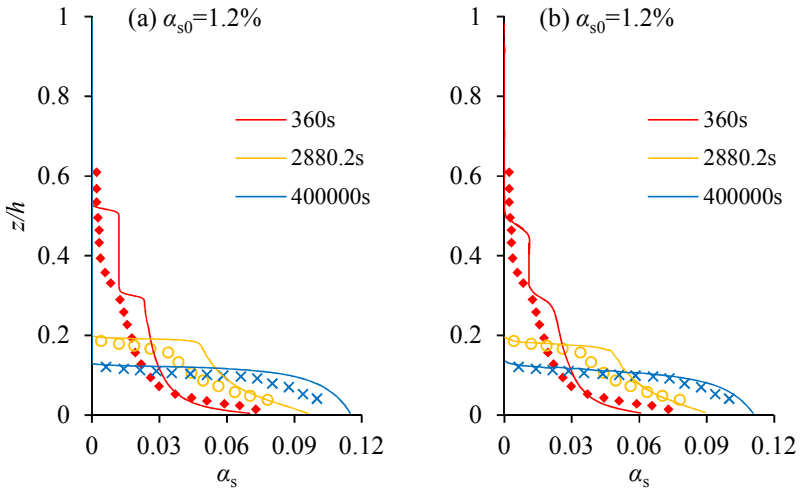

Figure 5.9 The experiments data (points) and numerical results (lines) of sediment concentration profile with initial volumetric sediment concentration of 1.2%. (a) numerical results by current study, (b) numerical results by Chauchat *et al.* (2013)

The measured sediment concentration profiles and numerical results are presented in Figure 5.9a (1.2%), Figure 5.10a (2.2%) and Figure 5.11a (5.2%). Unlike for the non-cohesive sediment case, the mud concentration keeps increasing with the interface between clear fluid and suspension moving upward. This is because for the non-cohesive sediment, a rigid bed is formed immediately almost as soon as the sand particles reaching the bottom and the concentration becomes almost constant. For the cohesive sediment case, due to the loose arrangement of fine primary particles in the flocs, tiny flow tubes are formed on the settling bed and the drainage processes last longer.

The model result of initial solid fraction of 2.2% case matches well with experiment data while for the case with initial solid fraction of 5.2% the comparison is worse. Because in this case the consolidation process starts at the very beginning of the experiment, the permeability characteristics are different from the experiment with initial solid fraction of 1.2%, but parameters used in the permeability closures were calibrated only for mud with initial solid fraction of 1.2%.

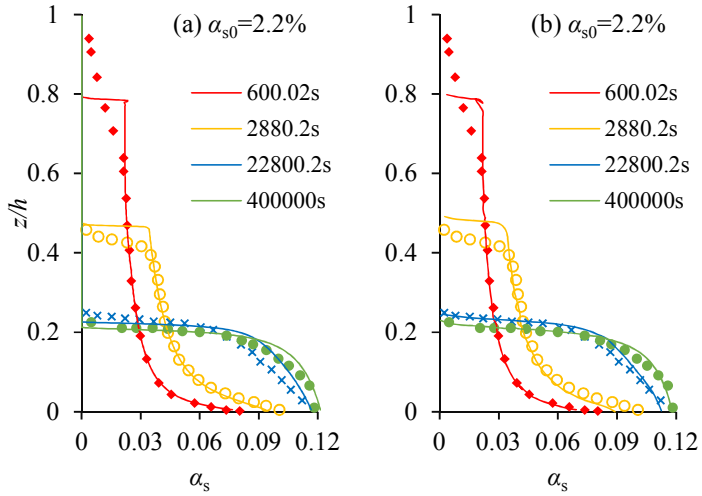

Figure 5.10 The experiments data (points) and numerical results (lines) of sediment concentration profile with initial volumetric sediment concentration of 2.2%. (a) numerical results by current study, (b) numerical results by Chauchat *et al.* (2013)

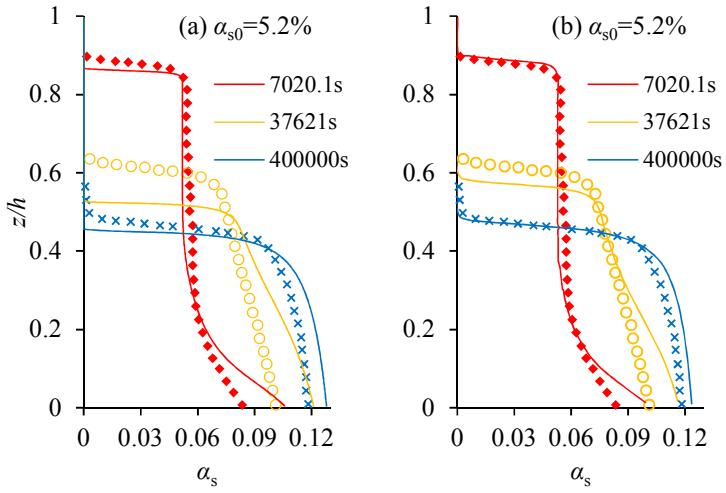

Figure 5.11 The experiments data (points) and numerical results (lines) of sediment concentration profile with initial volumetric sediment concentration of 5.2%. (a) numerical results by current study, (b) numerical results by Chauchat *et al.* (2013)

The numerical results from Chauchat *et al.* (2013) (Figure 5.8, Figure 5.9b, Figure 5.10b and Figure 5.11b), in which the flocculation process is not modelled, are presented as a comparator. As the modelling of sediment processes is only used to validate the

accuracy of two-phase model, to keep consistent with Chauchat et al. (2013), the flocculation process is not included. Instead a constant settling velocity of the flocs W_0 $=2.4\times10^{-4}$ m/s in dilute situation is used. In reality, the size and density of mud flocs change constantly during flocculation process and so is the settling velocity. The calculated results in this dissertation compare well with results from Chauchat *et al.* (2013). The presented two-phase model seems to be capable of capturing the main features of the cohesive sediment laboratory experiment.

Sensitivity analysis for cohesive sedimentation against grid and time step is presented in Figure 5.12-Figure 5.15. The calculated interface and concentration profile are not sensitive to selected time step (Figure 5.12 and Figure 5.13) when the time step is less than 1s and the model converges when time step reduces, whereas the model diverges when the time step larger than 1.4 s. From Figure 5.14 and Figure 5.15 show that the model results are not sensitive to grid size (grid size less than 0.001 m). When time step is set at 0.01 s, the model converges as expected when grid size less than 0.001 m.

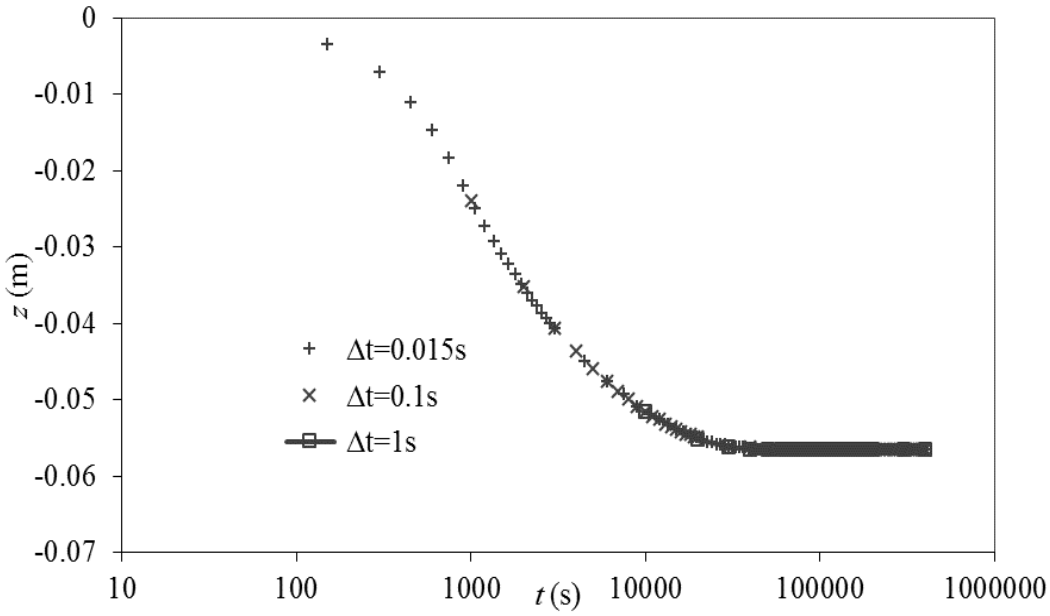

Figure 5.12 The calculated interface curves at Δz=0.00033 m, Δt=0.015 s, Δt=0.1 s and Δt=1 s with initial volumetric sediment concentration of 2.2%.

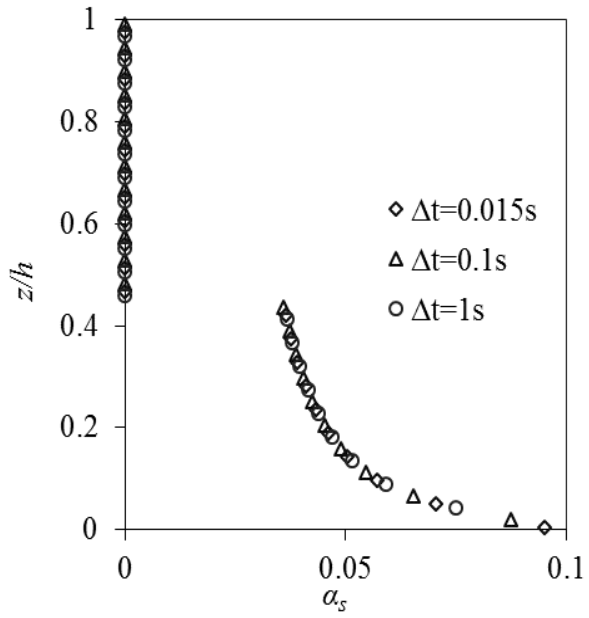

Figure 5.13 The calculated concentration profile at at Δz=0.00033 m, t=2700 s. Δt=0.015 s, Δt=0.1 s, and Δt=1 s with initial volumetric sediment concentration of 2.2%.

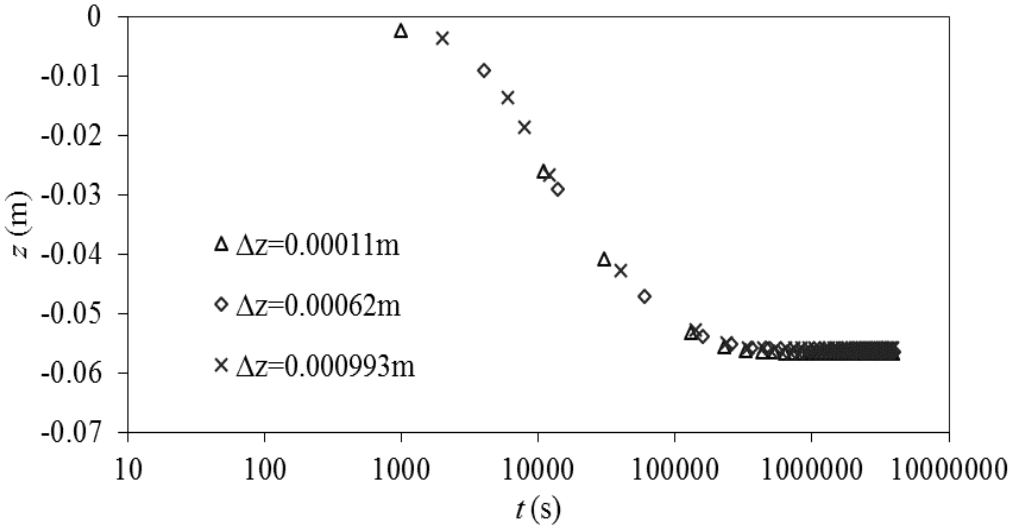

Figure 5.14 The calculated interface curves Δz=0.00011 m, Δz=0.00062 m and Δz=0.00093 m when Δt=0.01 s with initial volumetric sediment concentration of 2.2%.

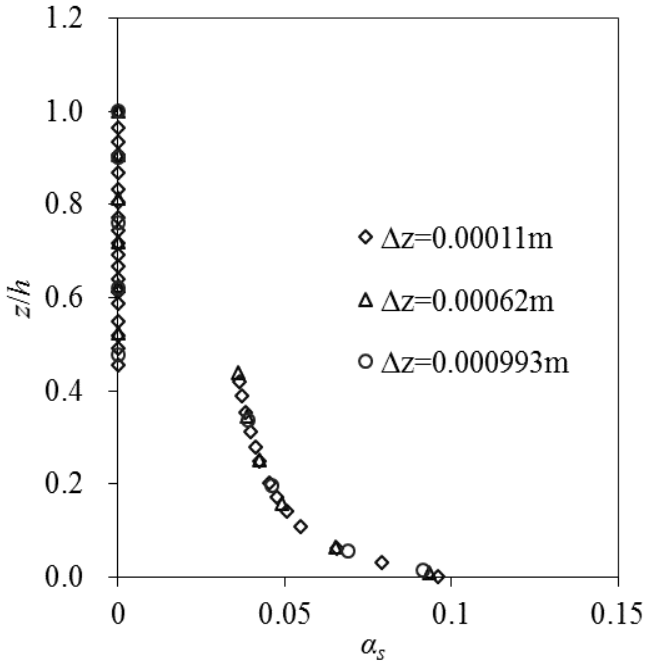

Figure 5.15 The calculated concentration profile at t=2700 s (Δt=0.01 s). Δz=0.00011 m, Δz=0.00062 m and Δz=0.00093 m with initial volumetric sediment concentration of 2.2%.

5.2 Numerical modeling of sediment suspension in the EMS/ Dollard estuary

5.2.1 Introduction

The EMS/ Dollard estuary is an ebb current dominated estuary (Dyer *et al.*, 2000; Talke and de Swart, 2006; van der Ham and Winterwerp, 2001). The intra-tidal variations in SSC are influenced by sediment availability, horizontal sediment transport and more importantly vertical mixing, as the horizontal sediment transport is also governed by local sedimentation/resuspension features (van Leussen, 2011). It is known the SSC in the water column during both flooding and ebbing phases does not show significant difference (Van der Lee, 2000) and sediment flux is even flood dominant (Dyer *et al.*, 2000). There also exist time lags between current velocity and SSC. It was also often observed that the SSC stops increasing before the maximum current velocity is being reached, which is a clear indication of limited sediment availability (van der Ham and Winterwerp, 2001; Van der Lee, 2000). During the deceleration period, the SSC decreases quickly commonly referred to as “rapid settling” which was explained as the results of over saturation or formation of large mud flocs (van Leussen, 2011).

A new closure of drag force, which combines the flocculation and hindered settling effects, is incorporated into the model. Once settled on the seabed, mud flocs normally start to consolidate, generating a network of permanent contacts between particles and causing the erodibility of the bed to change. This process, named as consolidation, has recently been considered in cohesive sediment transport models. In the present model, it is incorporated using the classic effective stress concept in soil mechanics. The new two-

phase model is applied to simulate sediment transport in Ems/Dollard estuary over two time periods during which tide currents are dominant. The results indicate that the model is capable of capturing the overall features of the sediment transport process and the proposed drag force closure can describe accurately the flocculation mechanism of cohesive sediment at this site.

5.2.2 Model set up and materials

In the current application, the suspended sediment concentration is around 1 kg/m^3 within the calculation domain. It means the consolidation stage does not appear because the sediment concentration is less than the gelling concentration the value of which suggested by Chauchat *et al.* (2013) is 0.025 (66.25 kg/m^3). Therefore, the effective stress σ_e term, which is introduced to describe the residence of solid compaction, is removed. And the EMS/Dollard Estuary is dominated by currents, Equation (4.31) and (4.41) are adopted as the boundary conditions.

In modeling cohesive sediment process, the time scale is an important factor. It has been found that a positive correlation between floc sizes and suspended sediment concentration (SSC) exists on a tidal time scale while on the seasonal time scale the floc sizes can be more crudely and simply described on the basis of the cohesive sediment characteristics (Van der Lee, 2000). The model application to be described is therefore intentionally focused on the tidal time scale so as to examine more critically the capability of the developed 1DV two-phase model.

High frequency field measurements of flow velocities and suspended sediment concentration (SSC) in a tidal channel of Ems/ Dollard Estuary are reported by Van Der Ham *et al.* (2001). As the horizontal variation of sediment flux is small, the horizontal

gradient of SSC may be taken as zero so that the present 1DV two-phase model is expected to be applicable to compare with the measured data.

The data for two time periods, one from 27/Jun/1996 at 02:00 to 28/Jun/1996 at 02:00 and the other one from 08/Aug/1996 at 00:00 to 09/Aug/1996 at 02:00, are considered. The former is denoted as Data 1 and the latter as Data 2. The time varying averaged flow velocity $\overline{U}$ and water depth h for Data 1 and Data 2 are used as inputs to the model. As a fixed time step t=1 s is used in the model all the inputs between the measured data points are determined using a linear interpolation.

The stratification effects are negligible with a low SSC, and a roughness height of 2×10-3 m and the erosion rate for mud M=1.54×10^{-8} m/s is selected following van der Ham and Winterwerp (2001). The settling velocity w_0=1.54×10^{-8} m/s that is adopted in the study is the same as suggested by van der Ham and Winterwerp (2001) and is in line with the range found by van Leussen (2011). The critical shear stress for erosion τ_{cr} is specified as 0.1 Pa, which is the average critical shear stress suggested by Kornman and De Deckere (1998) for sediment erosion studies in an adjacent tidal flat. Similarly, the critical shear stress for deposition is set as 0.1 Pa. The flocculation process is investigated only based on the relationship between sediment concentration and settling velocity given by Equation (4.19).

5.2.3 Model results and discussion

5.2.3.1 *June data*

The numerical simulation of the measurements from 27/Jun/1996 at 02:00 to 28/Jun/1996 at 02:00 with/without the effects of flocculation is addressed as Run

JWF/JNF. The Equations (4.14) and (4.19) are used in Run JWF, the new drag force closure is to take the flocculation effects into consideration, while in Run JNF Equations (4.14) and (4.18) are used in which the flocculation effects are ignored. van Leussen (1999) carried out in-situ measurements in Ems/Dollard and found a number of relationships exist between settling velocities and sediment concentration, even within a single estuary. As w_0 represents the averaged settling velocity of mud flocs and $k_1 C^m$ represents the settling velocities of mud flocs considering flocculation effects which relates to sediment concentration, here we follow van der Ham and Winterwerp (2001) and w_0, k_1 and m are specified as 5×10^{-4} m/s, $1.5\times10^{-3}(\mathrm{m/s})\bullet(\mathrm{g/L})^{-m}$ and 1.2 for Data 1 in which the sediment concentration is less than 1 g/L, while for Data 2 in which the sediment concentration is less than 0.5 g/L. w_0, k_1 and m are specified as 5×10^{-4} m/s, $2.5\times10^{-3}(\mathrm{m/s})\bullet(\mathrm{g/L})^{-m}$ and 1.2 respectively. More details about the parameters used in the model simulation can be seen in Table 5.2 for Data 1 and in Table 5.3 for Data 2.

Table 5.2 The fitting parameters used in the simulation of Data 1

Run	w_0 (m/s)	$k_1(\mathrm{m/s})\bullet(\mathrm{g/L})^{-m}$	m	M (m/s)	Buoyancy effects
JWF	5×10^{-4}	–	–	1.54×10^{-8}	Included
JNF	–	1.5×10^{-3}	1.2	1.54×10^{-8}	Included

Figure 5.16 presents the measured and calculated shear stress at 0.4 m above the bed. Figure 5.16 shows that the calculated curves for both Run JWF (solid line) and JNF (dashed line) compare well with the measured data. This proves the effectiveness of the presented 1DV two-phase model. It is can be noticed that the shear stress calculated from Run JWF (solid line) is coincident with shear stress calculated from Run JNF (dashed

line), which indicates that under low sediment concentration the effects of flocculation process on shear stress is negligible. The flow structure is hardly affected when the SSC is less than 1 kg/m^3, which is consistent with the conclusion from the work of van der Ham and Winterwerp (2001). It should be mentioned that the shear stresses calculated near the bed for Run JWF and Run JNF are almost the same as well as the values of critical shear stress for erosion and deposition adopted in the model. As there is no sediment availability limitation, the difference of the mass of sediment suspended in the water column for both Runs should be determined using Equation (4.41). From the discussion above, it is concluded that the different distribution of SSC for both Runs is mainly due to the different settling velocity w_s which will be illustrated in detail below.

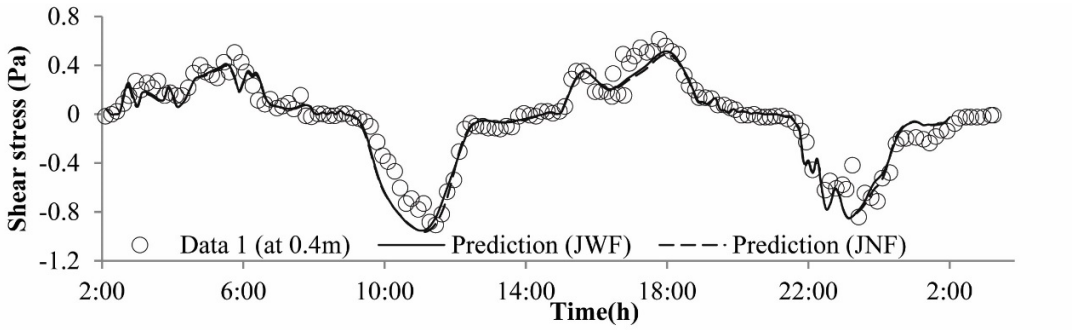

Figure 5.16.The measured shear stress by Van Der Ham *et al.* (2001) at 0.4 m above the bed (cycles) in June measuring period and numerical prediction from Run JWF (solid curve with the effects of flocculation) and Run JNF (dashed curve without the effects of flocculation)

The measured and calculated variations of sediment concentration at 0.7 m above the bed are presented in Figure 5.17. The numerical results of variations of sediment concentration during the two tidal cycles for both Runs (with/ without the effects of flocculation) seem to follow broadly the trend of measured data except for an abrupt increase of measured sediment concentration at the very start of the first tidal cycle, which is explained as a local increase of the rate of sediment erosion. The model results

with the effects of flocculation (solid line) match well with measured data while those ignoring the flocculation process (dashed line) show less favorable agreement. It can be easily noticed that a lower value of sediment concentration during the slack water time of tidal cycles is predicted by Run JNF, while during the acceleration time, a much higher sediment concentration is predicted compared with the measured data. During the acceleration time of the first tidal cycle, the calculated sediment concentration peaks can even be twice as the experiment data. The discrepancy does not appear between the numerical results from run JWF and field measurements. And it is more likely caused by different settling velocities calculated when flocculation process is incorporated. More details are illustrated below:

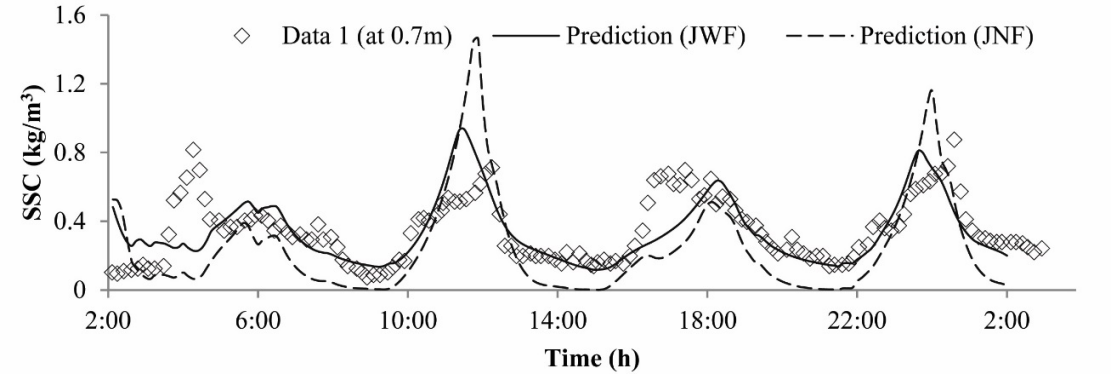

Figure 5.17.The measured variations of SSC by Van Der Ham *et al.* (2001) at 0.7m above the bed (diamonds) in June measuring period and numerical prediction from Run JWF (solid curve with the effects of flocculation) and Run JNF (dashed curve without the effects of flocculation)

In Equation (4.18), which is adopted for Run JNF, the first term on the right side is the settling velocity w_0, which is treated as a constant for mud flocs in dilute situation, while in Equation (4.19), adopted for Run JWF, the first term on the right side is $k_1 C^m$, which describes the effect of flocculation on the settling velocity. By solving the momentum equation of the two-phase model, a positive correlation between the value of

$k_1 C^m$ and the settling velocity w_s is found. As the term $k_1 C^m$ increases with the sediment concentration, the finally calculated settling velocity w_s will increase with sediment concentration (for C≤ 3 kg/m^3 the hindered settling effects are unimportant). According to Equation (4.41), the sediment is eroded when the bed shear stress exceeds the critical shear stress for erosion, otherwise the sediment will settle onto the bed. The settling velocity is the key parameter in determining the sediment flux on the bed surface. During the slack time, the SSC is lower due to the weak flow. A lower SSC corresponds to a lower settling velocity and thus less sediment deposit on the bed for Run JWF, while for Run JNF a larger settling velocity is obtained due to the constant value w_0 in the drag force closure, which causes the amount of sediment deposited on the bed to be overestimated. Therefore the variations of sediment concentration calculated for Run JNF are lower than field measurements. In the acceleration time of tidal cycle, the SSC is high due to the strong flow dynamics. A higher sediment concentration (but less than 3 kg/m^3) results in large settling velocities for Run JWF which prevents the sediment being diffused up in the water column, while for Run JNF the settling velocities are underestimated and higher sediment concentration peaks are calculated than that of the measurements.

5.2.3.2 *August data*

The model simulation of the measurements from 08/Aug/1996 at 00:00 to 09/Aug/1996 at 02:00 with/ without the consideration of flocculation process is denoted as Run AWF/ANF. Equations (4.14) and (4.19), which incorporate the effects of flocculation on the transport of cohesive sediment, are adopted in Run AWF while in Run ANF, which is the control study, Equations (4.14) and (4.18) are used without

considering the effects of flocculation on the transport of cohesive sediment. It has been found by Kornman and De Deckere (1998) that an increased critical shear stress for erosion will affect the availability of sediment in the adjacent tidal flat. As it is beyond the scope of the current study, here we follow van der Ham and Winterwerp (2001) using a maximum depth-averaged sediment concentration $C_{\max}$ to account for the mechanism in both Runs. All parameters that are used in the model simulation are listed in Table 5.3

Table 5.3 The fitting parameters used in the simulation of Data 2

Run	w_0 (m/s)	k_1(m/ s)•(g/ L)$^{-m}$	m	M (m/s)	$C_{\max}$ (kg/ m^3)	Buoyancy effects
AWF	5×10^{-4}	–	–	1.54×10^{-8}	0.25	Included
ANF	–	2.5×10^{-3}	1.2	1.54×10^{-8}	0.25	Included

The measured and calculated shear stresses from both Run AWF and Run ANF at 0.4m above the bed are presented in Figure 5.18. It can be seen that the shear stresses calculated in both Runs (solid curve for Run AWF and dashed curve for Run ANF) match the measurements well and there are almost no difference between the two numerical results. The shear stress seems to be hardly affected by the flocculation process for low sediment concentration which is consistent with the conclusion from the simulation of June measuring period.

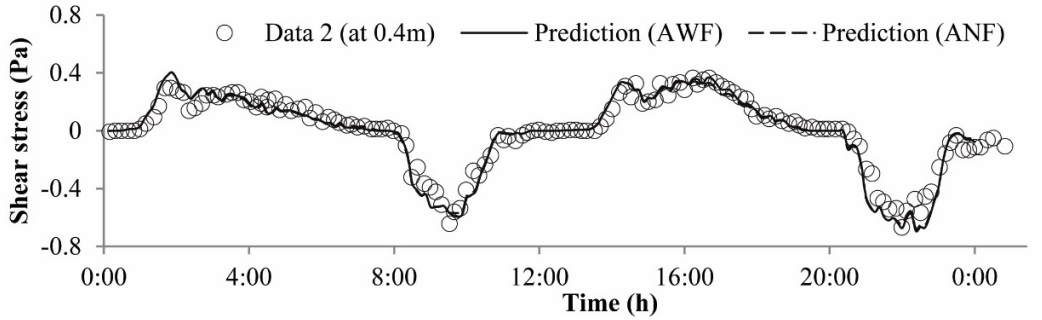

Figure 5.18.The measured shear stress by Van Der Ham *et al.* (2001) at 0.4m above the bed (cycles) in August measuring period and numerical prediction from Run AWF (solid curve with the effects of flocculation) and Run ANF (dashed curve without the effects of flocculation)

The model results for both Runs and measured sediment concentration at 0.7 m and 1.4 m above the bed are shown in Figure 5.19 and Figure 5.20, respectively. As shown in Figure 5.19, the numerical results generally follow the trend of measured data. However, the calculated sediment concentration peaks of Run ANF are higher during ebbs. The results of Run AWF, which includes the effects of flocculation through Equations (4.14) and (4.19), fit well with field measurements during both floods and ebbs. Figure 5.20 shows that the model results of Run AWF (solid curve) compare well with experimental data while a lower sediment concentration is predicted by Run ANF (dashed curve). It can be concluded that for Run ANF, a higher value of sediment concentration peaks is predicted in the lower part of the water column (0.7m Figure 5.19 The measured variations of SSC by Van Der Ham *et al.* (2001) at 0.7m above the bed (diamonds) in August measuring period and numerical prediction from Run AWF (solid curve with the effects of flocculation) and Run ANF (dashed curve without the effects of flocculation) This can be easily explained for Run ANF, which is under low sediment concentration and the effects of hindrance can be neglected. Without considering flocculation effects,

the settling velocities calculated in the model are almost constant throughout the water column. Therefore, the settling velocities are relatively small in the lower part of the column (0.7m), which cannot prevent the sediment being diffused up from the lower layer. Whereas, the settling velocities are relatively large in the upper part of the water column. The downward sediment flux is overestimated, which leads to the lower calculated SSC. In the Run AWF with flocculation effects included, the settling velocities predicted by the model vary over a large range throughout the water column, which is closer to the real situation. With a more realistic settling velocity profile in Run AWF, the discrepancy between the measured SSC and calculated results from Run AWF does not appear.

Overall, it can be concluded that more accurate predictions are obtained when the flocculation effects are considered. As the sediment concentration is less than 1 g/L for both measuring periods and even less than 0.5 g/L for the August measuring period, the results indicate that the flocculation process plays an important role even in a low sediment concentration environment.

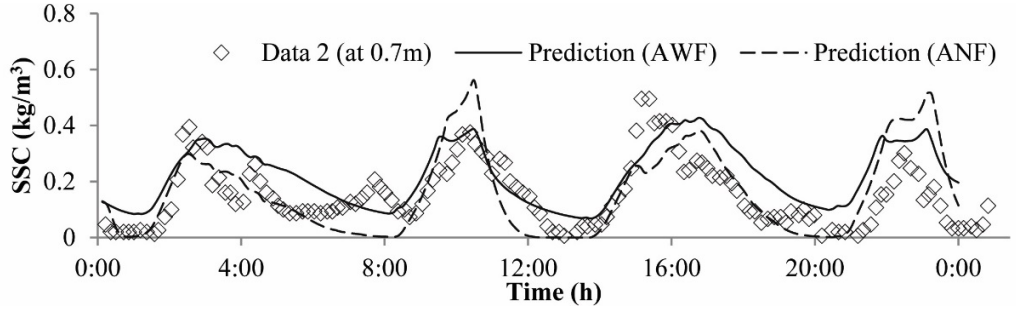

Figure 5.19 The measured variations of SSC by Van Der Ham *et al.* (2001) at 0.7m above the bed (diamonds) in August measuring period and numerical prediction from Run AWF (solid curve with the effects of flocculation) and Run ANF (dashed curve without the effects of flocculation)

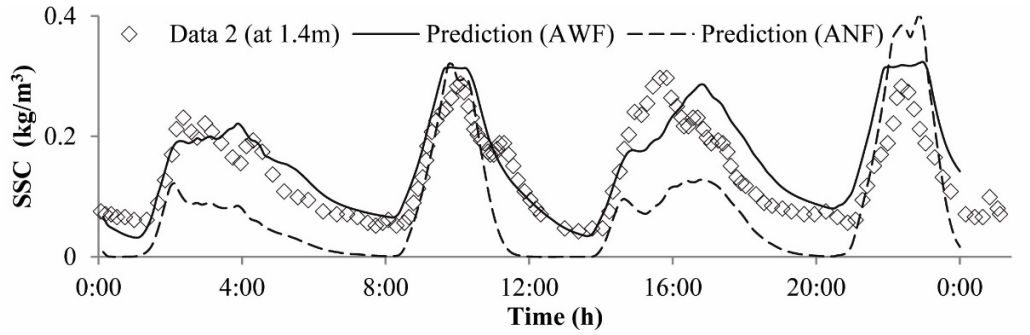

Figure 5.20 The measured variations of SSC by Van Der Ham *et al.* (2001) at 1.4m above the bed (diamonds) in August measuring period and numerical prediction from Run AWF (solid curve with the effects of flocculation) and Run ANF (dashed curve without the effects of flocculation)

5.2.4 Summary

The two-phase model is applied to the simulation of sediment suspension of EMS/Dollard estuary. A new drag force closure which takes the flocculation process into consideration is incorporated with the two-phase model and the model is validated with field measurements in Ems/Dollard estuary, which demonstrates the efficiency of the model in simulating sediment suspension with tidal currents. The model results indicate that the dissipation of turbulence caused by the existence of suspended sediment is so weak because of low sediment concentration (less than 1 kg/m^3 for Data 1 and less than 0.5 kg/m^3 for Data 2) that the shear stress can be hardly affected. However, the flocculation process has been proved important even under low sediment concentration. The models results considering the flocculation effects show a better prediction than that without flocculation effects. With a new drag force closure, which considered the flocculation process, a more realistic settling velocity profile is calculated and so is a more accurate sediment concentration profile. Apart from confirming the efficiency of new drag force closure, the accurate prediction further reveals that the flocculation effects have to be considered in the simulation of sediment suspension in EMS/Dollard estuary.

5.3 Studying sedimentary processes on an erosional mudflat at Yangtze River Delta

5.3.1 Introduction

Tidal wetlands are among the most economically important as well as the most vulnerable ecosystems in the coastal zones. Rapid economic development in large part of the world has resulted in the loss of tidal wetlands at an alarming rate due to their direct conversion into land for industrial and aquaculture uses. Understanding sedimentary processes in tidal wetlands in general and estuarine mudflats in particular, such as how they may adapt to sea-level rise, and what the key links between ecology and geomorphology are, is important for better preservation and sustainable development of these valuable resources (Liu *et al.*, 2015; Montserrat *et al.*, 2011; Shi *et al.*, 2012; Zhu *et al.*, 2014).

Apart from some areas where the evolution of tidal wetland is due to peat accumulation, most progradational wetlands are due to deposition of sediments (Shi *et al.*, 2012). Therefore, morphological evolution of these mudflats is significantly influenced by sedimentary processes including sediment settling, transport, deposition and re-suspension (Kirwan and Murray, 2007), driven usually by a combination of tides and waves (Shi *et al.*, 2012). Numerous numerical studies, laboratory experiments and field observations have been carried out on the sedimentary processes under various flow conditions (Davies, 1993; Héquette *et al.*, 2008; Liang *et al.*, 2008; Wang *et al.*, 2006). Most of the researches tend to focus on hydrodynamic forcing and their influence on sediment transport pathways, while some are directed especially on erosion/deposition

processes and studying morphological evolution. Based on the measurements taken in the mudflat and salt marsh transition on eastern Chongming Island, Shi *et al.* (2012) determined the combined current-wave shear stress and compared it with bed critical shear stress on the mudflats and saltmarsh respectively. They found that the sediment erosion was dominated on mudflats while sediment dynamics is mainly controlled by deposition on the salt marsh. Callaghan *et al.* (2010) investigated the development of salt marsh based on the hydrodynamic forcing and concluded that waves provided greater hydrodynamic force than currents and sediment dynamics were much active on shrinking marshes than expanding marshes, which is consistent with the conclusion of Shi *et al.* (2012).

In this chapter, the newly developed two-phase 1DV mud sedimentation model is applied to investigate sedimentary processes on an erosional intertidal mudflat based on two sets of intra-tide observations of currents, waves, suspended sediment concentration (SSC), sedimentary properties, and bed-level changes. It will focus on investigating the attenuation of turbulence, reduction of bed shear stresses due to the presence of fluid mud layer and the relative importance of waves in sediment dynamics on the mud flat under moderate sea conditions. This work is intended to improve our understanding of the processes of sediment dynamics on tidal flats as well as identify the uncertainties and improvements that are required to the model in order to predict more accurately the sedimentary processes under combined waves and tides action.

5.3.2 Results and discussion

5.3.2.1 *Data description*

A field measurement was recently carried out by Zhu *et al.* (2014) on the mudflat

within intertidal zones located in Nanhui foreland of which the coastal evolution is strongly influenced by Yangtze river. The measurement was conducted in two periods from 18/Dec/2009 at 9:00 h to 18/Dec/2009 at 16:00h and from 18/Dec/2009 at 21:00 to 19/Dec/2009 at 6:00h. The variations of water depths, current velocities, current directions, significant wave heights, wave periods and wave directions were all measured which allow the sediment settling processes under the combined wave and current actions to be studied. Like in many muddy tidal flats, estuaries and continental shelves where a layer of fluid mud can form just above the immobile sea bed (McAnally *et al.*, 2007; Yang *et al.*, 2003), a fluid mud layer was observed during the deceleration and slack time. Its influence on sedimentation process was found to be notable and has to be considered in modelling analysis. In terms of richness of the information provided, these data sets are uniquely suited to investigate how well the proposed model can simulate the effects of fluid mud on the flow structure and settling processes of the cohesive sediment.

As the measured net horizontal flux of sediments in the last part of acceleration time for both data periods is not zero, which implies the existence of a horizontal gradient in the sediment flux and is incompatible with the zero horizontal gradient assumption of the 1DV sediment transport model, only the measurements over two reduced time periods from 18/Dec/2009 at 9:00 h to 18/Dec/2009 at 14:00h and from 18/Dec/2009 at 21:00 to 19/Dec/2009 at 2:00 h are used as inputs to the model and denoted as Data D1 and Data D2, respectively. The model was run on a fixed time step and all the input values between the measured data points are determined using linear interpolation.

5.3.2.2 *Model setup*

The two-phase model adopted is the same as in section 5.2. As the study area is

under the action of combined waves and currents, the bed shear stress is calculated using Equation (4.37). Equation (4.14) and (4.18) are used for the drag force closures.

To study the effects of fluid mud on the cohesive sediment transport processes, two runs (with the effects of fluid mud run FM and without the effects of fluid mud run F) are carried out for comparison. For run F, an immobile fictive bed is assumed and the concentration gradient is small at the boundary. For run FM, the immobile bed is replaced as a layer of high concentrated fluid mud with constant concentration adopted in model calculation and a large concentration gradient exists at the surface of fluid mud. The concentration of fluid mud varies from several tens grams to several hundred grams per litre from the surface to the bottom layer of fluid mud (Winterwerp, 2006). In the current study, as only the concentration at the fluid mud surface are included in calculation, the constant concentration of fluid mud (surface) is specified as 32 kg/m^3 for both data cases. The sensitivity of the value adopted for the fluid mud (surface) is further discussed in section 5.3.3. From Equation (5.2)-(5.4) it can be seen that the friction velocity and thus the flow structure can be significantly influenced due to the large concentration gradient.

The main physical parameters required to run the model are the critical shear stress and settling velocity of mud flocs, in dilute flows none of which can be easily determined as they may vary significantly in time and location. For simplicity the critical shear stress is set as 0.1 Pa which is an average value calculated by Zhu *et al.* (2014) based on the method proposed by Taki (2000). The settling velocities of typical cohesive sediment flocs in the dilute situations are typically in the range of 0.04-4.5 mm/s (Hill *et al.*, 2000; Thorn, 1981). As silty mud found at the study site has a relatively weak flocculation

property, 0.08 mm/s is selected as the settling velocity in the dilute situations (w_0) for run FM in both data sets. Without accounting for fluid mud effects, which is unrealistic, it proved impossible to match the predictions with both sets of measurements using a single settling velocity value. Therefore, it was decided to use different settling velocity values to match as closely as possible the predicted and measured peak values of sediment concentration during the acceleration time. The settling velocities (w_0) finally used were 0.28 mm/s (Data D1) and 0.16 mm/s (Data D2) for run F. Based on the dissipation function deduced by Kranenburg (1998) with equilibrium conditions, the coefficients A and B are set as 0.1 as the concentration near bed is between 1 g/L-10 g/L, which is in the region of transport model Ⅱ of Cheng *et al.* (2015).

5.3.2.3 *Results*

Tidal flow velocity

As a common solution procedure (van der Ham and Winterwerp, 2001), the 1DV two phase model needs to be driven by the depth averaged flow velocity $\overline{U}$. As the depth averaged velocity was not a quantity that was measured in the field observation, the measured velocity at the depth of 5 cm above the bed is converted to the depth averaged flow velocity by assuming a standard logarithmic velocity law as:

$$\frac{u_c(z)}{\overline{U}} = \frac{1}{\kappa}\ln\left(\frac{z/z_0}{kh/z_0}\right) \tag{5.1}$$

where $u_c(z)$ is the current velocity at z, κ is the Von Karman constant and equals 0.4 and z_0 is the roughness length. Theoretically, the calculated velocity at 5 cm above the bed should equal the velocity measured at the same level, while flow structure may be

modified due to the presence of high suspended sediment concentration, which means the flow structure is no longer a standard logarithmic velocity profile. In that case the depth averaged velocity $\overline{U}$ driving the model, will be changed to make the calculated velocity at 5 cm above the bed approach the measured velocity at the same level until the difference smaller than a crucial value. Figure 5.21 shows the measured and calculated velocity variations at 5 cm above the bed.

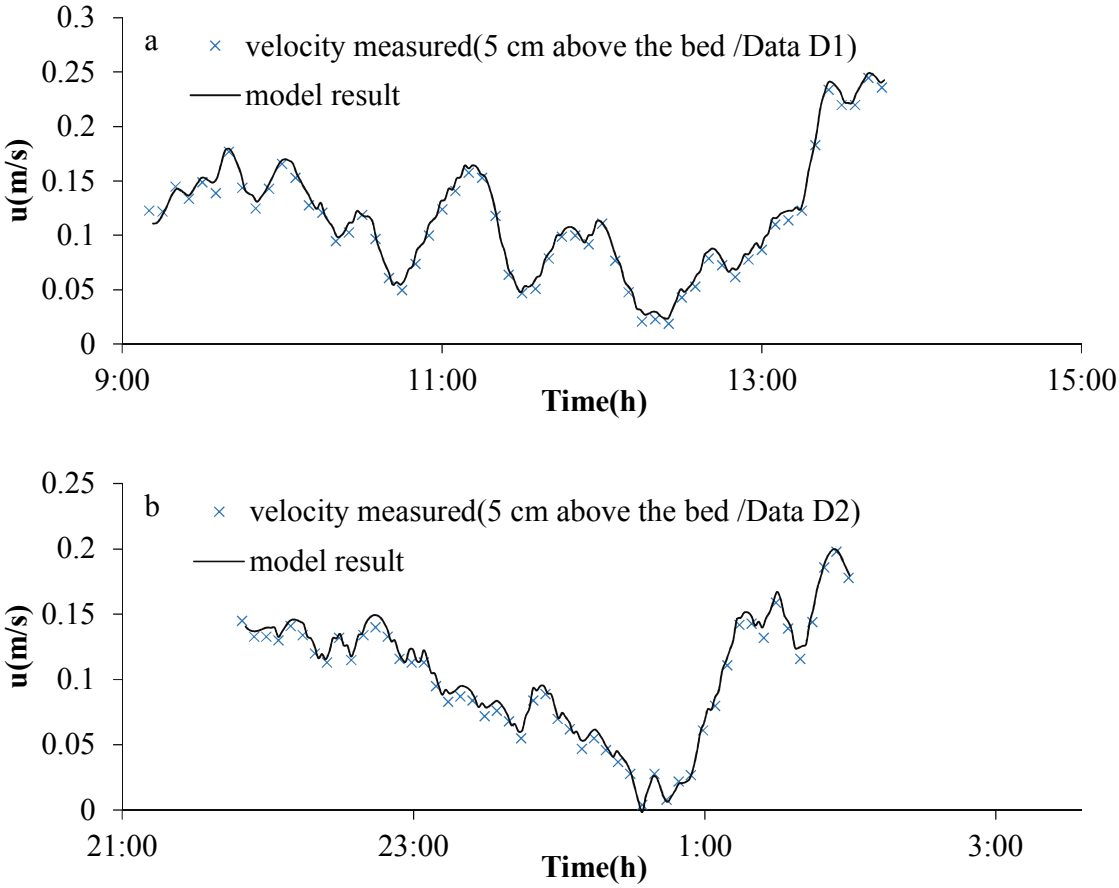

Figure 5.21 Measured and calculated velocity at 5cm above the bed for both data sets (a-Data D1, b-Data D2)

As the measurements are taken on an exposed mudflat and the current velocities measured are not complete within one tidal cycle the flow peak is difficult to be

determined. The eddy diffusivity, flow velocity and suspended sediment concentration profiles shown in Figure 5.22 are during the time when the sediment concentration is well mixed throughout the water column rather than right at the flow peak, while in Figure 5.23 they are during the slack water.

Figure 5.22a and Figure 5.23a show the calculated flow profiles with more details about parameters listed in Table 5.4. It can be noticed from Figure 5.22a that the thickness of boundary layer in run FM is smaller than that in run F, which means the dissipation of turbulence and mixing is due to the presence of fluid mud on the bottom. It can also be seen that the sediment concentration profile showed in Figure 5.22c for run F (dashed curve) is well mixed while a larger sediment concentration gradient is presented in run FM (solid curve). The calculated distribution of sediment concentration is consistent with the distribution of eddy diffusivity (Figure 5.22b). The curve of eddy diffusivity calculated in run F (dashed curve) is close to the clear fluid condition. The curve for run FM (solid curve) is weak and keeps almost constant in the middle part due to the large sediment concentration gradient. As the data point selected in Figure 5.23 is during the slack water, the flow velocities and eddy diffusivities throughout the profile approach zero. During the slack water for both cases the sediment concentration is large on the bottom, a sharp sediment concentration gradient appears near the bed and the concentration decays rapidly away from the bed.

Table 5.4 Fitting parameters used in simulation of Data D1

Run	w_0 (m/s)	M (s^{-1})	Fluid mud layer
FM	0.8×10^{-4}	4.67×10^{-8}	Included
F	0.28×10^{-3}	4.67×10^{-8}	Not included

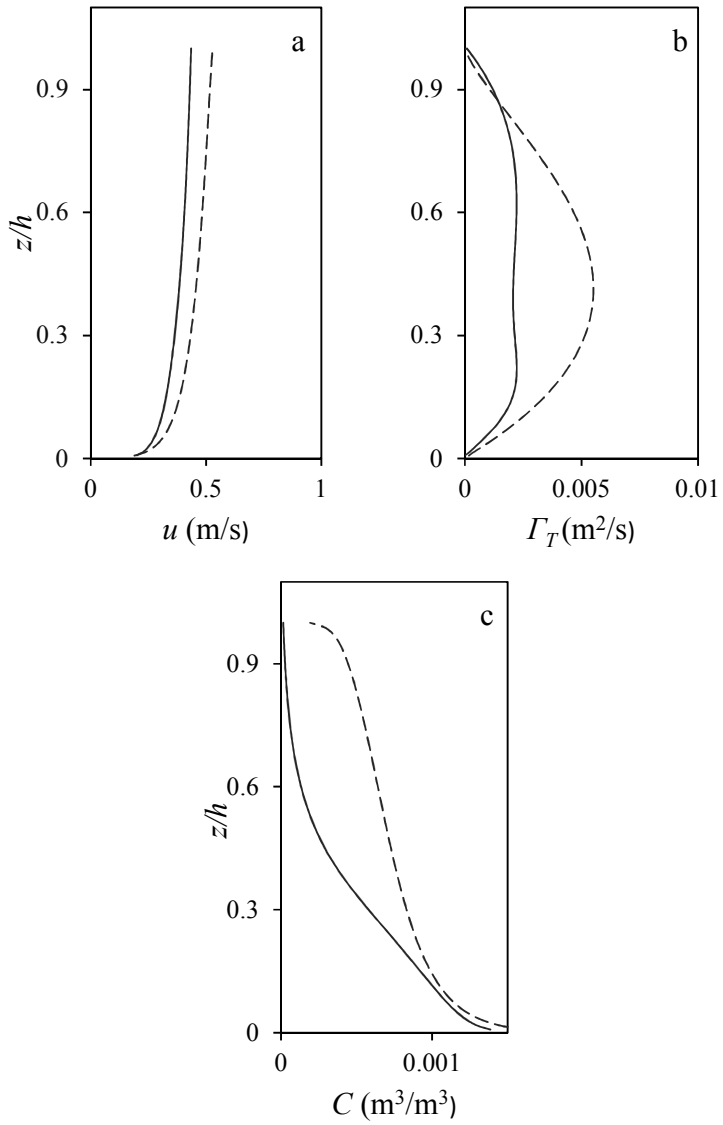

Figure 5.22 Velocity profile (a), distribution of eddy diffusivity (b) and sediment concentration (c) for run FM (solid curve) and run F (dashed curve) during the acceleration time of Data D1

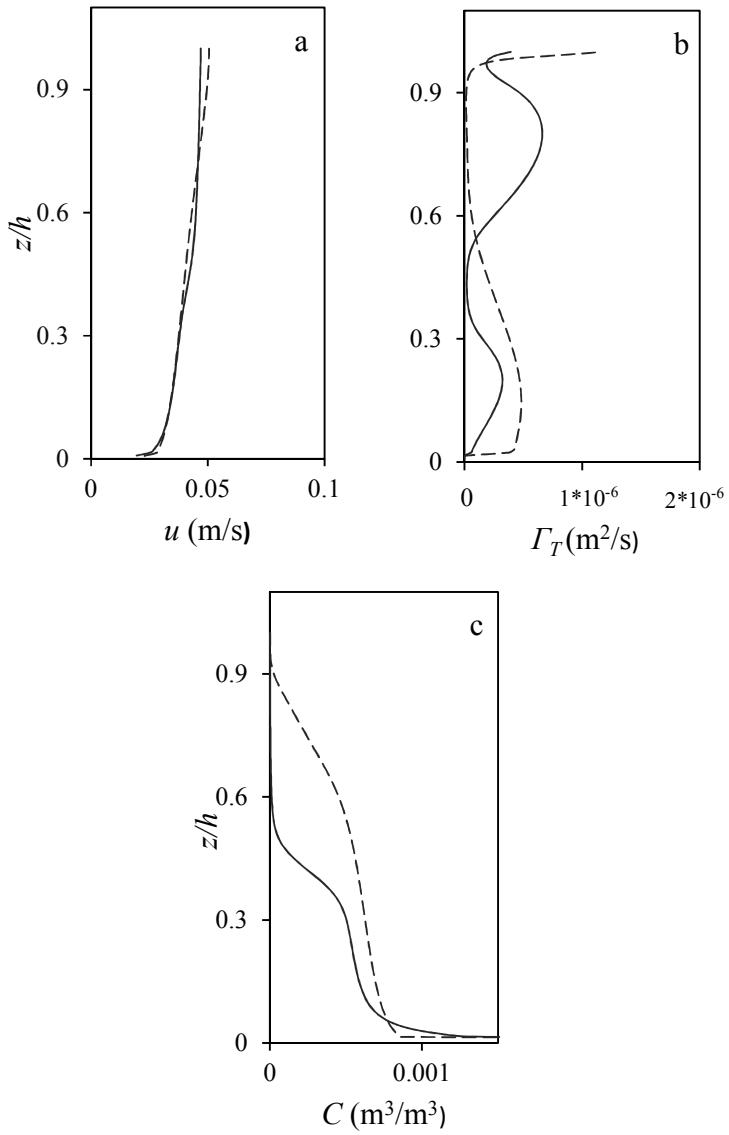

Figure 5.23 Velocity profile (a), distribution of eddy diffusivity (b) and sediment concentration (c) for run FM (solid curve) and run F (dashed curve) during the slack water time of Data D1

Bed shear stress under combined current and wave action

The bed shear stress induced by current, waves and combined currents and waves with/without the effects of presence of fluid mud are presented in Figure 5.24 (run FM)/Figure 5.25 (run F) respectively. As the interaction between waves and suspended sediment or fluid mud is beyond the scope of this study, the shear stress calculated due to

waves is assumed not to be influenced by the sediment. The shear stress due to waves (τ_w) is around 0.1pa-0.2pa. The variations of bed shear stress calculated due to currents (τ_c) presented in Figure 5.25 (run F), in which the effects of fluid mud is not introduced, are in line with the variations of velocities at 5cm above the bed. The U-shaped time series shear stress is consistent with the results presented by Zhu *et al.* (2014). When the effects of fluid mud are considered (Figure 5.24), the value is much lower as expected, because the shear stress is fully dissipated due to the presence of fluid mud. The shear stress is overestimated as the effects of turbulence damping is not introduced (Toorman *et al.*, 2002).

In most previous sediment dynamic models a solid boundary condition can be safely applied on the seabed. The situation here is more complicated due to the existence of the fluid mud layer within the lowest level (Zhu *et al.*, 2014). As a sharp concentration gradient is introduced into calculating gradient Richardson number which makes the stratification effects remarkable. The combined shear stress (τ_{cw}) for run F is dominated by current shear stress while waves are also important to the erosion especially during the slack water. Due to the turbulence dissipation, current shear stress is nearly annihilated and the combined shear stress is dominated by wave shear stress for run FM. The combined shear stress is almost equal to wave shear stress except for during the initial time and near the end of the simulation, which means that the wave shear stress make the most contribution to the erosion of sediment during the whole tidal cycle.

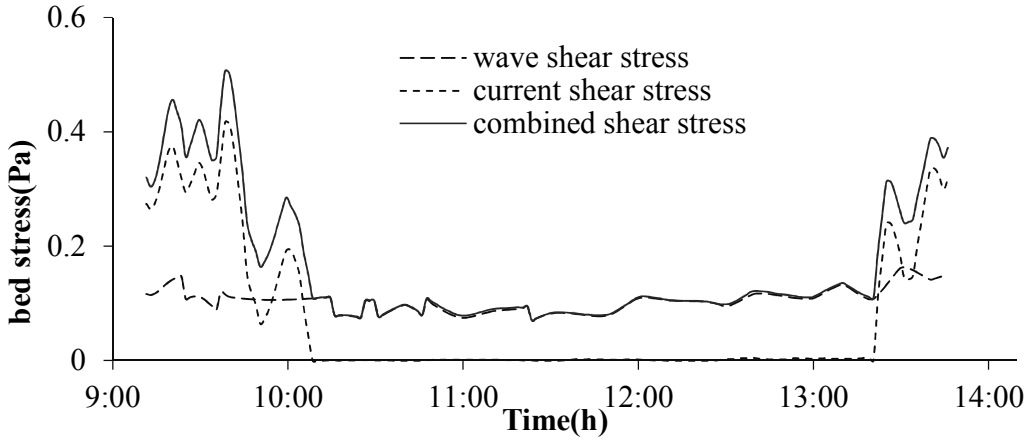

Figure 5.24 Calculated wave shear stress (long dashed curve), current shear stress (short dashed curve) and combined shear stress (solid curve) for run FM (fluid mud layer introduced) of Data D1

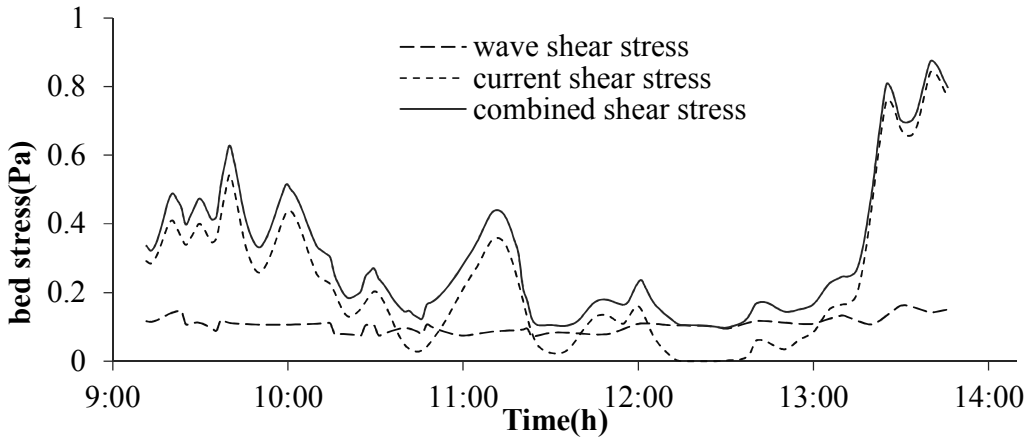

Figure 5.25 Calculated wave shear stress (long dashed curve), current shear stress (short dashed curve) and combined shear stress (solid curve) for run F (no fluid mud layer) of Data D1

Sediment concentration (Data D1)

The variations of model results (run FM and run F) and measured data of sediment concentration at 6 cm and 75 cm above the bed are presented in Figure 5.26 and Figure 5.27 respectively. To achieve a better result of sediment concentration that can fit the measured data well, two sets of parameters are used as inputs (see more details in Table 5.4).

It can be seen that the sediment concentration measured at 6 cm above the bed is increasing until 13:14 which is 1 hour after the slack water and then decreases very sharply. It is noticed that the results for run F do not compare well with the measured data as the values of calculated sediment concentration for run F are lower than measured data. The peak value of calculated sediment concentration is equal to the measured data but appears some time earlier. The result of run F shows that sediment concentration increases sharply sometime after the slack water and then decreases rapidly. The concentration curve forms a narrow peak which is not consistent with the measured data. The difference between measured concentration and result of run F is partly because the effects of fluid mud are ignored. Without the consideration of the dissipation due to the presence of fluid mud, the stratification effects may be underestimated and the sedimentation concentration increases rapidly until the peak value is reached. Then most of the deposited sediments during the slack water are re-suspended and the sediment concentration gradient becomes smaller which increases the rate of the sediment mixed up in the water column. The sediment concentration near bed (6 cm above the bed) decreases as the sediments are suspended in the upper part of the water column and sediment concentration distribution becomes more uniform.

The variations of sediment concentration calculated in run FM compare well with the measured data. Model results follow the trend of measurements at initial time and after that go through the central of measured data points. With the effects of fluid mud, the calculated sediment concentration starts to increase gradually sometime after the slack water and the slope of the curve is consistent with field measurements. From the results of run FM and F, it can be concluded that the concentration curve can be

significantly influenced by fluid mud on the bottom boundary and this effect needs to be introduced in two-phase flow models.

In the upper part of the water column the measured sediment concentration (at 75 cm above the bed) and model results are presented in Figure 5.27. The measured sediment concentration falls within a narrow interval compared to the variation of sedimentation concentration near bed. Both model results compare well and follow the trend of field data, though the model results almost keep constant.

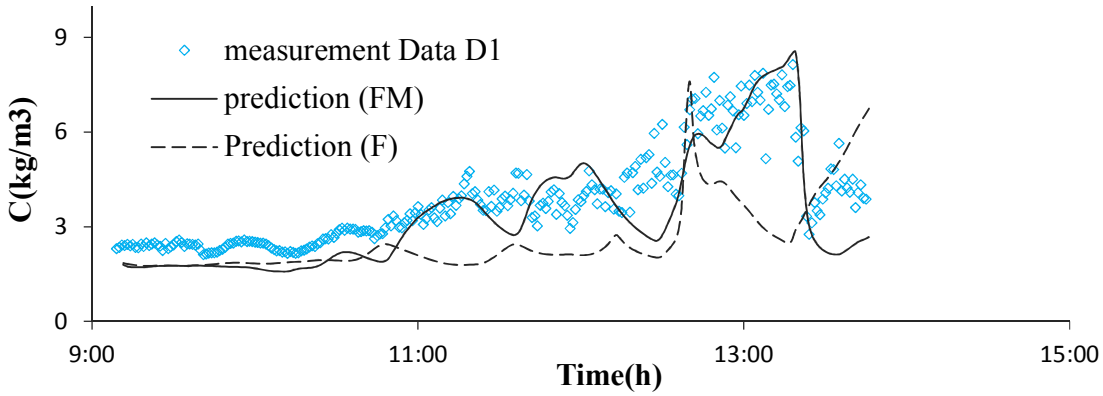

Figure 5.26 Measured and calculated sediment concentration at 6 cm above the bed of Data D1

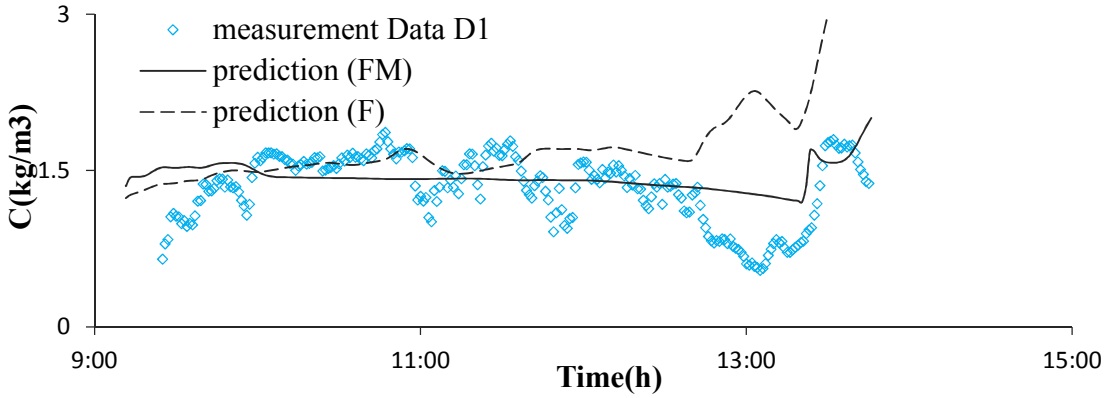

Figure 5.27 Measured and calculated sediment concentration at 75 cm above the bed of Data D1

Sediment concentration (Data D2)

The model parameters selected in run FM for Data D2 are the same as that adopted in run FM for Data D1 and the settling velocity for dilute situation is changed in run F (see Table 5.5) to achieve a reasonable result comparing to measured variations of sediment concentration.

Table 5.5 Fitting parameters used in simulation of Data D2

Run	w_0 (m/s)	M (s^{-1})	Fluid mud layer
FM	0.8×10^{-4}	4.67×10^{-8}	Included
F	0.16×10^{-3}	4.67×10^{-8}	Not included

The velocity profile, eddy diffusivity and sediment concentration are presented in Figure 5.28 and Figure 5.29 for run FM and Run F, respectively. There are some resemblance between the model results for Data D2 and the simulation results showed in Data D1. The flow velocity and eddy diffusivity approach zero during the slack water and the sediment concentration near the bed is large (Figure 5.29). As most of the sediment deposited, a sharp sediment concentration gradient appears near the bed and the sedimentation concentration above the region is relatively small. The results during acceleration time are presented in Figure 5.28. The eddy diffusivity calculated in run FM (solid curve Figure 5.28b) is much smaller than that calculated in run F (dashed curve Figure 5.28b). The peak value of eddy diffusivity in FM is only half of the peak value showed in F in the middle part of the water column. The distributions of eddy diffusivity are consistent with the distributions of sediment concentration which are presented in Figure 5.28c. Due to the large eddy diffusivity of run F (Figure 5.28b dashed line) the

sediment concentration is well mixed throughout the water column. Contrary to the results of run F, which is uniform, the sediment concentration of run FM (solid curve Figure 5.28c) decreases gradually upward from the bed.

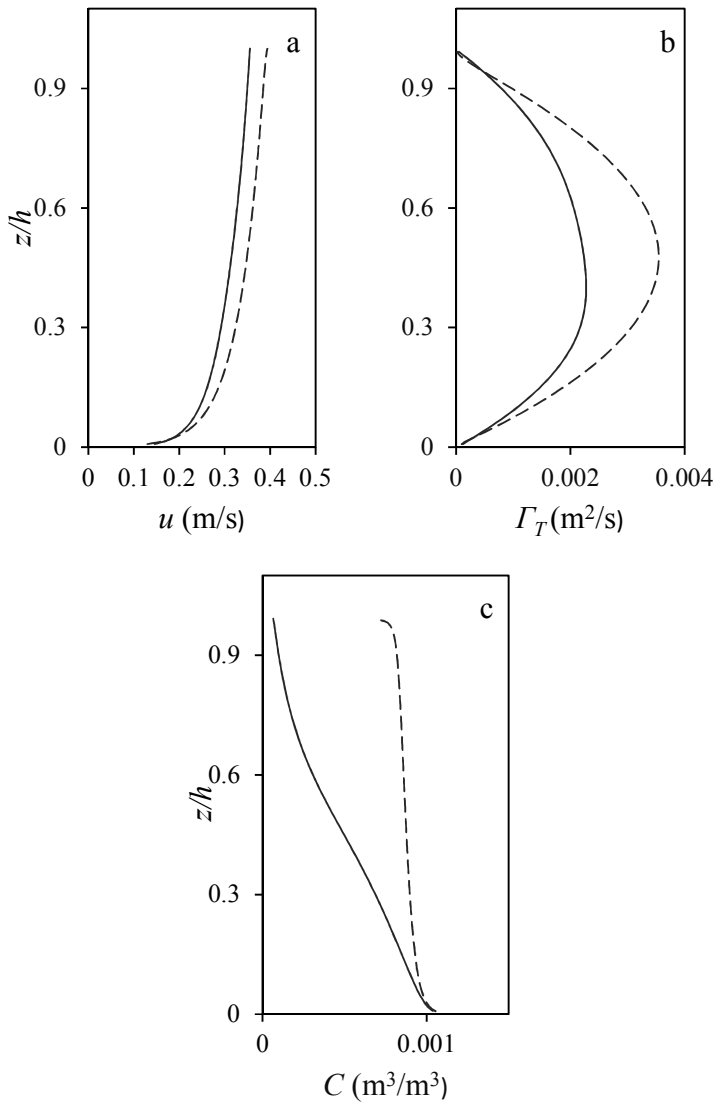

Figure 5.28 Velocity profile (a), distribution of eddy diffusivity (b) and sediment concentration (c) for run FM (solid curve) and run F (dashed curve) during the acceleration time of Data D2

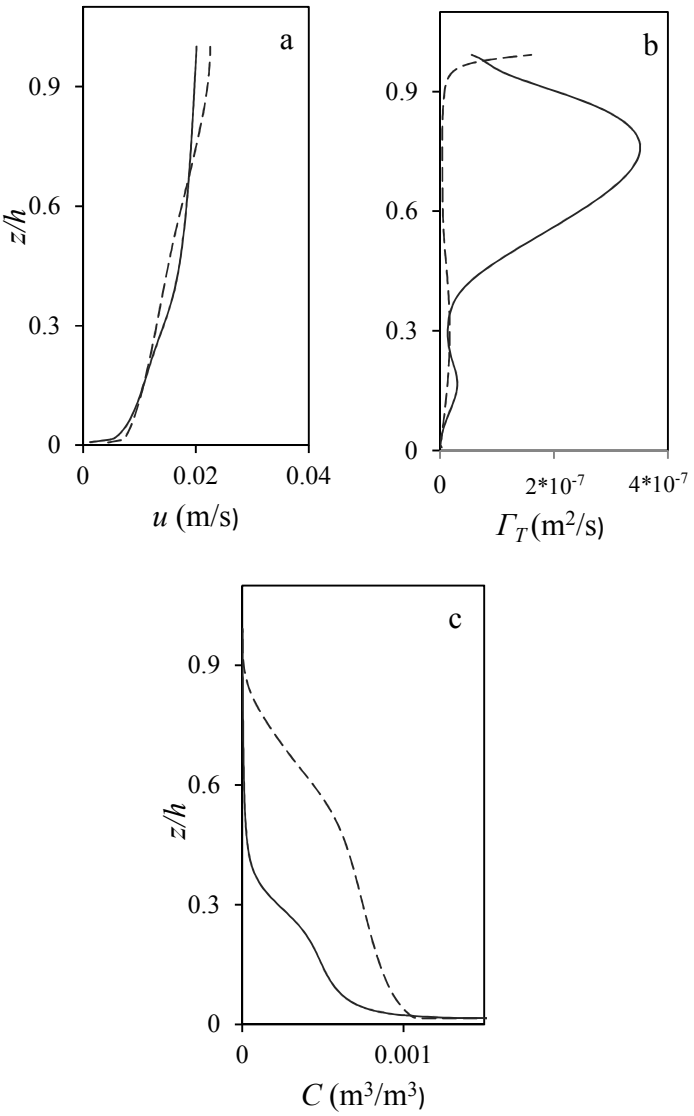

Figure 5.29 Velocity profile (a), distribution of eddy diffusivity (b) and sediment concentration (c) for run FM (solid curve) and run F (dashed curve) during the slack water time of Data D2

Shear stresses due to waves, currents and combined waves and currents are calculated in run FM/run F and presented in Figure 5.30/Figure 5.31. The wave shear stress (τ_w) is the same for reasons stated in the analysis of the Data D1. Both current shear stress and wave shear stress are significant in calculating the combined shear stress in run F. Compared to current shear stress calculated by Zhu *et al.* (2014) the present

results are smaller and this may be due to the traditional wall functions they had adopted, in which the interactions between suspended sediment concentration and flow structure are not considered. In fact the modification of flow structure due to the presence of suspended sediment can be significant (Villaret and Davies, 1995) and thus the bed shear stress. From Figure 5.30 and Figure 5.31 it can be noticed that the current shear stress calculated by run FM is much smaller than that in run F because the effects of fluid mud layer are considered.

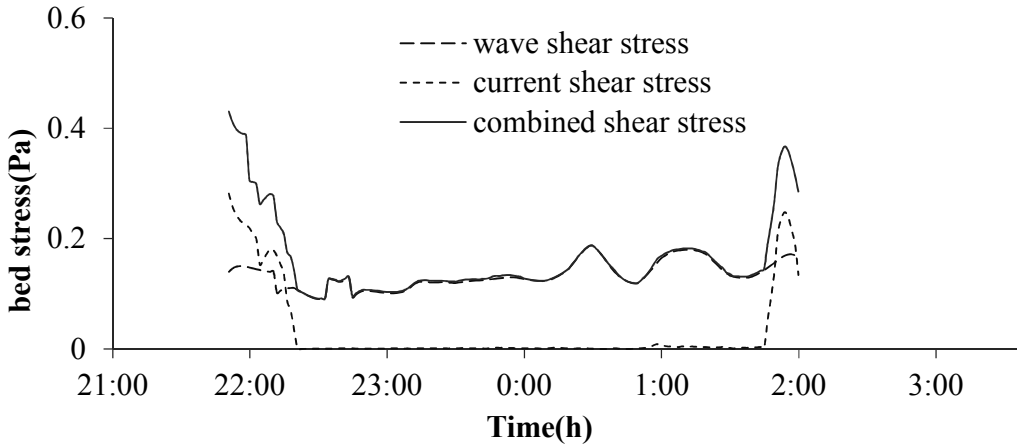

Figure 5.30 Calculated wave shear stress (long dashed curve), current shear stress (short dashed curve) and combined shear stress (solid curve) for run FM (fluid mud layer introduced) of Data D2

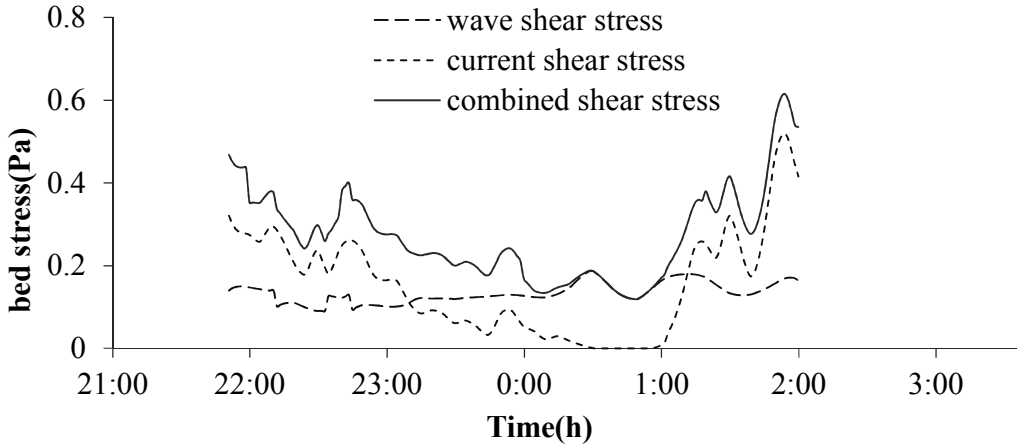

Figure 5.31 Calculated wave shear stress (long dashed curve), current shear stress (short dashed curve) and combined shear stress (solid curve) for run F (no fluid mud layer) of Data D2

To present a fuller picture of the predicted and measured flow and sediment structures through the water column, the model results for run FM and F and the measured sediment concentration at 6 cm and 75 cm above the bed are presented in Figure 5.32 and Figure 5.33 respectively. The sediment concentration at 75 cm varies very small. Model results of run FM compare well with measured data while the results of run F deviate from the measured data points except at the initial time. As to the variations of sediment concentration at 6 cm above the bed, the behavior of predictions from run F is quite similar to that of run F in the simulation of Data D1. The simulation results form a narrow peak sometime after slack water which suggests the concentration increases sharply and then a rapid decrease. The sediment concentration starts to increase again when it reaches a low value which is not consistent with measured data. This phenomenon is believed to be due to that the deposited sediment are all re-suspended when the low value is reached and more sediments are eroded from the bed.

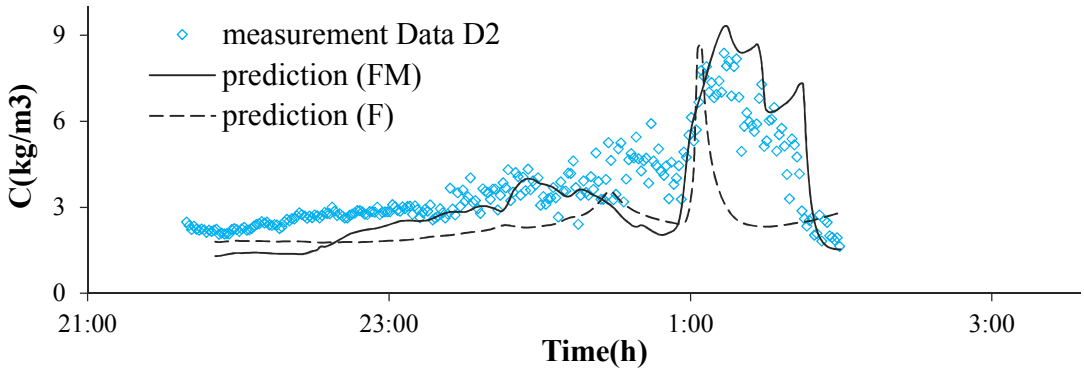

Figure 5.32 Measured and calculated sediment concentration at 6 cm above the bed for Data D2

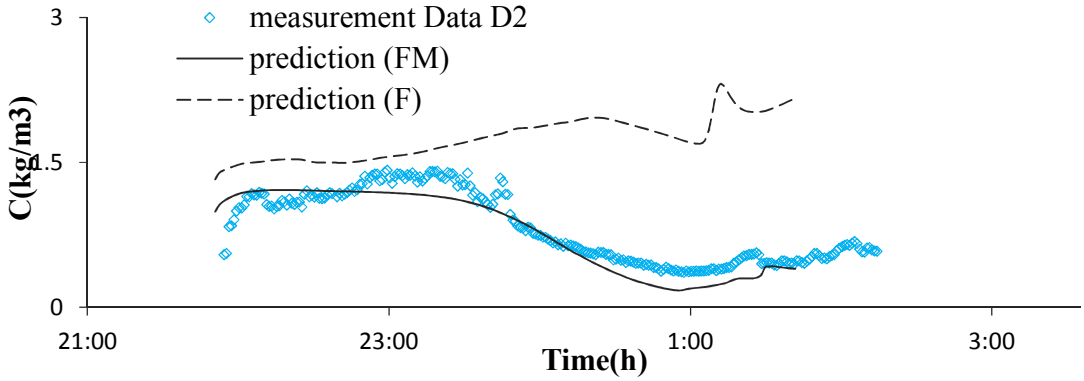

Figure 5.33 Measured and calculated sediment concentration at 75 cm above the bed for Data D2

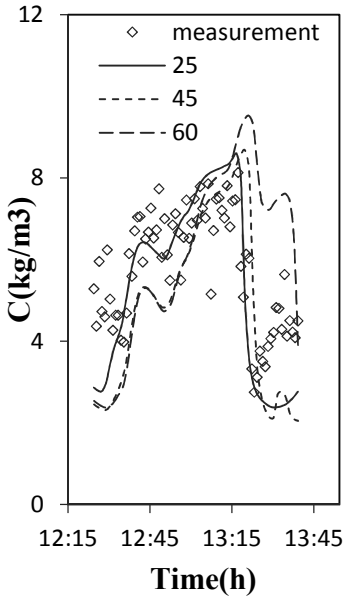

Figure 5.34 Measured and calculated sediment concentration peak at 6 cm above the bed during the acceleration time of Data D1. The inputs of concentration of surface of fluid mud are 25 kg/m^3 (solid curve), 45 kg/m^3 (short dashed curve) and 60 kg/m^3 (long dashed curve)

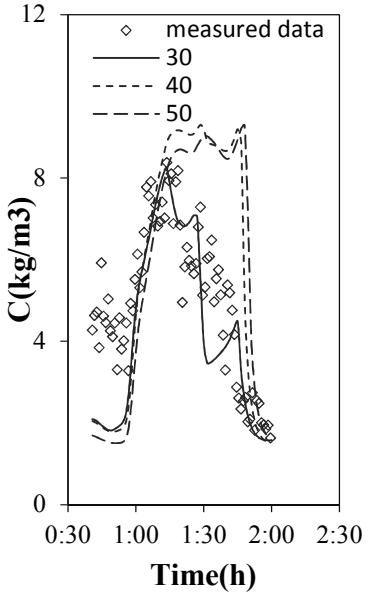

Figure 5.35 Measured and calculated sediment concentration peak at 6 cm above the bed during the acceleration time of Data D2. The inputs of concentration of surface of fluid mud are 25 kg/m^3 (solid curve), 45 kg/m^3 (short dashed curve) and 60 kg/m^3 (long dashed curve)

The model results by run FM about the sediment concentration at 6 cm above the bed show good agreement with field measurements. The predicted curve goes through most of the measured data points and especially during the accelerating time when the concentration peaks appear the model results perform well. It can be noticed that during the slack time (around 0:45), the model results compare less favorably with measured data. In the field measurements the sediment concentration keeps increasing during deceleration and slack water time. The concentration starts to drop at the measured height (6 cm above the bed) during the slack time as most of the suspended sediment deposited on the bed. This is may be due to the assumption of constant fractal dimension of mud flocs or because the formula for hindered settling velocity used in the model is incapable of describing accurately the settling characteristics of the mud flocs in the study area.

5.3.3 Further discussions on the mud layer effects

As discussed above the flow dynamics and settling processes are significantly influenced by fluid mud the concentration of which is an important parameter and should be specified. In terms of modelling, relationship between damping functions in the Prandtl mixing length model (PML) and Taylor Kolmogorov (TK) model can be expressed as below according to Kranenburg (1998):

$$F_v = F_{vis}^{\ 2} \tag{5.2}$$

$$F_d = F_{vis} F_{diff} \tag{5.3}$$

The friction velocity is calculated using Equation (5.4):

$$\frac{u(z_b)}{u^*} = \frac{\ln(\frac{z_b}{z_0})}{\kappa\sqrt{F_v}} \tag{5.4}$$

As a layer of fluid mud is introduced into the model, a large value will be obtained for the term $-\partial\rho_{mix}/\partial z$ in Equation (4.29). From Equation (4.29), (4.30) and (5.4) it can be seen that the friction velocity is reduced as the value of F_v is less than 1. It also can be concluded that the shear stress is reduced which is consistent with the simulation results. The differences of current shear stress in Figure 5.24 and Figure 5.25 for Data D1 (also see Figure 5.30 and Figure 5.31 for Data D2) indicates that the shear stress is significantly damped due to the presence of the fluid mud. Since sediment erosion is a key process in the sediment transport model (Cheng *et al.*, 2015), it is crucial to further understand the interaction between bed shear stress and fluid mud. The reduced eddy viscosity (see Figure 5.22b and Figure 5.28b solid curves) proves that turbulence attenuation is due to fluid mud layer. The calculated suspended sediment concentration profile is dependent on the distribution of eddy viscosity/eddy diffusivity and bed shear stress. Because eddy diffusivity corresponds to the mixing up of sediment and the bed shear stress corresponds to the availability of sediment. The good agreement of simulated sediment concentration profile with measured data (see solid curves in Figure 5.26, Figure 5.27, Figure 5.32 and Figure 5.33) confirms that fluid mud layer controls the suspended sediment concentration indirectly through modification of flow dynamics.

As in the current study the fluid mud is formed during the tide cycle which can be treated as fresh soft mud and the concentration introduced into the model is on the surface of the bed (fluid mud), the input value of sediment concentration should around several tens grams per liter. It proves that 32 kg/m^3 is the best option for the model

results. To analyze the sensitivity of sediment concentration of bed surface, Figure 5.34 (Data D1) and Figure 5.35 (Data D2) show the model results with different concentration inputs (25, 45 and 60 kg/m^3). As the model results are almost the same during the deceleration and slack water time, only variations of sediment concentration with peak value during the acceleration time are presented. As shown in both Figure 5.34 and Figure 5.35, the model results have agreement with the trend of the measured data, among which the simulation result with input of 25 kg/m^3 performs better than other two. When the concentration of fluid mud increases, the concentration increase point appears later. Also the peak value appears later but with a higher magnitude. It should be noticed that the predicted variations of sediment concentration change slightly when the inputs of fluid mud concentration increased from 45 kg/m^3 to 60 kg/m^3.

5.4 Summary

We have presented a model study of the sedimentation processes at mudflat near the estuary of Yangtze River. The model assumed an idealized 1DV flow driven by an oscillatory horizontal pressure gradient and is based on the two-phase continuity and momentum equations. The key features of the flow are the simultaneous interactions between the turbulent flow, suspended sediments, sediment entrainment and settling under combined waves and currents actions. The computational results and comparison with the measurements showed that the wave effects are significant at the study site and the sediment erosion has to be determined using the combined waves and currents shear stress. Apart from confirming the importance of buoyancy effects on the vertical distribution of mud floc concentration, the model results further demonstrated that the presence of fluid mud layer can significantly alter the flow structure and near bed

sediment settling processes mainly through dissipating the wave and current shear stress. When the fluid mud layer is introduced into the model the eddy diffusivity is more realistically redistributed and resulted in better prediction of near bed suspended sediment concentration. Interestingly, the measured concentration peak appears during the acceleration time instead of the slack time. This has been shown to be due to the fact that most of the sediment deposited below the observed height (6 cm above the bed) during the slack time. The average sediment concentrations from the bed to the height measured are 13.9 kg/m^3 (Data D1) and 17.3 kg/m^3 (Data D2), respectively. While the corresponding sediment concentrations at the level of 2 cm above the bed are 30 kg/m^3 (Data D1) and 32.3 kg/m^3 (Data D2). On the other hand, strong sediment re-suspension occurs during the acceleration time. The distribution of sediment concentration within the observed height is fairly uniform and the average sediment concentrations are 8.6 kg/m^3 (Data D1) and 11.4 kg/m^3 (Data D2), respectively.

Chapter 6 Conclusions and recommendations

This thesis investigated the sedimentation processes of cohesive sediment in coastal waters using a two-phase model. Despite its limitations, it help to understand the mechanisms (flocculation and fluid-mud interaction) controlling cohesive sediment transport processes. In this chapter, conclusions will be made and recommendations for the future work will also be given.

6.1 Conclusions

A two-phase model was developed to study the cohesive sediment transport processes, especially for the flocculation and interaction between fluid and high concentrated sediment, to be specific, the interaction between fluid and fluid mud.

Based on a normal distribution of fractal dimension of mud flocs and yield stress, a flocculation model is developed to predict the evolution of mud floc size in Chapter 3. In the break-up process of mud flocs, the distribution of fractal dimensions are implemented into the model to account for the large variation of settling velocities for floc class with a size of D. Within the flocs group with size of D, only flocs with yield stress less than the turbulent shear stress are allowed to break up. The new flocculation model is established by linearly combing the aggregation process and break-up process. Also, the flocculation model is applied to predict the time-growing floc size and is compared with four set of experimental data collected from the published literature. The following findings were confirmed:

- The proposed model is found to perform better in predicting the temporal evolution of floc size than that based on a single fixed floc-size dependent fractal dimension, especially under high shear conditions and with large

equilibrium floc size.

- The normal distribution of fractal dimension has a significant effect on the breakup process of mud flocculation process. With the consideration of multi fractal dimensions for floc class with size *D*, at the very start the floc size increases quicker compared to flocculation models with single fractal dimension for a fixed floc size. Also the floc size grows gently near the end of curves where mud flocs reach the equilibrium size.
- Flocculation model with single fractal dimension and yield stress may overestimate the breakup process at the beginning of flocculation.

In Chapter 4-5, the two-phase model was developed and validated using experiments data of vertical settling tanks. The model is based on solving the one-dimensional continuity and momentum equations for both fluid and solid phases through water depth (1DV). For the purpose of simulation sedimentation processes in which the consolidation process is included, the closure of effective stress is incorporated for both non-cohesive and cohesive sediment cases. As in the study, the simulation is only used to illustrate the validity of the presented two-phase model, only comparisons are briefly discussed and the results indicate that:

- The model predictions match well with the experiments data, which indicates a clear capability of the presented two-phase model in simulating sedimentation processes of cohesive sediment.
- The model results capture most of the main features of the sedimentation process of both non-cohesive and cohesive sediment.
- In the case of sedimentation simulation with initial cohesive sediment

concentration 5.2%, the predicted results compare less favorably with experiment data which may be due to the improper calibration of hindered settling regime.

The two-phase model developed in Chapter 5 was further extended to account for the horizontal tidal currents. The two-phase model was applied to simulate the sediment suspension of Ems/Dollard estuary using two series field measured data in June and August 1996. A new drag force closure was presented to consider the effects of flocculation. The flocculation effect was related to suspended sediment concentration. According to the model results, the main findings are listed below:

- The model results captured most of features of cohesive sediment transport processes and the data set. The time-lag between current velocity and suspended sediment concentration were well modelled.
- The 'rapid settling' which was explained by van der Ham and Winterwerp (2001) as the buoyancy effects, while in the current study it may be explained due to the flocculation process which is consistent with most of the field observations.
- As the sediment concentration is less than 1 g/L, the buoyancy effects is weak and the shear stress can be hardly affected.
- The model with the consideration of flocculation process predicted a better result compared with model results from run without consideration of flocculation process.
- Though the concentration is less than 1 g/L, the flocculation effects are significant in influencing the settling velocity directly and the cohesive

sediment suspension indirectly.

The two-phase model is also applied to cohesive sediment transport under the action of combined waves and currents at the mudflat near Yangtze River estuary. The key features of the flow are the interaction between high suspended sediment concentration and fluid. At the bottom of the water column, the shear stress was calculated by combing both the current and wave effects and implemented into the boundary condition of horizontal momentum equation. Model results indicated that:

- The effects of waves are important and the combined shear stresses of waves and currents have to be considered when calculation the erosion process at the mud flat.
- Due to the existence of a fluid mud layer, the flow structure is significantly altered and also the sediment settling process is indirectly influenced by the fluid mud layer.
- When the fluid mud layer was introduced to the model, the re-distributed eddy viscosity and eddy diffusivity were more realistic and a better prediction of sediment concentration was obtained.

6.2 Recommendations

The thesis developed a two-phase model and applied it to simulate sedimentation processes in coastal waters. The recommendations will be given about the structure of the two-phase model, the closure terms that are required to be further investigated and the problems that are still poorly understood in sediment transport.

- In the current study, the momentum equations for both fluid and solid phase in the horizontal direction were combined together as one equation as we assume

the velocities of fluid and mud are the same, however, a difference exists in reality. A more complete two-phase model can be developed in the future work to study the behavior of cohesive sediment transport when the horizontal velocities for both phases are calculated separately.

- For simplicity, the effective viscosity for both phases are assumed as the same, a more realistic expression need to be investigated and the effective viscosity incorporated into the momentum equations should be calculated separately.
- Cohesive sediment transport behavior near the bed, especially the erosion process is not fully understood. As the mud is in the intermediate state of fluid and solid, the non-Newtonian properties should be considered.
- Due to complexity of mud and sand behavior, the settling processes of mud and sand are usually studied separately. In natural environment, it appears as a mixture. Recently a few researches, most of which are experiments, were focused on the sedimentation processes of mixed sediment, which made it possible to study the behavior of sand-mud mixture.

Reference

Amoudry, L., Hsu, T.-J., Liu, P.L.-F., 2005. Schmidt number and near-bed boundary condition effects on a two-phase dilute sediment transport model. Journal of Geophysical Research 110, C09003.

Amoudry, L.O., 2008. Two-phase modeling of granular sediment for sheet flows and scour. Cornell University.

Baldock, T.E., Tomkins, M.R., Nielsen, P., Hughes, M.G., 2004. Settling velocity of sediments at high concentrations. Coastal Engineering 51, 91-100.

Been, K., Sills, G.C., 1981. Self-weight consolidation of soft soils: An experimental and theoretical study. Geotechnique 31, 519-535.

Bian, C., Jiang, W., Quan, Q., Wang, T., Greatbatch, R.J., Li, W., 2013. Distributions of suspended sediment concentration in the yellow sea and the east china sea based on field surveys during the four seasons of 2011. Journal of Marine Systems 121-122, 24-35.

Biggs, C., Lant, P., 2000. Activated sludge flocculation: On-line determination of floc size and the effect of shear. Water research 34, 2542-2550.

Boulton, S.J., Robertson, A.H.F., Ünlügenç, U.C., 2006. Tectonic and sedimentary evolution of the cenozoic hatay graben, southern turkey: A two-phase model for graben formation. Geological Society, London, Special Publications 260, 613-634.

Burban, P.-Y., Lick, W., Lick, J., 1989. The flocculation of fine-grained sediments in estuarine waters. Journal of Geophysical Research 94, 8323-8330.

Burban, P.Y., Xu, Y.J., McNeil, J., Lick, W., 1990. Settling speeds of floes in fresh water and seawater. Journal of Geophysical Research: Oceans (1978–2012) 95, 18213-18220.

Callaghan, D.P., Bouma, T.J., Klaassen, P., van der Wal, D., Stive, M.J.F., Herman, P.M.J., 2010. Hydrodynamic forcing on salt-marsh development: Distinguishing the relative importance of waves and tidal flows. Estuarine, Coastal and Shelf Science 89, 73-88.

Camenen, B., 2008. Settling velocity of sediments at high concentrations, Proceedings in Marine Science. Elsevier, Saga, Japan, pp. 211-226.

Camenen, B., Pham van Bang, D., 2011. Modelling the settling of suspended sediments for concentrations close to the gelling concentration. Continental Shelf Research 31, S106-S116.

Chauchat, J., Guillou, S., 2013. A vertical one-dimensional two-phase flow model for sedimentation-consolidation of mud, Coastal Dynamics, Arcachon, France., pp. 327 - 338.

Chauchat, J., Guillou, S., Barbry, N., Nguyen, K.D., 2009. Simulation of the turbidity maximum in the seine estuary with a two-phase flow model. Comptes Rendus Geoscience 341, 505-512.

Chauchat, J., Guillou, S., Pham Van Bang, D., Dan Nguyen, K., 2013. Modelling sedimentation–consolidation in the framework of a one-dimensional two-phase flow model. Journal of Hydraulic Research 51, 293-305.

Cheng, N.S., 1997a. Effect of concentration on settling velocity of sediment particles. Journal of hydraulic engineering 123, 728-731.

Cheng, N.S., 1997b. Simplified settling velocity formula for sediment particle. Journal of hydraulic engineering 123, 149-152.

Cheng, Z., Yu, X., Hsu, T.-J., Ozdemir, C.E., Balachandar, S., 2015. On the transport modes of fine sediment in the wave boundary layer due to resuspension/deposition: A turbulence-resolving numerical investigation. Journal of Geophysical Research: Oceans 120, 1918-1936.

Colomer, J., Peters, F., Marrase, C., 2005. Experimental analysis of coagulation of particles under low-shear flow. Water research 39, 2994-3000.

Cuthbertson, A., Dong, P., King, S., Davies, P., 2008. Hindered settling velocity of cohesive/non-cohesive sediment mixtures. Coastal Engineering 55, 1197-1208.

Cuthbertson, A.J.S., Dong, P., Davies, P.A., 2010. Non-equilibrium flocculation characteristics of fine-grained sediments in grid-generated turbulent flow. Coastal Engineering 57, 447-460.

Dankers, P.J.T., Winterwerp, J.C., 2007. Hindered settling of mud flocs: Theory and validation. Continental Shelf Research 27, 1893-1907.

Davies, A.G., 1993. Modelling the vertical distribution of suspended sediment in combined wave‐current flow, Dynamics and exchanges in estuaries and the coastal zone. Wiley Online Library, pp. 441-466.

De Sutter, R., Huygens, M., Verhoeven, R., 1999. Bed shear stress governing erosion on cohesive mixtures, 28TH IAHR CONGRESS, Grenoble, France.

Dong, P., Zhang, K., 1999. Two-phase flow modelling of sediment motions in oscillatory sheet flow. Coastal Engineering 36, 87-109.

Dyer, K.R., 1989. Sediment processes in estuaries: Future research requirements. Journal of Geophysical Research: Oceans (1978–2012) 94, 14327-14339.

Dyer, K.R., Christie, M.C., Feates, N., Fennessy, M.J., Pejrup, M., van der Lee, W., 2000. An investigation into processes influencing the morphodynamics of an intertidal mudflat, the dollard estuary, the netherlands: I. Hydrodynamics and suspended sediment. Estuarine, Coastal and Shelf Science 50, 607-625.

Dyer, K.R., Manning, A.J., 1999. Observation of the size, settling velocity and effective density of flocs, and their fractal dimensions. Journal of Sea Research 41, 87-95.

Einstein, A., 1905. Eine neue bestimmung der moleküldimensionen. Annalen der Physik 324, 289-306.

Fennessy, M.J., Dyer, K.R., Huntley, D.A., 1994. Inssev: An instrument to measure the size and settling velocity of flocs in situ. Marine Geology 117, 107-117.

Frankel, N.A., Acrivos, A., 1967. On the viscosity of a concentrated suspension of solid spheres. Chemical Engineering Science 22, 847-853.

Gibbs, R.J., 1985. Estuarine flocs: Their size, settling velocity and density. Journal of Geophysical Research: Oceans (1978–2012) 90, 3249-3251.

Gibson, R.E., England, G.L., Hussey, M.J.L., 1967. The theory of one-dimensional consolidation of saturated clays. Geotechnique 17, 261-273.

Gibson, R.E., Schiffman, R.L., Cargill, K.W., 1981. The theory of one-dimensional consolidation of saturated clays. Ii. Finite nonlinear consolidation of thick homogeneous layers. Canadian Geotechnical Journal 18, 280-293.

Graham, A.L., 1981. On the viscosity of suspensions of solid spheres. Applied Scientific Research 37, 275-286.

Héquette, A., Hemdane, Y., Anthony, E.J., 2008. Sediment transport under wave and current combined flows on a tide-dominated shoreface, northern coast of france. Marine Geology 249, 226-242.

Hawlader, B.C., Muhunthan, B., Imai, G., 2008. State-dependent constitutive model and numerical solution of self-weight consolidation. Geotechnique 58, 133-141.

Heiliger, C.S., 2010. A numerical and experimental study of differential settling in cohesive sediments. Clemson University.

Hill, P.S., Milligan, T.G., Geyer, W.R., 2000. Controls on effective settling velocity of suspended sediment in the eel river flood plume. Continental Shelf Research 20, 2095-2111.

Hir, P.L., Cann, P., Waeles, B., Jestin, H., Bassoullet, P., 2008. Erodibility of natural sediments: Experiments on sand/mud mixtures from laboratory and field erosion tests, Proceedings in Marine Science. Elsevier, Saga, Japan, pp. 137-153.

Hsu, T.-J., 2003. On two-phase sediment transport: Dilute flow. Journal of Geophysical Research 108, 3057.

Hsu, T.-J., Balachandar, S., 2009. High resolution numerical modeling of cohesive sediment transport. Delaware univ newark centre for applied coastal research.

Hsu, T.-J., Jenkins, J.T., Liu, P.L.F., 2004. On two-phase sediment transport: Sheet flow of massive particles, 2048 ed. The Royal Society, pp. 2223-2250.

Hsu, T.-J., Ozdemir, C.E., Traykovski, P.A., 2009. High-resolution numerical modeling of wave-supported gravity-driven mudflows. Journal of Geophysical Research 114, 1289-1301.

Hsu, T.-W., Chang, H.-K., Hsieh, C.-M., 2003. A two-phase flow model of wave-induced sheet flow. Journal of Hydraulic Research 41, 299-310.

Hsu, T.J., Traykovski, P.A., Kineke, G.C., 2007. On modeling boundary layer and gravity-driven fluid mud transport. Journal of Geophysical Research 112, C04011.

Huang, Z., Aode, H., 2009. A laboratory study of rheological properties of mudflows in hangzhou bay, china. International Journal of Sediment Research 24, 410-424.

Imai, G., 1981. Experimental studies on sedimentation mechanism and sediment formation of clay materials. Soils found 21, 7-20.

Jacobs, W., Le Hir, P., Van Kesteren, W., Cann, P., 2011. Erosion threshold of sand–mud mixtures. Continental Shelf Research 31, S14-S25.

Jiang, J., Law, A.W.-K., Cheng, N.-S., 2004. Two-phase modeling of suspended sediment distribution in open channel flows/modélisation diphasique de la distribution de sédiments en suspension dans un écoulement à surface libre. Journal of Hydraulic Research 42, 273-281.

Keyvani, A., Strom, K., 2014. Influence of cycles of high and low turbulent shear on the growth rate and equilibrium size of mud flocs. Marine Geology 354, 1-14.

Khelifa, A., Hill, P.S., 2006. Models for effective density and settling velocity of flocs. Journal of Hydraulic Research 44, 390-401.

Kirwan, M.L., Murray, A.B., 2007. A coupled geomorphic and ecological model of tidal marsh evolution. Proc Natl Acad Sci U S A 104, 6118-6122.

Klimpel, R., Hogg, R., 1986. Effects of flocculation conditions on agglomerate structure. Journal of Colloid and Interface Science 113, 121-131.

Kornman, B.A., De Deckere, E.M.G.T., 1998. Temporal variation in sediment erodibility and suspended sediment dynamics in the dollard estuary. Geological Society, London, Special Publications 139, 231-241.

Kranenburg, C., 1994. The fractal structure of cohesive sediment aggregates. Estuarine, Coastal and Shelf Science 39, 451-460.

Kranenburg, C., 1998. Saturation concentrations of suspended fine sediment: Computations with the prandtl mixing-length model, Report No. 5 - 98. TU Delft.

Kynch, G.J., 1952. A theory of sedimentation. Transactions of the Faraday society 48, 166-176.

Lee, B.J., Toorman, E., Molz, F.J., Wang, J., 2011. A two-class population balance equation yielding bimodal flocculation of marine or estuarine sediments. Water research 45, 2131-2145.

Lee, S.-I., Seo, I.-S., Koopman, B., 1994. Effect of mean velocity gradient and mixing time on particle removal in seawater induced flocculation. Water, Air, & Soil Pollution 78, 179-188.

Leupi, C., 2005. Numerical modeling of cohesive sediment transport and bed morphology in estuaries. ÉCOLE POLYTECHNIQUE FÉDÉRALE DE LAUSANNE.

Levich, V., 1963. Physicochemical hydrodynamics. American Journal of Physics 31, 892-892.

Li, D.H., Ganczarczyk, J., 1989. Fractal geometry of particle aggregates generated in water and wastewater treatment processes. Environmental science & technology 23, 1385-1389.

Li, X., Logan, B.E., 1995. Size distributions and fractal properties of particles during a simulated phytoplankton bloom in a mesocosm. Deep Sea Research Part II: Topical Studies in Oceanography 42, 125-138.

Liang, B.-c., Li, H.-j., Lee, D.-y., 2008. Bottom shear stress under wave-current interaction. Journal of Hydrodynamics, Ser. B 20, 88-95.

Lick, W., Huang, H., Jepsen, R., 1993. Flocculation of fine-grained sediments due to differential settling. Journal of Geophysical Research 98, 10279-10210,10288.

Lick, W., Lick, J., Ziegler, C.K., 1992. Flocculation and its effect on the vertical transport of fine-grained sediments. Hydrobiologia 235, 1-16.

Liu, H., Sato, S., 2005. Modeling sediment movement under sheetflow conditions using a two-phase flow approach. Coastal Engineering Journal 47, 255-284.

Liu, X.J., Gao, S., Wang, Y.P., 2015. Modeling the deposition system evolution of accreting tidal flats: A case study from the coastal plain of central jiangsu, china. Journal of Coastal Research 299, 107-118.

Lopes, J.F., Dias, J.M., Dekeyser, I., 2006. Numerical modelling of cohesive sediments transport in the ria de aveiro lagoon, portugal. Journal of Hydrology 319, 176-198.

Lumborg, U., 2005. Modelling the deposition, erosion, and flux of cohesive sediment through resund. Journal of Marine Systems 56, 179-193.

Lumborg, U., Pejrup, M., 2005. Modelling of cohesive sediment transport in a tidal lagoon—an annual budget. Marine Geology 218, 1-16.

Maggi, F., 2005. Flocculation dynamics of cohesive sediment. Delft University of Technology.

Maggi, F., Mietta, F., Winterwerp, J.C., 2007. Effect of variable fractal dimension on the floc size distribution of suspended cohesive sediment. Journal of Hydrology 343, 43-55.

Manning, A., 2004a. The observed effects of turbulence on estuarine flocculation. Journal of Coastal Research SI 41, 90-104.

Manning, A.J., 2004b. Observations of the properties of flocculated cohesive sediment in three western european estuaries. Journal of Coastal Research SI 41, 70-81.

Manning, A.J., Baugh, J.V., Spearman, J.R., Pidduck, E.L., Whitehouse, R.J.S., 2011. The settling dynamics of flocculating mud-sand mixtures: Part 1—empirical algorithm development. Ocean Dynamics 61, 311-350.

Martinis, M., Risovic, D., 1998. Fractal analysis of suspended particles in seawater. FIZIKA B-ZAGREB- 7, 65-72.

Masliyah, J.H., 1979.] hindered settling in a multi-species particle system. Chemical Engineering Science 34, 1166-1168.

McAnally, W., Mehta, A., 2000. Aggregation rate of fine sediment. Journal of hydraulic engineering 126, 883-892.

McAnally, W.H., Friedrichs, C., Hamilton, D., Hayter, E., Shrestha, P., Rodriguez, H., Sheremet, A., Teeter, A., 2007. Management of fluid mud in estuaries, bays, and lakes. I: Present state of understanding on character and behavior. Journal of hydraulic engineering 133, 9-22.

McCave, I.N., 1984. Size spectra and aggregation of suspended particles in the deep ocean. Deep Sea Research Part A. Oceanographic Research Papers 31, 329-352.

Meakin, P., 1983. Formation of fractal clusters and networks by irreversible diffusion-limited aggregation. Physical Review Letters 51, 1119-1122.

Mehta, A.J., 1986. Characterization of cohesive sediment properties and transport processes in estuaries. Lecture notes on coastal and estuarine studies 14, 290-325.

Merckelbach, L.M., Kranenburg, C., 2004. Equations for effective stress and permeability of soft mud–sand mixtures. Geotechnique 54, 235-243.

Montserrat, F., Suykerbuyk, W., Al-Busaidi, R., Bouma, T.J., van der Wal, D., Herman, P.M.J., 2011. Effects of mud sedimentation on lugworm ecosystem engineering. Journal of Sea Research 65, 170-181.

Nguyen, K.D., Guillou, S., Chauchat, J., Barbry, N., 2009. A two-phase numerical model for suspended-sediment transport in estuaries. Advances in Water Resources 32, 1187-1196.

Reed, C., Anderson, J.L., 1980. Hindered settling of a suspension at low reynolds number. AIChE Journal 26, 816-827.

Richardson, J.F., Zaki, W.N., 1954. The sedimentation of a suspension of uniform spheres under conditions of viscous flow. Chemical Engineering Science 3, 65-73.

Risović, D., Martinis, M., 1996. Fractal dimensions of suspended particles in seawater. Journal of Colloid and Interface Science 182, 199-203.

Safak, I., Allison, M.A., Sheremet, A., 2013. Floc variability under changing turbulent stresses and sediment availability on a wave energetic muddy shelf. Continental Shelf Research 53, 1-10.

Safak, I., Sheremet, A., Allison, M.A., Hsu, T.-J., 2010. Bottom turbulence on the muddy atchafalaya shelf, louisiana, USA. Journal of Geophysical Research 115, C12019.

Shi, B.W., Yang, S.L., Wang, Y.P., Bouma, T.J., Zhu, Q., 2012. Relating accretion and erosion at an exposed tidal wetland to the bottom shear stress of combined current–wave action. Geomorphology 138, 380-389.

Son, M., Hsu, T.-J., 2008. Flocculation model of cohesive sediment using variable fractal dimension. Environmental Fluid Mechanics 8, 55-71.

Son, M., Hsu, T.-J., 2011. The effects of flocculation and bed erodibility on modeling cohesive sediment resuspension. Journal of Geophysical Research 116, C03021.

Son, M., Hsu, T.J., 2009. The effect of variable yield strength and variable fractal dimension on flocculation of cohesive sediment. Water Reseach 43, 3582-3592.

Soulsby, R.L., Clarke, S., 2005. Bed shear-stresses under combined waves and currents on smooth and rough beds, Report TR137. HR Wallingford.

Spearman, J.R., Manning, A.J., Whitehouse, R.J.S., 2011. The settling dynamics of flocculating mud and sand mixtures: Part 2—numerical modelling. Ocean Dynamics 61, 351-370.

Spicer, P.T., Pratsinis, S.E., 1996. Shear-induced flocculation: The evolution of floc structure and the shape of the size distribution at steady state. Water research 30, 1049-1056.

Spicer, P.T., Pratsinis, S.E., Raper, J., Amal, R., Bushell, G., Meesters, G., 1998. Effect of shear schedule on particle size, density, and structure during flocculation in stirred tanks. Powder Technology 97, 26-34.

Strom, K., Keyvani, A., 2011. An explicit full-range settling velocity equation for mud flocs. Journal of Sedimentary Research 81, 921-934.

Taki, K., 2000. Critical shear stress for cohesive sediment transport. Proceedings in Marine Science 3, 53-61.

Talke, S.A., de Swart, H.E., 2006. Hydrodynamics and morphology in the ems/dollard estuary: Review of models, measurements, scientific literature, and the effects of changing conditions.

Teisson, C., Simonin, O., Galland, J., Laurence, D., 1992. Turbulence and mud sedimentation: A reynolds stress model and a two-phase flow model, 23rd international conference on coastal engineering. ASCE, Venice, pp. 2853-2866.

Thomsen, L., Gust, G., 2000. Sediment erosion thresholds and characteristics of resuspended aggregates on the western european continental margin. Deep Sea Research Part I: Oceanographic Research Papers 47, 1881-1897.

Thorn, M.F.C., 1981. Physical processes of siltation in tidal channels, Hydraulic Modelling applied to Maritime Engineering Problems. ICE, London, pp. 47-55.

Tomkins, M.R., Baldock, T.E., Nielsen, P., 2005. Hindered settling of sand grains. Sedimentology 52, 1425-1432.

Toorman, E., 1999. Sedimentation and self-weight consolidation: Constitutive equations and numerical modelling. Geotechnique 49, 709-726.

Toorman, E., 2002. Modelling of turbulent flow with suspended cohesive sediment. Proceedings in Marine Science 5, 155-169.

Toorman, E., Bruens, A., Kranenburg, C., Winterwerp, J., 2002. Interaction of suspended cohesive sediment and turbulence. Proceedings in Marine Science 5, 7-23.

Toorman, E.A., 1996. Sedimentation and self-weight consolidation: General unifying theory. Geotechnique 46, 103-113.

Torres-Freyermuth, A., Hsu, T.-J., 2010. On the dynamics of wave-mud interaction: A numerical study. Journal of Geophysical Research 115, C07014.

Vahedi, A., Gorczyca, B., 2011. Application of fractal dimensions to study the structure of flocs formed in lime softening process. Water research 45, 545-556.

Vahedi, A., Gorczyca, B., 2012. Predicting the settling velocity of flocs formed in water treatment using multiple fractal dimensions. Water research 46, 4188-4194.

Van Bang, D.P., Lefrançois, E., Sergent, P., Bertrand, F., 2008. Expérimentation par irm et modélisation par éléments finis de la sédimentation-consolidation des vases. La Houille Blanche, 39-44.

Van Der Ham, R., Fontijn, H., Kranenburg, C., Winterwerp, J., 2001. Turbulent exchange of fine sediments in a tidal channel in the ems/dollard estuary. Part i: Turbulence measurements. Continental Shelf Research 21, 1605-1628.

van der Ham, R., Winterwerp, J.C., 2001. Turbulent exchange of fine sediments in a tidal channel in the ems/dollard estuary. Part ii. Analysis with a 1dv numerical model. Continental Shelf Research 21, 1629-1647.

Van der Lee, W.T.B., 2000. Temporal variation of floc size and settling velocity in the dollard estuary. Continental Shelf Research 20, 1495-1511.

Van, L.A., 2013. Modélisation du transport des sédiments mixtes sable-vase et application à la morphodynamique de l'estuaire de la gironde. Citeseer.

van Leussen, W., 1999. The variability of settling velocities of suspended fine-grained sediment in the ems estuary. Journal of Sea Research 41, 109-118.

van Leussen, W., 2011. Macroflocs, fine-grained sediment transports, and their longitudinal variations in the ems estuary. Ocean Dynamics 61, 387-401.

Van Maren, D.S., Winterwerp, J.C., Wang, Z.Y., Pu, Q., 2009. Suspended sediment dynamics and morphodynamics in the yellow river, china. Sedimentology 56, 785-806.

Villaret, C., Davies, A., 1995. Modeling sediment-turbulent flow interactions. Applied mechanics reviews 48, 601-609.

Wang, Y., Gao, S., Jia, J., 2006. High-resolution data collection for analysis of sediment dynamic processes associated with combined current-wave action over intertidal flats. Chinese Science Bulletin 51, 866-877.

Whitehouse, R.J.S., Bassoullet, P., Dyer, K.R., Mitchener, H.J., Roberts, W., 2000. The influence of bedforms on flow and sediment transport over intertidal mudflats. Continental Shelf Research 20, 1099-1124.

Winterwerp, J.C., 1998. A simple model for turbulence induced flocculation of cohesive sediment. Journal of Hydraulic Research 36, 309-326.

Winterwerp, J.C., 2002. On the flocculation and settling velocity of estuarine mud. Continental Shelf Research 22, 1339-1360.

Winterwerp, J.C., 2006. Stratification effects by fine suspended sediment at low, medium, and very high concentrations. Journal of Geophysical Research 111, C05012.

Winterwerp, J.C., Manning, A.J., Martens, C., de Mulder, T., Vanlede, J., 2006. A heuristic formula for turbulence-induced flocculation of cohesive sediment. Estuarine, Coastal and Shelf Science 68, 195-207.

Winterwerp, J.C., Van Kesteren, W.G., 2004. Introduction to the physics of cohesive sediment in the marine environment. Elsevier Science Limited.

Yang, S.-L., Friedrichs, C.T., Shi, Z., Ding, P.-X., Zhu, J., Zhao, Q.-Y., 2003. Morphological response of tidal marshes, flats and channels of the outer yangtze river mouth to a major storm. Estuaries 26, 1416-1425.

Ying, X., Ding, P., Wang, Z.B., Van Maren, D.S., 2012. Morphological impact of the construction of an offshore yangshan deepwater harbor in the port of shanghai, china. Journal of Coastal Research 278, 163-173.

Zhang, K., Dong, P., 2000. A computer code for simulating hyper-concentrated sediment motions in steady and unsteady flows. Applied Mathematical Modelling 24, 495-510.

Zhang, Y., Campbell, C.S., 1992. The interface between fluid-like and solid-like behaviour in two-dimensional granular flows. Journal of Fluid Mechanics 237, 541-568.

Zhou, C., Dong, P., Li, G., 2015. Hydrodynamic processes and their impacts on the mud deposit in the southern yellow sea. Marine Geology 360, 1-16.

Zhu, Q., Yang, S., Ma, Y., 2014. Intra-tidal sedimentary processes associated with combined wave–current action on an exposed, erosional mudflat, southeastern yangtze river delta, china. Marine Geology 347, 95-106.